MDPI

Review

A Review on Metal Ions Modified TiO$_2$ for Photocatalytic Degradation of Organic Pollutants

Dafu Jiang [1], Tunmise Ayode Otitoju [2,3], Yuanyuan Ouyang [1], Noor Fazliani Shoparwe [3], Song Wang [1], Ailing Zhang [1] and Sanxi Li [1,]*

[1] School of Environmental and Chemical Engineering, Shenyang University of Technology, Shenyang 110870, China; jiangdafubs@163.com (D.J.); ouyangyuanyuanbs@163.com (Y.O.); wangsong@sut.edu.cn (S.W.); zhangal718@sina.com (A.Z.)

[2] School of Materials Science and Engineering, Shenyang University of Technology, Shenyang 110870, China; timopd1@gmail.com

[3] Faculty of Bioengineering and Technology, Jeli Campus, Universiti Malaysia Kelantan, Jeli 17600, Malaysia; fazliani.s@umk.edu.my

* Correspondence: lisx@sut.edu.cn

Abstract: TiO$_2$ is a semiconductor material with high chemical stability and low toxicity. It is widely used in the fields of catalysis, sensing, hydrogen production, optics and optoelectronics. However, TiO$_2$ photocatalyst is sensitive to ultraviolet (UV) light; this is why its photocatalytic activity and quantum efficiency are reduced. To enhance the photocatalytic efficiency in the visible light range as well as to increase the number of the active sites on the crystal surface or inhibit the recombination rate of photogenerated electron–hole pairs electrons, various metal ions were used to modify TiO$_2$. This review paper comprehensively summarizes the latest progress on the modification of TiO$_2$ photocatalyst by a variety of metal ions. Lastly, the future prospects of the modification of TiO$_2$ as a photocatalyst are proposed.

Keywords: photocatalysts; TiO$_2$; metal ions; pollutant degradations

1. Introduction

In the past, industrial development has been accompanied by the discharge of a large number of organic pollutants, which has caused great harm to the environment and living beings in general [1,2]. Research on the purification of wastewater is currently available and ongoing. Various traditional methods including physical adsorption, biodegradation, catalytic oxidation, and high-temperature incineration have been proposed [3]. Table 1 presents the traditional treatment methods and their limitations. These treatment methods have some shortcomings, and the treatment effect on organic wastewater is not very ideal. Recent studies have been devoted to a promising approach, the advanced oxidation processes (AOP) for the degradation of organic pollutants from wastewaters [3–10], due to its ability to completely mineralize the targeted pollutants [11]. There are various types of AOPs including ozone (photo-ozonation, ozonation, O$_3$+Fe^{2+}/Fe^{3+}, and ozonation + catalyst and O$_3$+H$_2$O$_2$), photolysis (VUV or UV), hydrogen peroxide (photo-Fenton: H$_2$O$_2$+Fe^{2+}/Fe^{3+}+UV, Fenton-like reagents: H$_2$O$_2$+Fe^{2+}-solid/Fe^{3+}-solid, Fenton: H$_2$O$_2$+Fe^{2+}/Fe^{3+}, and H$_2$O$_2$+UV), and photocatalysis [12,13].

The ordinary chemical oxidation process has limitations in degrading some harmful substances because of its poor oxidation ability. The intermediate products in the advanced oxidation process can react with hydroxyl radicals to oxidize harmful substances into carbon dioxide and water. AOPs are a chemical purification treatment used to remove inorganic/organic materials in wastewater and water via oxidation through reactions with hydroxyl radicals ($\cdot$OH). AOPs can be categorized as heterogeneous systems (semiconductor photocatalytic process) and homogeneous systems (Fenton and photo-Fenton systems,

ozone, UV/H$_2$O$_2$) [14]. Photocatalytic degradation is a part of AOP for the degradation of organic pollutants which has proven as an effective technology [15,16]. It is more effective in comparison with the AOP as it can easily mineralize various organic components and the semiconductors used are not expensive.

Table 1. Traditional photodegradation methods and limitations.

Approach	Limitations
Biological treatment	Chlorinated phenols are resistant to biodegradation and can accumulate in sediments. They transfer the contaminants from one medium to another and require disposal or further treatment The biodegradation of organic pollutants such as 4-CP is slow and incomplete, and its byproducts are more toxic compared to other pollutants. Biological processes usually require considerable processing time to decompose 4-CP. By use of the biological treatment, it cannot be degraded due to a large number of aromatic structures in the dye molecules and the stability of modern dyes. Azo bond is reduced to form a colorless but toxic and potentially carcinogenic aromatic amine.
Adsorption technology and activated carbon adsorption method	The post-treatment of wastewater and regeneration of adsorbent materials requires an expensive operation. Activated carbon adsorption requires the safe disposal of carbon. During the adsorption process, the system cannot tolerate the suspended solids in the influent water as a result of blockage. The operating cost is high due to the requirements of the carbon system. The treatment may be problematic if the polluted carbon is not regenerated.
Chemical precipitation	Requirements for a large amount of chemicals and a large amount of sludge produced. Requires further treatment or disposal. Due to the large amount of sludge needing to be treated, the method is not feasible economically.
Air stripping	It is susceptible to pollution. Aesthetic limitations due to tower height. Challenges involving mechanical reliability.
Membrane adsorption	The purchasing cost of membranes and residues (very concentrated filtrate) is high and must be collected or may require further processing. The physical method is not destructive, but only transfers pollutants to other media, causing secondary pollution.

2. TiO$_2$ Photocatalysis

Photocatalysis is a general term for a photoinduced reaction that is accelerated in the presence of a catalyst. Heterogeneous photocatalysis is the most widely used and effective process for the degradation of organic pollutants and does not produce harmful intermediates at ambient temperature and pressure [17,18]. This process starts with electron excitation, which is transferred from the valence band (VB) to the empty conduction band (CB). In the presence of light, the catalyst absorbs adequate energy to become excited from the light which is equal to its energy bandgap. The excited electrons move toward the conduction band via the holes acting as a positive charge in the valence band, owing to which photogenerated species, including e$^-$/h$^+$ pair, are created in the photocatalytic system. The generated species react with -OH groups or oxygen molecules to further produce reactive oxygen species such as superoxide anion radicals (O$_2\bullet^-$) and hydroxyl radicals (•OH). Thereafter, these reactive oxygen species attack the organic molecules, decomposing them via oxidation. Finally, the e-/h$^+$ pairs are formed on the photoexcited catalyst's surface [19,20].

These materials are generally N-type semiconductors with discontinuous band structures different from metals, usually composed of low-valence bands full of electrons. Common semiconductor photocatalysts include ZnO, TiO_2, $Bi_{20}Ti_{20}$, Bi_2WO_6, Nb_2O_5, Fe_2O_3, $SrTiO_3$, $BiTiO_3$, CuS/ZnS, $ZnWO_4$, WO_3, ZnS, Ag_2CO_3, and SnO_2, etc., but most photocatalysts have an impact on the photocatalytic performance due to the photocorrosion phenomenon. Among the aforementioned photocatalysts, Titanium dioxide (TiO_2) has been widely studied by researchers due to its low cost, high efficiency, and stability. The disadvantage of TiO_2 is that it cannot be activated by visible irradiation, but by UV. Its advantages over other semiconductors include being biologically and chemically inert, relatively easy to use and produce, photo-catalytically stable, relatively cheap, and able to efficiently catalyze reactions, with no risk to humans or the environment [11]. TiO_2 exists in three polymorphs such as rutile, anatase, and brookite. Both rutile and anatase have tetragonal crystal lattices while brookite appears as orthorhombic crystal lattices [21]. Rutile form is more stable than the other polymorphs among these three phases. TiO_2 has applications in various products including sunscreen lotions, capacitors, paint pigments, toothpaste, food coloring agents, solar cells, and electrochemical electrodes [22].

In 1967, Kenichi Honda and Akira Fujishima jointly discovered that light irradiating a titanium dioxide electrode can carry out the electrolysis of water. The ionized water or oxygen was converted into photo-living groups with oxidizing ability. Their energy was equivalent to a high temperature of 3600 K and is highly oxidizing. In 1972, Fujishima et al. first proposed the theory of photocatalytic water splitting on TiO_2 electrodes, and then in 1973, they proposed the use of titanium dioxide photocatalyst for environmental remediation, thus promoting the development of photocatalytic technology [23]. In 1995, Fujishima et al. [24] discovered that a film containing a certain amount of TiO_2 was super-hydrophilic under ultraviolet light, which promoted the derivation of the field of photocatalyst and film binding. This technology utilizes some special photocatalyst powder into sewage, which could decompose toxic metal substances in the water to obtain pure water under the irradiation with ultraviolet rays. This technology was also used to remediate polluted rivers and found harmless to the environment. Since then, researchers have found ways to modify the TiO_2 photocatalyst in a large amount. By 2004, Sonawane reported that Fe-TiO_2 film could degrade methyl orange solution within 4 h under sunlight, with a degradation efficiency (95%) [25].
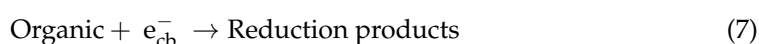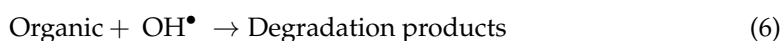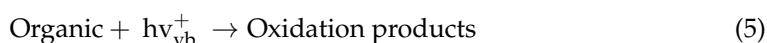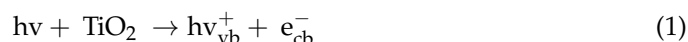
The bandgap of pure nano-titanium dioxide powder is about 3.2 eV, which can only absorb ultraviolet light below 400 nm. In the natural environment, ultraviolet light is less than 10%, so pure nano-titanium dioxide does not have the function of a photocatalyst. This greatly affects the utilization rate of the catalyst to sunlight. Other key factors that limit the practical application of photocatalysts are the low quantum yield of the catalyst and the faster recombination of electrons and photogenerated holes. Generally, the recombination efficiency of photogenerated carriers determines the quantum quality of the photocatalyst, which affects carrier recombination. The main factors of the surface charge transfer process are the surface morphology, grain size, crystal phase structure, and surface lattice defects of the catalyst, as well as the intensity of light radiation.

To make the TiO_2 photocatalyst absorb visible light and far-infrared light and improve the photocatalytic efficiency, the photocatalyst needs to be modified. At present, researchers have proposed two ways to enhance the photocatalytic performance of TiO_2: one is to prevent photogenerated electrons from recombining with photogenerated holes so that they can effectively participate in the catalytic degradation reaction process; the other is to introduce other elements into TiO_2 lattice, thereby reducing the bandgap energy of the catalyst and expanding its photoresponse range. Generally, the activated CB electrons and VB holes recombine into a neutral body to generate energy, which is lost in the form of light energy or heat. Therefore, the photogenerated electrons can be captured by the catalyst or the mobility of the surface charge of the catalyst can be improved. To slow down the recombination of hole–electron pairs, modification of TiO_2 lattice with metal ions is an effective way to improve photocatalytic performance. In the subsequent sections,
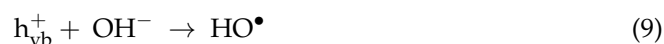
recent studies on metal ion modified TiO_2 (with morphologies such as nanoparticles, microspheres, nanofibers, nanocrystals, nanosheets, nanotubes, nanopowders) were summarized and reported.

3. Mechanisms of TiO₂ Photocatalysts for Organic Pollutants

The mechanism of the photocatalytic reaction in the presence of TiO_2 photocatalysts consists of a free radical reaction initiated by light irradiation (photons) [26]. When the energy of solar radiation exceeds the bandgap of TiO_2 (i.e., photon energy reaches or exceeds its bandgap energy), the surface of the photocatalyst becomes excited, and the electrons transit from the valence band (VB) to the conduction band (CB). In the CB, corresponding electron holes are derived in the VB at the same time, forming electron–hole pairs (i.e., generating electron (e^-) and hole (H^+) pairs). VB holes have strong oxidation reaction activity (1.0~3.5 V) because they lose electrons and act as reducing agents, and electrons in the conduction band have good reducibility 0.5~1.5 V when they undergo reduction. Under light irradiation, positive holes and electrons are generated in the VB (hv_{vb}^+) and CB (e_{cb}^-) of TiO_2 as presented in Equation (1) [27]. These holes can either form hydroxyl radicals (Equation (3)) or react directly with organic molecules (Equation (5)) which subsequently oxidize the organic molecules (Equation (6)) [28]. The electrons can also react with organic compounds to produce reduction products (Equations (1)–(7)). The role of oxygen is important as it reacts with the photogenerated electrons. Organic compounds can then undergo oxidative degradation through their reactions with hydroxyl and peroxide radicals, VB holes, as well as reductive cleavage via reactions with electrons yielding various byproducts and finally mineral end-products [29].

$$hv + TiO_2 \rightarrow hv_{vb}^+ + e_{cb}^- \tag{1}$$

$$OH_{surface}^- + hv_{vb}^+ \rightarrow OH^\bullet \tag{2}$$

$$H_2O_{absorbed} + hv_{vb}^+ \rightarrow H^+ + OH^\bullet \tag{3}$$

$$O_{absorbed} + e_{cb}^- \rightarrow OH_2^{-\bullet} \tag{4}$$

$$Organic + hv_{vb}^+ \rightarrow Oxidation\ products \tag{5}$$

$$Organic + OH^\bullet \rightarrow Degradation\ products \tag{6}$$

$$Organic + e_{cb}^- \rightarrow Reduction\ products \tag{7}$$

Additionally, VB holes (h_{vb}^+) react with water (H_2O) and the hydroxyl ion (OH^-) to form hydroxyl radicals ($HO^\bullet$), while electrons (e_{cb}^-) react with adsorbed oxygen molecule (O_2), thus reducing it to superoxide radical anion ($O_2^{\bullet-}$) which reacts with protons (H^+) to form peroxide radicals ($HO_2^\bullet$) as shown in Equations (8)–(11) [30].

$$h_{vb}^+ + H_2O \rightarrow HO^\bullet + H^+ \tag{8}$$

$$h_{vb}^+ + OH^- \rightarrow HO^\bullet \tag{9}$$

$$e_{cb}^- + O_2 \rightarrow O_2^{\bullet-} \tag{10}$$

$$O_2^{\bullet-} + H^+ \rightarrow HO_2^\bullet \tag{11}$$

In the presence of light irradiation using metal ion modified TiO_2 and because the metal ions create intermediate states in the TiO_2 structure, the surface electrons in the intermediate states become excited, having sufficient energy to access more light absorption and transfer electrons to the TiO_2 surface that stimulate more electrons under light, which as a consequence advances the redox reactions [31–33]. These properties being displayed by the metal ions help to improve the photocatalytic reactions. The transfer of electrons takes place at the VB to the CB via the creation of holes in the former and these holes subsequently react with H_2O molecules present in the pollutant as well as helping to form

the OH radicals [31–34]. The formed OH radicals are supportive and found significant success in degrading various dyes under light irradiation [35–37]. The photocatalytic mechanism of metal-ion modified TiO$_2$ for organic pollutants is illustrated in Figure 1.
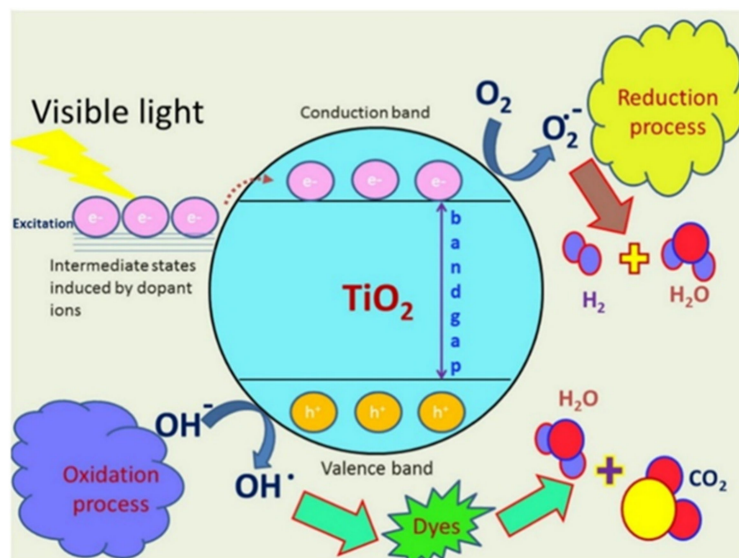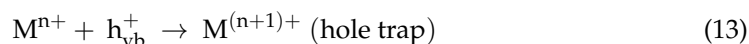

Figure 1. Mechanism of photocatalytic activity of metal-ion modified TiO$_2$ in the presence of visible light [38].

4. Modification with Metal Ions

Modification with metal-ion can act as electron/hole traps and alter e$^-$/h$^+$ recombination rate, according to the below mechanisms [39]:

$$M^{n+} + e_{cb}^- \rightarrow M^{(n-1)+} \text{ (electron trap)} \tag{12}$$

$$M^{n+} + h_{vb}^+ \rightarrow M^{(n+1)+} \text{ (hole trap)} \tag{13}$$

where energy level for $M^{n+}/M^{(n-1)+}$ lies below the CB edge (e$_{cb}$) and the energy level for $M^{n+}/M^{(n+1)+}$ above the VB edge (e$_{vb}$).

The presence of metal ions allows visible light absorption and introduces trap/recombination sites within the TiO$_2$ bands which may as a result increase the life span of photoinduced charge carriers as well as the reduction in quantum efficiency. Modifications with metal ions can influence TiO$_2$ photocatalysis according to these principles: (i) improve the electron–hole separation (strength) by selective trapping [40,41]; (ii) due to their ability to act as recombination centers, they reduce carriers' lifespan (weakness) [42,43], and (iii) enhance optical absorption in visible light range. The commonly used metal ions are the metals, transition metal, rare earth metal, or noble metal [44]. Modification of TiO$_2$ by metal ions is generally carried out via sputtering [45], ion implantation [46], or via chemical processes (for example sol–gel) [47–50]. Figure 2 presents a table of commonly used metallic ions to enhance the photocatalytic degradation of organic pollutants.

In general, various types of metals (Transition, rare earth, or other metals) have been used to modify TiO$_2$ photocatalysts. Table 2 presents the general properties and principal applications of the metals. In the subsequent sections, the modifications using metal ions TiO$_2$ photocatalysts are described and discussed. The following section starts with the modification using transition metal, which is subsequently followed by lanthanides or rare earth metal modifications. At the end of this section, the modifications of other metals were presented.

Figure 2. Table of commonly used metallic ions to enhance the photocatalytic degradation of organic pollutants.

Table 2. General properties and principal applications of the metals.

Classes of Metals	Features/Properties	Principal Applications
Transition metals	They have incompletely filled d orbitals. The transition metals are more electronegative than the other metals and form stable compounds with neutral molecules (such as water or ammonia). The main advantages of these metals are malleability and ductility. Examples of transition metals used to modify TiO_2 photocatalysts include vanadium (V), nickel (Ni), copper (Cu), manganese (Mn), zirconium (Zr), iron (Fe), chromium (Cr), molybdenum (Mo), cobalt (Co), niobium (Nb), tungsten (W), and zinc (Zn). The density of V, Ni, Cu, Mn, Zr, Fe, Cr, Mo, Co, Nb, W, and Zn are 6.0, 8.90, 8.96, 7.3, 6.52, 7.87, 7.15, 10.2, 8.86, 8.57, 19.3, and 7.134 g cm^{-3}, respectively.	Luminescence, electronic device, and water pipes applications.
Noble metals	These metals are known as iron lovers due to their ability to dissolve in iron either as solid solutions or in the molten state. They have outstanding resistance to chemical attacks even at high temperatures. Furthermore, they are well known for their catalytic properties and associated capacity to facilitate or control the rates of chemical reactions. Examples of noble metals used to modify TiO_2 photocatalysts include ruthenium (Ru), palladium (Pd), platinum (Pt), gold (Au), and silver (Ag). The density of Ru, Pd, Pt, Au, and Ag are 12.1, 12.0, 21.5, 19.3, and 10.5 g cm^{-3}, respectively.	Hydrogenation, total oxidation and, more recently, partial oxidation heterogeneous catalysts.
Rare-earth metals	Rare earth metals possess good magnetic and luminescent properties. The common rare earth metals used to modify TiO_2 photocatalysts include cerium (Ce), erbium (Er), holmium (Ho), gadolinium (Gd), terbium (Tb), neodymium (Nd), ytterbium (Yb), samarium (Sm), lanthanum (La), europium (Eu), and yttrium (Y). The density of Ce, Er, Ho, Gd, Tb, Nd, Yb, Sm, La, Eu, and Y is 6.77, 9.07, 8.80, 7.90, 8.23, 7.01, 6.90, 7.52, 6.15, 5.24 and 4.47 g cm^{-3}, respectively.	Cellphones, electrical and electronic components, lasers, glass, magnetic materials, fluorescent lights, defense, clean energy.
Metals	Metals are malleable, ductile, good conductors of heat and electricity. Metals have a luster with high tensile strength. Typical metals used to modify TiO_2 photocatalysts include gallium (Ga), indium (In), aluminum (Al), and tin (Sn). The density of Ga, In, Al, and Sn is 5.91, 7.31, 2.70, and 7.287 g cm^{-3}, respectively.	Automobiles, electronic devices.

4.1. Modification with Transition Metals

Modifying TiO_2 with transition metals has shown great promise through the extension of spectral response and the ability to achieve visible light-activated photocatalysis [51]. Modifying with transition metal including Cu, Cr, Mn, Fe, V, and Zn can reduce the e^-/h^+ recombination and decrease the bandgap by creating an intra-bandgap state, which shifts the light absorption into the visible light region [52,53]. The formation of additional energy levels in the bandgap of TiO_2 can be described below [54]:

$$(1) \ M^+ + hv \ \rightarrow \ M^{(n+1)+} + \ e^- \tag{14}$$

$$(2) \ M^+ + hv \ \rightarrow \ M^{(n-1)+} + \ h^+ \tag{15}$$
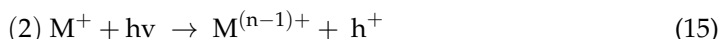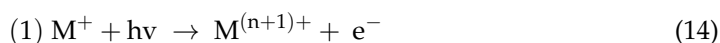
where M is the metal.

The energy necessary for reducing the metal ion should be less negative than the conduction band edge of titania while its oxidation energy should be less positive than the valence band edge of TiO_2. Additionally, photocatalytic reactions can occur only if the trapped holes and electrons are transferred to the catalyst's surface. Therefore, metal ions should be situated near the surface of TiO_2 crystallites for a better charge transfer [55]. If the amount of metal ions is more than optimal, the metal ions tend to behave as recombination centers and the transfer of h^+/e^- pairs to the interface is more complex. Generally, the metal ions are precipitated on the surface as oxides forming a MO_x/TiO_2 nanocluster and not incorporated in the structure of TiO_2. If the energetic positions of CB and VB of components forming the composite are suitable (i.e., a type II heterojunction), beneficial charge transfer occurs within the photocatalyst where e^- is accumulated in the CB edge of one component and h^+ is accumulated in the VB edge of the other component. Therefore, the charge carriers are separated efficiently, leading to improved photocatalytic property [56,57].

4.1.1. Modification with Vanadium (V)

Vanadium exists in several oxidation states (V^{2+} to V^{5+}) and a variety of species. The types of species and oxidation state are a function of the redox potential, pH, concentration, and other factors [58]. The radius of the V ion is nearly identical to that of titanium (Ti) and can be conveniently introduced into titania [59]. V ions with different valence states (V^{3+} to V^{5+}) can transfer between V^{3+} to V^{5+} under oxidizing and reducing conditions. For example, the tetragonal crystal structure of VO_2 is similar to that of titania, which is responsible for an increase in visible light absorption and photogenerated holes and electrons [60]. The photogenerated holes and electrons can be migrated, trapped, and released on the TiO_2 surface by V^{4+} ions, and play a role in charge transfer species. It is very difficult for V^{5+} ions to enter the lattice of TiO_2, making it appropriate to form V_2O_5 on the surface and thus responsible for h^+ and e^- separation [61]. Subsequently, this photogenerated e^- and h^+ can be accepted by the adsorbed O_2 and surface hydroxyl group (OH^-), and therefore transform OH^- and O_2 into hydroxyl radical ($\bullet OH$) and superoxide radicals ($\bullet O_2^-$) active species, respectively.

Vanadium-TiO_2 (V-TiO_2) at low concentrations has been found to improve TiO_2 photocatalytic behavior via the existence of the photogenerated charge and the more efficient expansion of absorption spectrum as compared to other metals [62,63]. V-TiO_2 has an enhanced photocatalytic activity due to the following reasons: (i) improving the absorption in the visible light range, (ii) improved quantum efficiency due to effective h^+ to e^- pair separation, and (iii) presence of both V^{5+} and V^{4+} species in the V-TiO_2. Additionally, the second reason can contribute to the increased electron transfer and visible light absorption, whereas the latter enhances e^-–h^+ separation and is a potential electron acceptor [64–66]. V-TiO_2 have been extensively studied in experiments and theory due to evidence of ferromagnetism above room temperature or at room temperature [67,68]. Vanadium with a narrow bandgap can be coupled with TiO_2 by various approaches such as metal-ion implantation, sol–gel, hydrothermal, and coprecipitation approach. Generally, the sol–gel method is frequently used for depositing the V-TiO_2 films while the

coprecipitation approach is used to prepare V-TiO$_2$ powders. Among these approaches, (compared with the hydrothermal approach), the sol–gel and coprecipitation approach is quite harsh and complicated; however, the hydrothermal approach is easy to execute and involves low cost [69,70]. Table 3 presents the summary of recent progress on V-TiO$_2$ photocatalysts for organic pollutants degradation.

Table 3. Summary of recent progress on V-TiO$_2$ photocatalysts for organic pollutants degradation.

Material (TiO$_2$ Phase Transition)	Optimum	Catalyst Dosage	Synthetic Methods	Pollutant (Volume)	Light Source	Unmodified	Modified	Ref.
V-TNT nanosheet (mixed crystal of anatase and rutile phases)	1.0% V-TNT	0.1 g	Hydrothermal method	20 mg/L RhB (100 mL)	UV/Visible light	70% within 70 min for TNT	The reaction rate was 3.26-fold and 9.27-fold as compared to unmodified TNT under visible light and UV–vis irradiation, respectively.	[71]
V$_2$O$_5$/TiO$_2$ nanoparticles (anatase phase)	3 wt% V$_2$O$_5$/TiO$_2$	0.05 g	Incipient wet impregnation method	0.2 mg/L Eosin Y (200 mL)	Visible light	8% within 180 min for V$_2$O$_5$	93% within 180 min, the stability only decreased by 20% for the first run	[72]
V$_2$O$_5$/P25 nanoparticles (anatase phase)	3 wt% V$_2$O$_5$/P25	0.05 g	Incipient wet impregnation method	0.2 mg/L Eosin Y (200 mL)	Visible light	8% within 180 min for V$_2$O$_5$	81% within 180 min	[72]
V$_2$O$_5$/TiO$_2$ nanoparticles (anatase phase)	3 wt% V$_2$O$_5$/TiO$_2$	0.05 g	Incipient wet impregnation method	0.2 mg/L Eosin Y (200 mL)	Visible light	100% within 180 min for TiO$_2$ and P25, 33% within 180 min for V$_2$O$_5$	40% within 180 min	[72]
V$_2$O$_5$/TiO$_2$ coatings (anatase phase)	2.0 wt% V$_2$O$_5$/TiO$_2$	15 mm × 10 mm	Sol–gel method	8 mg/L MO (10 mL)	Sunlight	35% within 8 h	53% within 8 h	[73]
V-TiO$_2$ nanoparticles (rutile to stable anatase phase)	1.0% V-TiO$_2$	0.05 g	Sol–gel method	10 mg/L RhB (100 mL)	Xenon Lamp	21.56% within 300 min	53.74% within 300 min	[74]
V-TiO$_2$ nanopowders (anatase phase)	50 wt% V$_2$O$_5$/TiO$_2$	0.1 g	Solid-state dispersion method	25 mg/L 2,4-CP (50 mL)	UV-B	72% within 30 min for pure V$_2$O$_5$, 66% within 30 min for pure TiO$_2$	85% within 30 min	[75]
V-TiO$_2$ coupons (rutile to stable anatase phase)	6.0 wt% V-TiO$_2$	15 mm × 10 mm	PEOx	10 mg/L MB (100 mL)	Tungsten-halogen	55% within 180 min for pure TiO$_2$	85% within 180 min	[76]
V-TiO$_2$ nanoparticles (anatase to brookite and rutile phases)	0.125 mol%-V-TiO$_2$	0.1 g/L	MWASG	85 mg/L MB and SMX (100 mL)	UV	0.031 min^{-1} for MB within 60 min	0.035 and 0.0262 min^{-1} for MB and SMX, respectively within 60 min	[77]

MWASG: Microwave-assisted sol–gel method; PEOx: plasma electrolytic oxidation; RhB: rhodamine B; 2,4-CP: 2,4-dichlorophenol; MB: methylene blue; SMX: sulfamethazine.

4.1.2. Modification with Nickel (Ni)

Nickel (Ni) has good activity and it is less expensive than noble metals [78]. This element is used in many applications due to its physicochemical properties. Ni is a good candidate for substituting Ti atoms in the TiO_2 structure [79]. The incorporation of Ni ions into the TiO_2 lattice can actively modify the TiO_2 physical properties via the creation of an impurity energy level. Upon modifying TiO_2 with Ni, the recombination of photogenerated hole–electron pairs is suppressed effectively, thus resulting in an enhanced photocatalytic activity [79–81]. The structure of the Ni^{2+} valence band is 3d8. When the Ni ions trap the photogenerated hole–electron pairs, the valence layer (d) is converted from a high to low spin state, and thus results in a significant spin energy loss. Based on the crystal field theory, charge carriers that are being trapped by Ni ions tend to migrate to the H_2O molecules (adsorbed on the surface) to restore their energy, and as a consequence will prevent the recombination of hole–electron pairs [82]. Furthermore, Ni^{2+} plays an important role in the improvement of thermal stability as well as controlling the morphology of TiO_2 photocatalysts. Table 4 presents the summary of recent progress on Ni-TiO_2 photocatalysts for organic pollutants degradation.

Table 4. Summary of recent progress on Ni-TiO$_2$ photocatalysts for organic pollutants degradation.

Material (TiO$_2$ Phase Transition)	Optimum	Catalyst Dosage	Synthetic Methods	Pollutant (Volume)	Light Source	Unmodified	Modified	Ref.
Ni-TiO$_2$ nanotubes (mixed crystal of anatase and rutile phases)	10% Ni-TNT	0.1 g	Hydrothermal method	5 mg/L MB (50 mL)	Sunlight	71.4% within 90 min for pure TiO$_2$	~65% within 90 min	[83]
Ni-TiO$_2$ nanoparticles (mixed crystal of anatase and rutile phases)	0.9 wt% Ni- TiO$_2$	1.5 g/L	Sol–gel method	10 mg/L MB (100 mL)	Hg vapor lamp	62% within 120 min for pure TiO$_2$	50% within 120 min	[84]
Ni-TiO$_2$ nanoparticles (anatase phases)	0.01% Ni-TiO$_2$	0.1 g	Hydrothermal method	10 mg/L MB (100 mL)	Tungsten-halogen lamp	-	75% within 300 min	[85]
Ni-TiO$_2$ inverse opal photonic microarray (IOPM) (anatase phases)	3.0 wt% Ni-TiO$_2$	-	Sol–gel method	10 mg/L MB (100 mL)	Sunlight	60% within 90 min for TiO$_2$ IOPM	95% within 90 min (1.58 times larger compared to that over TiO$_2$ IOPM)	[86]
Ni-TiO$_2$ nanoparticles (anatase phases)	1.0 wt% Ni-TiO$_2$	1 g/L	MWASG	10 mg/L BPA (200 mL)	Phillip lamp	60.1% (0.0098 min^{-1}) within 120 min	93% (0.0255 min^{-1}) within 120 min	[87]
Ni-TiO$_2$ nanoparticles (anatase phases)	0.50 wt% Ni-TiO$_2$	2 g/L	Sol–gel method	25 mg/L IBP (50 mL)	Solar light	76% within 6 h for pure TiO$_2$	78% (0.0046 min^{-1}) within 6 h	[88]
Ni-TiO$_2$ nanoparticles (anatase to rutile phase)	10 wt% Ni-TiO$_2$	2 g/L	Coprecipitation method	100 mg/L ECR (200 mL)	Visible light	20.9% within 120 min for pure TiO$_2$	37.4% within 120 min	[89]
NiO/TiO$_2$ nanopowders (mixed phase of rutile and anatase)	0.5 wt% NiO/TiO$_2$	0.05 g	Modified combustion-based method	15 mg/L MB (50 mL)	Daylight emission	85% within 210 min	90% within 210 min	[90]
Ni-TiO$_2$ nanopowders (anatase phase)	0.05 mol% Ni	1 g L^{-1}	Sol–gel method (non-aqueous)	10 mg L^{-1} MB (500 mL)	Xenon Lamp	88.0% within 180 min for pure TiO$_2$	98.9% within 180 min	[91]
Ni-TiO$_2$ nanoparticles (anatase phase)	1.0% Ni-TiO$_2$	0.025 g	Sol–gel method	10^{-5} mol/L MO (50 mL)	Visible light	0.00075 and 0.002631 min^{-1} for visible and UV irradiation, respectively. 16.3 and 95.6% for visible and 95.6 for visible and UV light, irradiation within 120 min	13.8% for visible light irradiation within 120 min. 0.00063 min^{-1} and 0.00390 min^{-1} for visible and UV light irradiation, respectively	[92]

Table 4. *Cont.*

Material (TiO$_2$ Phase Transition)	Optimum	Catalyst Dosage	Synthetic Methods	Pollutant (Volume)	Light Source	Unmodified	Modified	Ref.
Ni-TiO$_2$ nanoparticles (anatase phase)	1.0% Ni- TiO$_2$	0.05 g/0.5 g	Sol–gel method	10 mg/L 4-CP, NPX (250 mL)	UV	68.9 and 84.9% for 4-CP and NPX, respectively within 6 h	89.5 and 84% for 4-CP and NPX, respectively within 6 h	[93]
Ni-TiO$_2$ nanoparticles (anatase phase)	1 wt% Ni-TiO$_2$	0.1 g	Sol–gel method	5 mg/L MO, MB (100 mL)	Visible light	44.18 and 26.80% degradation rates for MB and MO, respectively for unmodified TiO$_2$ within 5 h. 45% of MB for Degussa P25 within 5 h.	71.18 and 39.57% for MB and MO, respectively within 5 h	[94]

MWASG: Microwave-assisted sol–gel method; MB: methylene blue; MO: methyl orange; NPX: naproxen; ECR: Eriochrome cyanine red; IBP: ibuprofen; BPA: bisphenol A; MG: malachite green; 4-CP: 4-chlorophenol.

4.1.3. Modification with Copper (Cu)

The introduction of Cu ion can directly trap generated electrons by excitation of light, and thus prevents the rapid recombination of hole–electron pairs [95]. It can increase the surface diffusivity of the TiO_2 [96], and thereby enables the interaction of holes and electrons with other compounds (e.g., H_2O) more quickly [97], generating feasible reactive species, and subsequently bypassing the recombination of the hole–electron pair [98]. Cu with redox potentials of 0.16 V (Cu^{2+}/Cu^+) and 0.52 V (Cu^{2+}/Cu) has been used as a suitable modifier for various visible light responsive photocatalysts. Ti^{4+} and Cu^{2+} have similar ionic radii and therefore Cu^{2+} can easily penetrate into TiO_2 matrixes as a deep acceptor in conjunction with neighboring oxygen vacancies or substitute the positions of Ti^{4+} [99]. In addition, modification with Cu shifts the absorption edges of both the photocatalysts towards the visible region [100].

The behavior involved in modifying TiO_2 with Cu is strongly linked to parameters of synthesis and diverse approaches used for fabrication of materials as well as analysis, and has led to various experimental findings in the past. Studies have observed the diverse speciation of Cu-TiO_2 with the majority of studies reporting the presence of Cu in a Cu^{2+} valence. These species are frequently reported to substitute for Ti^{4+} to give a solution phase with the composition $Cu_xO_2Ti_{1-x}$ and an increased lattice density of oxygen vacancies [101], and reportedly may also occupy interstices in anatase [102]. In addition to solid solutions, Cu^{2+} has been found to exist in amorphous or crystalline CuO nanoclusters as well as surface localized $Cu(OH)_2$ in titania [103–105]. The presence of monovalent Cu^+ (less common as compared to Cu^{2+}) has also been reported, both in Cu_2O nanoclusters and in substitutional positions [102,106]. The CB edges of CuO_2 and CuO are suitable for the enhancement of TiO_2 photocatalytical effect [107–109]. Generally, an efficient photocatalytic activity is understood to be driven by a reduced charge carrier recombination in Cu-TiO_2 photocatalyst. This was found to arise as a result of photogenerated electrons which facilitates the reduction of $Cu^{2+} + e^- \rightarrow Cu^+$, and thus extends the valence band hole lifetimes at the surfaces, which are able to react with adsorbed species to form active radical species [103,104]. Alternatively, the presence of Cu_2O or CuO phase in TiO_2 may improve exciton lifetime through electron capture in the secondary phase [110] or improve the activity via the increment in surface area [111]. Table 5 presents the summary of recent progress on Cu-TiO_2 photocatalysts for organic pollutants degradation.

Table 5. Summary of recent progress on Cu-TiO$_2$ photocatalysts for organic pollutants degradation.

Materials (TiO$_2$ Phase Transition)	Optimum	Catalyst Dosage	Synthetic Methods	Pollutants (Volume)	Light Source	Unmodified	Modified	Ref.
Cu-TiO$_2$ nanoparticles (anatase phase)	1.0% Cu-TiO$_2$	0.5 g/0.05 g	Sol–gel method	10 mg/L 4-CP (250 mL)	UV	79% (0.1210 L g^{-1} min^{-1}) within 6 h.	90% (0.1827 L/g^{-1} min^{-1}) within 6 h	[93]
Hybrid Cu-TiO$_2$/polythiophene nanorods (rutile phase)	-	0.1 g	Sol–gel method	5 mg/L RhB (150 mL)	Visible light	6.9% within 75 min	70.5% within 75 min. Furthermore, there was no significant decrease in photocatalytic activity after three continuous cycles.	[112]
Cu-TiO$_2$ nanoparticles (anatase phase)	1.0% Cu-TiO$_2$	0.05 g/0.5 g	Sol–gel method	10 mg/L NPX (250 mL)	UV	84.9% (0.0124 L g^{-1} min^{-1}) within 6 h.	87.4% (0.0259 L g^{-1} min^{-1}) within 6 h.	[93]
Hybrid Cu-TiO$_2$/polythiophene nanorods (rutile phase)	-	0.1 g	Sol–gel method	5 mg/L OG (150 mL)	Visible light	6.9% within 75 min	98% within 75 min. Furthermore, there was no significant decrease in photocatalytic activity after three continuous cycles.	[112]
Cu-TiO$_2$ nanoparticles (anatase phase)	0.2 wt% Cu-TiO$_2$	-	Sol–gel method	50 mg/L MO (50 mL)	UV	27% (0.45 min^{-1}) within 30 min	73% (2.83 min^{-1}) within 30 min	[113]
Cu-TiO$_2$ nanocrystals (mixed anatase and brookite phases)	0.1% Cu-TiO$_2$	1 g/L	Sol–gel method	10 mg/L PNP (10 mL)	Visible irradiation (halogen lamp)	12% for P25 within 24 h	65% (5 times more efficient than P25) within 8 h	[114]
Cu-TiO$_2$ nanoparticles (stable anatase phase)	2% Cu-TiO$_2$	0.002 g	Sol–gel method	10 mg/L MB (50 mL)	150 W Xenon lamp	0.0046 min^{-1} within 2 h	0.0082 min^{-1} within 2 h	[115]
Cu-TiO$_2$ nanoparticles (stable anatase phase)	2% Cu-TiO$_2$	0.002 g	Sol–gel method	10 mg/L PNP (50 mL)	150 W Xenon lamp	18% (0.0016 min^{-1}) within 2 h	29% (0.0027 min^{-1}) within 2 h	[115]
Cu-TiO$_2$ nanoparticles (anatase to rutile phase)	1.2% Cu-TiO$_2$	0.08 g	Sol–gel method	35 mg/L E131 VF (100 mL)	UV	0.083 min^{-1} within 30 min	0.0044 min^{-1} within 100 min	[116]
Cu-TiO$_2$/GO nanoparticles (anatase phase)	1 wt% Cu-TiO$_2$/GO	0.05 g	Impregnation method	20 mg/L TC (50 mL)	300 W mercury lamp	23.1% within 90 min for pure TiO$_2$	98% within 90 min (reaction rate constant was about 1.4 times than that of TiO$_2$/GO), the removal ratio of Cu-TiO$_2$/GO exceeded 98% after five cycles.	[117]
Cu-TiO$_2$ nanopowders (anatase to rutile phase)	Cu: TiO$_2$ both in powder (42.35%)	0.3 g	Sol–gel method	10 mg/L MB (50 mL)	Visible light	2.6% (0.00008 min^{-1}) within 6 h	42.4% (0.00140 min^{-1}) within 6 h	[98]

Table 5. *Cont*.

Materials (TiO$_2$ Phase Transition)	Optimum	Catalyst Dosage	Synthetic Methods	Pollutants (Volume)	Light Source	Unmodified	Modified	Ref.
Cu-TiO$_2$ film (anatase to rutile phase)	Cu: TiO$_2$ both in film (25.10%)	0.3 g	Sol–gel method	10 mg/L MB (50 mL)	Visible light	2.6% (0.00008 min^{-1}) within 6 h	25.1% (0.00082 min^{-1}) within 6 h	[98]
Cu-TiO$_2$ nanopowders (Anatase phase)	2.0% Cu-TiO$_2$	1 g/L	Sol–gel method	20 mg/L DFC (100 mL)	Visible light	25% within 7 h	33.26% within 7 h	[118]
Cu-TiO$_2$ nanopowders (Anatase to rutile phase)	3% Cu-TiO$_2$	0.125 mol L^{-1}	Sol–gel method	20 mg/L MB (50 mL)	Xenon Lamp	0.08124 min^{-1} within 6 h	0.00575 min^{-1} within 6 h	[119]
Cu-TiO$_2$ nanoparticles (anatase phase)	-	0.1 g	MWASG	30 mg/L MO (100 mL)	Visible light	1.4 × 10^{-3} min^{-1} within 6 h	7.0 × 10^{-3} min^{-1} within 6 h	[120]
Cu-TiO$_2$ nanoparticles (anatase phase)	-	0.1 g	MWASG	30 mg/L MB (100 mL)	Visible light	7.0 × 10^{-4} min^{-1} within 6 h	5.6 × 10^{-3} min^{-1} within 6 h	[120]
Cu-TiO$_2$ nanoparticles (anatase phase)	-	0.1 g	MWASG	30 mg/L MO (100 mL)	UV	5 × 10^{-3} min^{-1} within 6 h	1.2 × 10^{-2} min^{-1} within 6 h	[120]
Cu-TiO$_2$ nanoparticles (anatase phase)	-	0.1 g	MWASG	30 mg/L MB (100 mL)	UV	2.5 × 10^{-3} min^{-1} within 6 h	8.6 × 10^{-3} min^{-1} within 6 h	[120]
Cu-TiO$_2$ nanoparticles (anatase phase)	2 wt% Cu-TiO$_2$	0.38 g/L	Sol–gel method	10 mg/L Phenol (100 mL)	UV	82% within 60 min for P25	98% within 60 min	[121]
Cu-TiO$_2$ nanoparticles (anatase phase)	2 wt% Cu-TiO$_2$	0.38 g/L	Sol–gel method	10 mg/L Phenol (100 mL)	Visible light	35 and 75% after 60 min and 180 min, respectively for P25	22 and 37% after 60 min and 180 min, respectively	[121]
Cu-TiO$_2$ nanopowders (anatase phase)	0.21 mol% Cu-TiO$_2$	3 g·dm^{-3}	Sol–gel method	20 mg/L 2-CP (50 mL)	UV	-	98.92% within 6 h	[122]
Cu/TiO$_2$/bentonite composite nanoparticles (anatase phase)	-	0.02 g	Thermal decomposition and reduction method	10 mg/L Deltamethrin insecticide (50 mL)	Sunlight	87.01% within 120 min for TiO$_2$/bentonite	97% within 120 min	[123]
Cu-TiO$_2$ nanoparticles (anatase phase)	3% Cu-TiO$_2$	0.1 g	Sol–gel method	15 mg/L MO (100 mL)	Xenon Lamp	0.0011 min^{-1} within 60 min	61% (0.0166, min^{-1}) within 60 min	[124]
Cu-TiO$_2$ films (anatase phase)	4% Cu-TiO$_2$	0.1 g	Sol–gel method	25 mg/L MB (100 mL)	UV	92% ((0.015 min^{-1}) within 180 min	16% (0.001 min^{-1}) within 180 min	[125]
Cu/TiO$_2$ nanoparticles (anatase to rutile phase)	10% Cu-TiO$_2$	0.5 g	Coprecipitation method	100 mg/L ECR (200 mL)	Visible light	20.9% within 120 min	60.6% within 120 min	[89]

Table 5. *Cont.*

Materials (TiO$_2$ Phase Transition)	Optimum	Catalyst Dosage	Synthetic Methods	Pollutants (Volume)	Light Source	Unmodified	Modified	Ref.
Cu-TiO$_2$ nanoparticles (anatase phase)	1% Cu-TiO$_2$	2 g/L	Sol–gel method	100 mg/L MO, MB (100 mL)	Visible light	45% for MB within 5 h for Degussa P25	81.22 and 44.05% for MB and MO, respectively within 5 h.	[94]
Cu-TiO$_2$ nanoparticles (anatase phase)	5% Cu-TiO$_2$	0.5 g/L	Sol–gel method	60 mg/L Orange II (35 mL)	UV	95% for P25 within 180 min	82% within 180 min	[126]
Cu-TiO$_2$ nanoparticles (anatase phase)	5% Cu-TiO$_2$	0.5 g/L	Impregnation method	60 mg/L Orange II (35 mL)	UV	99% for P25 within 180 min	90% within 180 min	[126]
Cu^{2+}/TiO$_2$ nanoparticles (mixed anatase and brookite phases)	0.5 mol% Cu^{2+}/TiO$_2$	1 g/L	Sol–gel method	10 mg/L PNP (100 mL)	UV/Visible light	20 and 50% and under visible and UV/Visible light, respectively for Degussa P25 within 24 h	42 and 55% under visible and UV/visible light, respectively within 24 h	[127]
Cu-TiO$_2$ nanoparticles (mixed anatase and rutile phases)	-	0.1 g	Sol–gel method	20 mg/L MB (50 mL)	Visible light	89.69% within 60 min	27.5% within 60 min	[128]

MB: methylene blue; PNP: *p*-nitrophenol; MO: methyl orange; 2-CP: 2-chlorophenol; ECR: Eriochrome cyanine red; DFC: diclofenac; TC: tetracycline; OG: orange G; E131 VF: food colorant; MWASG: microwave-assisted sol–gel method; NPX: naproxen; RhB: rhodamine B; 4-CP: 4-chlorophenol.

4.1.4. Modification with Manganese (Mn)

Manganese (Mn) has a great potential to permit significant optical absorption in infrared solar light or visible light, via the introduction of intermediate bands within the forbidden gap as well as the combined effects of narrowed bandgap [129,130]. The intermediate bands provide adequate carrier mobility and hence significant curvature [131]. Mn ions can be easily incorporated into the lattice of TiO_2 to obtain a deformed structure. It has been reported that Mn in 3d states has some contributions to the TiO_2 conduction band, which will further impact the bandgap of TiO_2. Modifying with Mn cations has been reported to favor the charge separation acting like electrons trap as Mn^{4+} or Mn^{3+} [129] and holes trap as Mn^{2+} [132,133], thus prolonging the separation of photoinduced carriers and increasing the photocatalytic activity [134].

In Mn-photocatalytic materials with a mixture of oxidation states could be seen as a limitation because it is impossible to easily control the amount of one specific oxidation state [135]. However, this can be approached as a benefit since the oxidation state of Mn can act as a charge separator, attracting photogenerated holes in the Mn^{2+}/Mn^{3+} state or as a photogenerated electron in the Mn^{4+}/Mn^{3+} state, the oxidation states mixture can improve the photocatalytic activity [133]. When TiO_2 semiconductors are modified with Mn and applied in the photocatalytic degradation of organic dyes, the reduction in bandgap can be achieved, thereby improving the performance [136–138]. This is due to the following reasons: when Mn is introduced in the TiO_2 network at different oxidation states (2+, 3+, or 4+), there is a deformation of the TiO_2 crystalline structure and optimization of its optical properties [139–141]. Ref. [142] confirmed a high stability feature when TiO_2 was modified with Mn^{1+} to Mn^{6+}. Mn^{2+} can enter the lattice of TiO_2, replacing the position of the original titanium atom while forming a new chemical bond. In addition, modifying with Mn^{2+} can also increase the number of hydroxyl groups on the surface of TiO_2 in the aqueous solution, forming an active center for the adsorption of water [143].

Mn-TiO_2 nanoparticles can be prepared by (i) sol–gel technique [131,144], (ii) hydrothermal treatment [145], (iii) ultrasonic synthesis [146], (iv) liquid flame aerosol synthesis technique [32], (v) impregnation method [147], (vi) calcination [148], and (vii) thermal treatment [149]. Table 6 presents the summary of recent progress on Mn-TiO_2 photocatalysts for organic pollutants degradation.

Table 6. Summary of recent progress on Mn-TiO$_2$ photocatalysts for organic pollutants degradation.

Materials (TiO$_2$ Phase Transition)	Optimum	Catalyst Dosage	Synthetic Methods	Pollutants (Volume)	Light Source	Unmodified	Modified	Ref.
Mn-TiO$_2$ nanoparticles (anatase phase)	10% Mn-TiO$_2$	0.025 g	Sol–gel method	10^{-5} mol/L MO (50 mL)	UV/Visible light	0.00075 min^{-1} and 0.002631 min^{-1} for visible light and UV light, respectively within 120 min. 95.6 and 16.3% under UV light and visible light, respectively	0.00070 min^{-1} and 0.00074 min^{-1} for visible light and UV light, respectively within 120 min. Modifying with Mn presents a negative effect on the photocatalytic degradation of MO. 12.8% under UV light	[92]
Mn^{2+}/TiO$_2$ nanoparticles (mixed crystal of anatase and rutile phases)	1.90 wt% Mn^{2+}/TiO$_2$	0.05 g	Hydrothermal method	50 mg/L MG (50 mL)	Visible light	48% within 180 min for pure TiO$_2$	81% within 180 min	[150]
Mn-TiO$_2$ nanopowders (anatase phase)	0.6% Mn-TiO$_2$	0.05 g/L	Sol–gel method	10 mg/L DCF (100 mL)	UV	51% within 240 min	0.0033 min^{-1} within 240 min	[151]
Mn-TiO$_2$ nanoparticles (mixture of anatase and rutile phases)	0.1% Mn-TiO$_2$	0.1 g	Modified sol–gel method	Benzene, Xylene, toluene (100 mL)	UV/Visible light	60, 60 and 55% for benzene, xylene and toluene, respectively under UV light.	60, 60, and 40% for benzene, xylene and toluene, respectively under UV light. 34 and 22% for toluene and xylene, respectively under visible irradiation within 60 min	[152]
Mn-TiO$_2$ nanopowders	4 wt% Mn-TiO$_2$	0.1 g/L	Hydrothermal route	10 mg/L Phenol (50 mL)	UV	30% within 7 h	90% within 7 h	[153]
Mn-TiO$_2$ nanoparticles (anatase phase)	1 wt% Mn-TiO$_2$	1 g	Sol–gel method	30 mg/L Toluene (100 mL)	VUV	70% without photocatalyst	89.8% within 120 min	[154]
Mn-TiO$_2$ nanoparticles (anatase phase)	0.3 wt% Mn-TiO$_2$	0.1 g	Sol–gel method	5 mg/L MO, MB (100 mL)	Visible light	26.80 and 44.18% degradation rates for MO and MB, respectively for unmodified TiO$_2$ within 5 h. 45% of MB for Degussa P25 within 5 h.	15.48 and 16.41% for MO and MB, respectively within 5 h	[94]
Mn-TiO$_2$ films (anatase phase)	5 wt% Mn-TiO$_2$	0.5 g/L	Sol–gel method	6 mg/L Orange II (50 mL)	UV	95% for P25 within 180 min	97% within 180 min	[126]
Mn-TiO$_2$ nanoparticles (anatase-brookite phase)	5 wt% Mn-TiO$_2$	0.5 g/L	Impregnation method	6 mg/L Orange II (100 mL)	UV	99% for P25 within 180 min	97% within 180 min	[126]

Table 6. *Cont.*

Materials (TiO₂ Phase Transition)	Optimum	Catalyst Dosage	Synthetic Methods	Pollutants (Volume)	Light Source	Unmodified	Modified	Ref.
Mn-TiO₂ nanoparticles (mixed anatase and brookite phases)	0.5 mol% Mn-TiO₂	1 g/L	Sol–gel method	10 mg/L PNP (100 mL)	UV/Visible light	50 and 20% under UV/Visible and visible light irradiation for Degussa P2 within 8 h.	19 and 5% under UV/Visible and visible light irradiation, respectively within 8 h.	[127]
Mn-TiO₂ nanoparticles (anatase phase)	5 wt% Mn-TiO₂	0.1 g	Sol–gel method	5 mg/L MB, MO (100 mL)	UV/Visible light	65.3 and 72.4% under UV irradiation for MO and MB, respectively within 60 min. 4.1 and 6.2% for MO and MB, respectively under visible irradiation within 240 min	85.2.1 and 93.6% under UV irradiation for MO and MB, respectively within 60 min. 65.2 and 73.2% for MO and MB, respectively under visible irradiation within 240 min	[38]

MB: methylene blue; PNP: *p*-nitrophenol; MO: methyl orange; DCF: diclofenac.

4.1.5. Modification with Zirconium (Zr)

Zirconium (Zr) has a wide bandgap with a more positive (4.0 V vs. NHE) VB and a more negative (−1.0 V vs. NHE) CB than titania [155]. The tetravalent cations of both Ti and Zr have a comparable atomic radius, and their oxides have similar physicochemical properties. It has been previously reported that the modification of TiO_2 with Zr can improve physicochemical characteristics including an increase in the specific surface area [156], decrease in crystallite size as a result of dissimilar coordination geometry and nuclei [157]; enhance surface acidity [158], the transition temperature between anatase and rutile [156,158], and the adsorption and the hydrophilic properties [159], and enhance thermal stability and imbalance of charge resulting from the formation of capture traps as well as the formation of Ti-O-Zr bonds. These features favor a higher efficiency while separating photogenerated carriers, thus improving the photocatalytic efficiency [160,161]. Moreover, the hydroxyl groups that are trapped on the catalyst surface by holes improve the quantum yield and reduce the recombination reactions [159,162]. Modifying with Zr conquers charge recombination by electron trapping [163].

Liu et al. [164] prepared mesoporous Zr-TiO_2 NPs via the solvothermal approach and observed a higher photocatalytic activity in comparison with the commercialized P25 titania. Li et al. [165] reported a macro–mesoporous Zr-TiO_2 material via the facile surfactant self-assembly approach and observed a remarkable photocatalytic activity towards RhB decomposition under UV light radiation as compared to pure ZrO_2 and unmodified TiO_2 materials. A study by [166] found that modifying with Zr^{4+} can increase the surface area, and suppress crystal growth. Table 7 presents the summary of recent progress on Zr-TiO_2 photocatalysts for organic pollutants degradation.

Table 7. Summary of recent progress on Zr-TiO$_2$ photocatalysts for organic pollutants degradation.

Materials (TiO$_2$ Phase Transition)	Optimum	Catalyst Dosage	Synthetic Methods	Pollutant (Volume)	Light Source	Unmodified	Modified	Ref.
Zr-TiO$_2$ nanoparticles (mixed anatase and rutile phases)	0.01% Zr.TiO$_2$	0.1 g	Sol–gel method	20 mg/L *MB* (50 mL)	Visible light	89.69% within 60 min	81.9% within 60 min	[128]
Zr-TiO$_2$ films (stable anatase phase)	0.05% Zr/TiO$_2$	0.005 g	EISA via dip-coating	0.001 mM herbicide chloridazon, henol, 4-CP (50 mL)	Xenon lamp	42% within 4 h for phenol, 58% within 4 h for 4-CP	The Zr-TiO$_2$ film showed the superior photocatalytic activity for all pollutants but showed lowest rate using phenol	[167]
Zr-TiO$_2$ nanoparticles (anatase phase)	0.2% Zr-TiO$_2$	0.4 g	Sol–gel method	1.0±0.5 mg/m^3 formaldehyde	UV	10% within 48 h for P25	95.14% within 48 h. Furthermore, 94.38% removal efficiency was achieved even after seven cycles	[168]
Zr-TiO$_2$ nanoparticles (anatase phase)	Zr:TiO$_2$ = 0.08:0.92	0.005 g	EISA method	0.001 mM formaldehyde	Xenon lamp	45% within 48 h for TiO$_2$	92% after 48 h	[166]
Zr-TiO$_2$ nanoparticles (anatase phase)	5% Zr-TiO$_2$	0.04 g/L	A combined sol–gel and CVD method	10 ppm IBP	UV	-	80% after 40 min	[33]
Zr.TiO$_2$ nanoparticles (mixed anatase and brookite phase)	2.0% Zr.TiO$_2$	1 g/L	Sol–gel method	10 mg/L PNP (100 mL)	UVA/Visible light	20 and 84% for pure TiO$_2$ and commercial Evonik P25, respectively UV-A light. 25 and 12% for pure TiO$_2$ and Evonik P25, respectively under visible irradiation within 17 h	96% under UV-A light, 38% under visible irradiation within 17 h	[169]
Zr.TiO$_2$ nanoparticles (anatase phase)	0.5% Zr.TiO$_2$	0.25 g	Sol–gel method	10 mg/L antipyrine (phenazone) (10 mL)	Visible light	-	90% within 360 min. Furthermore, 8% lower degradation rate was achieved, even after six hours of irradiation	[170]
Zr.TiO$_2$ hollow microspheres (anatase phase)	12.6 wt% Zr.TiO$_2$	0.02 g	Facile solvothermal method	20 mg/L RhB (50 mL)	UV	14.6% within 60 min	96.3% within 60 min	[171]
Zr.TiO$_2$ nanoparticles (mixed anatase and brookite phase)	2.0% Zr.TiO$_2$	1 g/L	Sol–gel method	10 mg/L PNP (100 mL)	UV/Visible light	20 and 84% for pure TiO$_2$ and commercial Evonik P25, respectively within 24 h under UV–Visible light. 25 and 12% for pure TiO$_2$ and commercial Evonik P25, respectively within 24 h under visible light.	96% within 24 h under UV-Visible light. 38% within 24 h under visible light	[169]

Table 7. *Cont.*

Materials (TiO$_2$ Phase Transition)	Optimum	Catalyst Dosage	Synthetic Methods	Pollutant (Volume)	Light Source	Unmodified	Modified	Ref.
Zr-TiO$_2$/reduced Graphene Oxide nanoparticles (mixed anatase and brookite phase)	3% ZrO$_2$–TiO$_2$	0.025 g	Sol–gel method	20 mg/L EB (100 mL)	Visible light	-	75.75% within 90 min	[172]
ZrO$_2$/TiO$_2$ nanofibers (anatase phase)	40 wt% ZrO$_2$/TiO$_2$ (Zr:Ti = 1:3)	0.02 g	Sol–gel method	10 mg/L MB (50 mL)	Mercury lamp	43.3% within 180 min.	82.7% within 180 min	[173]
ZrO$_2$/TiO$_2$ nanoparticles (anatase phase)	6.9% ZrO$_2$–TiO$_2$	0.02 g	Facile surfactant self-assembly	5 mg/L RhB (100 mL)	UV	52.5% within 3 h.	86.9% within 3 h. Rate constant was 3.0 times higher than unmodified TiO$_2$ within 3 h	[165]
ZrO$_2$/TiO$_2$ nanoparticles (anatase phase)	5% ZrO$_2$/TiO$_2$	0.1 g	Sol–gel method	5×10^{-5} mol/L MB, MO (100 mL)	UV/Visible light	65.3 and 72.4% for MO and MB, respectively within 60 min under UV light. 4.1 and 6.2% for MO and MB, respectively within 240 min under visible light.	70.1 and 77.3% for MO and MB, respectively within 60 min under UV light. 22.6 and 38.2% for MO and MB, respectively within 240 min under visible light.	[38]
Zr-TiO$_2$ nanoparticles (anatase phase)	6 mol% Zr-TiO$_2$	1 g/L	Sol–gel method	5 mg/L Ponceau BS (180 mL)	UV	24.45% (0.0107 min^{-1}) within 30 min	99.3% (0.1810 min^{-1}) within 30 min	[155]

PNP: *p*-nitrophenol; MO: methyl orange; RhB: rhodamine B; MB: methylene blue; EB: eosin blue; 4-CP: 4-chlorophenol; IBP: ibuprofen.

4.1.6. Modification with Iron (Fe)

Iron (Fe) has a half-filled (3d5) electronic configuration, similar ionic radii of Fe^{3+} to that of Ti^{4+} and can be easily incorporated into the crystal lattice of TiO_2 [174,175], and it has been documented that modifying the crystal lattice of TiO_2 with Fe^{3+} ions weakens the surrounding oxygen atoms bonding. Consequently, the oxygen atoms are readily released from the lattice causing an oxygen vacancy, hence more oxygen/H_2O/OH- can be adsorbed onto the TiO_2 surface resulting in the decrease in CB electrons. In addition, Fe^{3+} ions can perform as a shallow charge trap in the TiO_2 lattice, because the energy level (redox potential) of Fe^{2+}/Fe^{3+} lies close to that of Ti^{3+}/Ti^{4+}, which favors the development of charge carrier separation, further causing a decrease in the e^-/h^+ pair recombination and expanding the photoresponse of TiO_2 into the visible light range [175,176].

Ali et al. [174] used the sol–gel method for the successful synthesis of Fe-TiO_2 NPs which could be activated in the presence of visible light. Naghibi et al. [177] also studied the properties of TiO_2 modified with four metals including Cu, Fe, Cd, and Ce, and observed that the Fe-TiO_2 presents the smallest crystal size with forbidden bandwidth among these four metals-modified TiO_2. [178] found that the Fe^{3+}-TiO_2 powder showed strong absorption characteristics in the visible region and [179] observed that introducing Fe^{3+} into the TiO_2 lattice facilitates the formation of a redox site, enabling absorption of the visible portion. The semi-filled electronic structure of Fe^{3+} ions not only facilitates the separation of photoelectrons and holes but also reduces the bandgap of TiO_2 [180]. In addition, modifying with Fe^{3+} can introduce more oxygen vacancies in TiO_2 surface and lattice [181], which is beneficial for increasing the number of surface OH groups and improvement in photocatalytic degradation. Table 8 presents the summary of recent progress on Fe-TiO_2 photocatalysts for organic pollutants degradation.

Table 8. Summary of recent progress on Fe-TiO$_2$ photocatalysts for organic pollutants degradation.

Materials (TiO$_2$ Phase Transition)	Optimum	Catalyst Dosage	Synthetic Methods	Pollutants (Volume)	Light Source	Unmodified	Modified	Ref.
Fe-TiO$_2$ nanopowders (mixture of anatase and rutile phases)	2wt% Fe-TiO$_2$	0.01 g	Conventional solid-state reaction	20 mg/L MB (50 mL)	Xenon arc lamp	90.80% within 210 min	94.93% within 210 min	[182]
Fe-TiO$_2$ nanoparticles (anatase phase)	1 wt% Fe-TiO$_2$	0.1 g	Sol–gel method	5 mg/L MO, MB (100 mL)	Visible light	44.18 and 26.80% degradation rates for MB and MO, respectively for unmodified TiO$_2$ within 5 h; 45% for MB using Degussa P25 within 5 h	1.41 and 7.94% for MB and MO, respectively within 5 h	[94]
Fe-TiO$_2$ nanoparticles (anatase phase)	0.1 mol% Fe-TiO$_2$	0.03 g/L	Precipitation method	MO, 4-CP (100 mL)	Xenon arc lamp	30 and 45% of 4-CP and MO, respectively within 4 h	65 and 95% for 4-CP and MO, respectively within 4 h	[183]
Fe-TiO$_2$ nanoparticles (anatase phase)	0.0017 mol% Fe-TiO$_2$	3 g/L	Sol–gel method	10 mg/L AO7 (100 mL)	Visible light	10% within 60 min	80% within 60 min	[184]
Fe-TiO$_2$ nanoparticles (anatase phase)	1.0% Fe-TiO$_2$	0.05 g/0.5 g	Sol–gel method	10 mg/L NPX, 4-CP (100 mL)	UV	68.9% (0.1069 L g^{-1} min^{-1}) and 84.9% (0.0124 L g^{-1} min^{-1}) for 4-CP and NPX, respectively for unmodified TiO$_2$ within 6 h	97.7% (0.1111 L g^{-1} min^{-1}) and 37% (0.0053 L g^{-1} min^{-1}) for NPX and 4-CP, respectively within 6 h	[93]
Fe-TiO$_2$ nanoparticles (anatase phase)	0.5% Fe-TiO$_2$	0.5 g/L	Sol–gel method	10 mg/L Phenol (200 mL)	Visible light	33% within 90 min	57% (about 73% increase) within 90 min. that the activity of pristine TiO$_2$ was higher than that of the modified catalysts with high content	[185]
Fe-TiO$_2$ nanoparticles (anatase phase)	0.1 wt% Fe-TiO$_2$	0.5 g	Sol–gel method	20 mg/L AO7 (500 mL)	Visible light	25% within 300 min	54% within 300 min	[186]
Fe-TiO$_2$ nanoparticles (mixture of anatase and rutile phases)	0.05 mol% Fe-TiO$_2$	0.5 g/L	Facile ultrasonic assisted hydrothermal method	10 mg/L PNP (50 mL)	Visible light	42% within 5 h for pure TiO$_2$	92% within 5 h	[187]
Fe-TiO$_2$ nanoparticles (mixture of anatase and rutile phases)	0.075 mol% Fe-TiO$_2$ NPs	0.5 g/L	Facile ultrasonic assisted hydrothermal method	10 mg/L MB (50 mL)	Visible light	50% within 180 min for pure TiO$_2$	93% within 180 min	[187]
Fe^{3+}/TiO$_2$ nanoparticles (anatase phase)	3% Fe^{3+}/TiO$_2$	25 cm × 25 cm	Sol–gel spin coating technique	5 mg/L MO (50 mL)	Visible light	34% within 360 min.	95.25% within 360 min.	[188]

Table 8. *Cont.*

Materials (TiO$_2$ Phase Transition)	Optimum	Catalyst Dosage	Synthetic Methods	Pollutants (Volume)	Light Source	Unmodified	Modified	Ref.
Fe^{3+}/TiO$_2$ nanoparticles (anatase phase)	3% Fe^{3+}/TiO$_2$	25 cm × 25 cm	Sol–gel spin coating technique	5 mg/L MB (50 mL)	Visible light	34% within 360 min.	Fe-TiO$_2$ (3% Fe^{3+}) film exhibits high efficiency of about 97.8% after 10 cycling runs of MB degradation.	[188]
Fe-TiO$_2$ nanoparticles (anatase phase)	0.5%Fe-TiO$_2$	0.20 g/L	Wet-impregnation method	5 ppm MO (200 mL)	UV/Visible light	85 and 11% under UV light and visible light irradiation, respectively within 2 h.	82.8 and 74.4% under UV light and visible light irradiation, respectively. within 2 h	[189]
Fe-TiO$_2$ thin films (anatase phase)	0.5% Fe-TiO$_2$	-	Sol–gel method	2.51 × 10^{-4} M NB (-)	UV	70.52% within 240 min	88.45% within 240 min	[190]
Fe-TiO$_2$ nanoparticles (mixture of anatase and rutile phases)	2.5 wt% Fe-TiO$_2$	0.1 g	Sol–gel method	10 mg/L MB (50 mL)	UV	~17% within 240 min. 54% within 90 min	40% within 240 min. 78% within 90 min. Furthermore, the photocatalytic activity only decreased 7.7% after three runs.	[191]
Fe-TiO$_2$ nanoparticles (anatase phase)	0.5 mol% Fe-TiO$_2$	0.5 g/L	Ultrasonic dispersion method	10 mg/L RhB (50 mL)	UV	60% within 150 min	91.11% within 150 min	[192]
Fe-TiO$_2$ microsized powder (anatase phase)	-	0.2 g	sol–gel and hydrothermal treatment	50 mg/L BO2 (3 L)	Solar	25% within 180 min.	≥90% within 180 min.	[193]
Fe-TiO$_2$ nanoparticles (anatase phase)	6 wt% Fe-TiO$_2$	-	Sol–gel method	10 mg/L MB (100 mL)	Visible light	36% without irradiation for Fe-TiO$_2$	99.5% within 3 h	[194]
Fe-TiO$_2$ nanoparticles (anatase phase)	0.4 wt% Fe-TiO$_2$	0.2 g/L	Sol–gel method	10 mg/L Acid Blue 80 (50 mL)	UV	27.86% (1.6 × 10^{-3} min^{-1}) within 120 min	31.13% (2.0 × 10^{-3} min^{-1}) within 120 min	[195]
Fe-TiO$_2$ nanoparticles (anatase phase)	0.4 wt% Fe-TiO$_2$	0.2 g/L	Ultrasound assisted approach	10 mg/L Acid Blue 80 (50 mL)	UV	27.86% (1.6 × 10^{-3} min^{-1}) within 120 min	38.01% (2.4 × 10^{-3} min^{-1}) within 120 min	[195]
Fe-TiO$_2$ nanoparticles (anatase phase)	1.5 wt% Fe-TiO$_2$	0.4 g/L	Hydrothermal	20 mg/L Diazinon (100 mL)	UV	~20% within 100 min	75% within 100 min	[196]
Fe-TiO$_2$ nanoparticles (anatase phase)	10% Fe-TiO$_2$	0.005 g	Sol–gel method	20 mg/L MB (250 mL)	UV	76.09% within 150 min	96.66% within 150 min	[197]

Table 8. *Cont.*

Materials (TiO$_2$ Phase Transition)	Optimum	Catalyst Dosage	Synthetic Methods	Pollutants (Volume)	Light Source	Unmodified	Modified	Ref.
Fe-TiO$_2$ nanoparticles (anatase phase)	2% Fe-TiO$_2$	0.5 g/L	Sol–gel method	50 mg/L AO7 (2.5 L)	UV/Visible/Solar light	9.2% within 6 h	UV (100%), visible (100%) and solar light (90%) within 6 h. Furthermore, the Fe-TiO$_2$ photocatalysts were stable and can maintain performance up to 6 recycle use.	[198]
Fe-TiO$_2$ nanotubes (anatase phase)	Hydrothermal temperature of 150 °C for 3 h	-	Hydrothermal	5 mg/L CR (35 mL)	Visible light	26.32% within 180 min	92.5% within 180 min	[199]
Fe-TiO$_2$ thin films (anatase phase)	0.02% Fe/TiO$_2$	-	Sol–gel method	20 mg/L MB (100 mL)	Visible light	~84 within 200 min	No enhancement in photocatalytic activity of Fe-TiO$_2$ thin films was achieved. This was be attributed to sodium diffusion from the substrate used.	[200]
Fe^{3+}/TiO$_2$ nanoparticles (anatase phase)	7% Fe^{3+}/TiO$_2$	-	Simple spin coating technique	3 mg/L MB (50 mL)	Xenon arc lamp	80% within 4 h	96.7% within 4 h. Furthermore, the degradation rate of MB was ~83.8% after 10 cyclic runs.	[201]
Fe-TiO$_2$ nanoparticles (anatase phase)	0.5 wt% Fe-TiO$_2$	-	Sol–gel method	20 mg/L MO (200 mL)	Visible light	24% within 60 min	98% within 60 min	[202]
Fe-TiO$_2$ nanoparticles (anatase phase)	3% Fe-TiO$_2$	0.2 g	Sol–gel method	20 mg/L RhB (100 mL)	Solar	34% within 120 min	64% within 120 min	[203]
Fe-TiO$_2$ nanoparticles (anatase-brookite phase)	5 wt% Fe-TiO$_2$	0.5 g/L	Impregnation method	6 mg/L Orange II (100 mL)	UV	99% for P25 within min	69% within 180 min	[126]
Fe-TiO$_2$ nanoparticles (anatase-brookite phase)	5 wt% Fe-TiO$_2$	0.5 g/L	Sol–gel method	6 mg/L Orange II (100 mL)	UV	95% for P25 within min	95% within 180 min	[126]
Fe-TiO$_2$ nanopowders (anatase phase)	0.5% Fe-TiO$_2$	0.1 g/L	Sol–gel method	2.45×10^4 M NB (-)	Mercury lamp	32.14% within 240 min for pure TiO$_2$	84.91% within 240 min	[204]

Table 8. *Cont.*

Materials (TiO$_2$ Phase Transition)	Optimum	Catalyst Dosage	Synthetic Methods	Pollutants (Volume)	Light Source	Unmodified	Modified	Ref.
Fe-TiO$_2$ nanopowders (anatase phase)	1 wt% Fe-TiO$_2$	0.1 g	Sol–gel method	10 mg/L MO, 4-CP (100 mL)	Visible light	31 and 28% for MO and 4-CP, respectively within 180 min	54 and 49% for MO and 4-CP, respectively within 180 min	[205]
Fe^{3+}/TiO$_2$ nanoparticles (mixed anatase and brookite phases)	0.5 mol% Fe^{3+}/TiO$_2$	1 g/L	Sol–gel method	10 mg/L PNP (100 mL)	UV/Visible light	50 and 20% under UV/Visible light and visible light, respectively using Degussa P25 within 8 h	56 and 44% under UV/Visible light and visible light, respectively within 8 h	[127]
Fe-TiO$_2$ nanoparticles (mixture of anatase and rutile phases)	2 wt% Fe-TiO$_2$	0.25 g/L	Surface impregnation method	0.0755 mg/L Carbendazim and 0.0096 mg/L for propiconazole(-)	Sunlight	-	98.5 and 92% of carbendazim and propiconazole, respectively within 60 min	[206]
Fe-TiO$_2$ nanotube (anatase phase)	1% Fe-TNAs	0.001 g/L	solvothermal method	20 mg/L MB (100 mL)	Solar	-	98.79% within 120 min	[207]
Fe-TiO$_2$ nanotube (anatase phase)	0.1 mol% Fe-TiO$_2$	1 g	Sol–gel method	10 mg/L AR-27 (1000 mL)	Visible light	78% within 2 h.	99% within 2 h. The removal efficiency was kept at 89% after catalyst used for 4 times.	[208]
Fe-TiO$_2$ thin films (anatase phase)	25 wt% Fe-TiO$_2$	-	Sol–gel method	4 mg/L MB (200 mL)	Visible light	0.018/h within 8 h	0.038/h within 8 h	[209]
Fe-TiO$_2$ nanoparticles (anatase phase)	1 wt% Fe-TiO$_2$	0.03 g	Sol–gel method	10 mg/L Orange II (500 mL)	UV/Visible light	30% within 60 min	24% within 60 min	[210]
Fe^{3+}/TiO$_2$ nanoparticles (anatase phase)	0.1% Fe^{3+}/TiO$_2$	0.2 g	Sol–gel method	10 mg/L MB (100 mL)	Xenon arc lamp	90% within 6 h	0.716 min^{-1} within 6 h	[211]
Fe^{3+}/TiO$_2$ thin films (anatase phase)	25 wt% Fe^{3+}/TiO$_2$	-	Sol–gel method	10 mg/L MB (100 mL)	Visible light	13.4% within 8 h	24.9% within 8 h	[212]
Fe-TiO$_2$ nanoparticles (anatase phase)	0.5 wt% Fe-TiO$_2$	0.25 g/L	Sol–gel method	(0.37–8.45) × 10^{-4} M NB (-)	Mercury lamp	48% within 240 min	99% within 240 min	[213]
Fe-TiO$_2$ nanotube (anatase phase)	5 wt% Fe/TNAs	0.5 mol·L^{-1}	Electrochemical anodization and subsequent dip-coating	10 mg/L BPA (200 mL)	Xenon lamp	-	18.3% within 240 min	[214]
Fe-TiO$_2$ nanoparticles (anatase phase)	0.15% Fe-TiO$_2$	0.3 g/L	Sol–gel method	20 mg/L RB5 (250 mL)	Xenon lamp	0.0180 min^{-1} within 60 min	0.0875 min^{-1} within 60 min	[215]

Table 8. *Cont.*

Materials (TiO$_2$ Phase Transition)	Optimum	Catalyst Dosage	Synthetic Methods	Pollutants (Volume)	Light Source	Unmodified	Modified	Ref.
Fe-TiO$_2$ nanoparticles (anatase phase)	0.5 wt.% Fe-TiO$_2$	0.25 g/L	Sol–gel method	$(0.37–8.45) \times 10^{-4}$ M NB (-)	Medium-pressure mercury lamp	48% within 240 min	99% within 240 min	[213]
Fe-TiO$_2$ nanoparticles (anatase phase)	1.0% Fe-TiO$_2$	0.05 g/0.5 g	Sol–gel method	10 mg/L NPX,4-CP (100 mL)	UV	79% (0.1210 L g^{-1} min^{-1}) within 6 h	97% (0.1111 L g^{-1} min^{-1}) within 6 h	[93]
Fe-TiO$_2$ nanoparticles (anatase phase)	0.05 wt% Fe-TiO$_2$	0.001 g/cm^2	Sol–gel method	25 mg/L DB15 (100 mL)	UV	3.3% within 1 h	31% within 1 h	[216]
Fe-TiO$_2$ nanoparticles (anatase phase)	1.75 wt% Fe-TiO$_2$	0.03 g/L	Nanosol/dip-coating method.	30 mg/L MB (50 mL)	UV	-	76% within 2 h	[217]

A07: acid orange 7; RB5: reactive black 5; 4-CP: 4-chlorophenol; NPX: naproxen; MB: methylene blue; MO: methyl orange; BO2: basic orange 2; RR 198: reactive red 198; PNP: *p*-nitrophenol; AR-27: acid red 27; NB: nitrobenzene; BPA: bisphenol A; RhB: rhodamine B; NB: nitrobenzene; CR: Congo red; PNP: 4-nitrophenol.

4.1.7. Modification with Chromium (Cr)

Chromium (Cr) has received many considerations owing to its partially filled d shell, and optically active nature. Cr^{3+} is suitable with an abundant electron shell structure [78]. Cr^{3+} ions have fewer valence electrons in comparison with Ti^{4+}. TiO_2 crystalline lattice deformation is evoked by substitution of Ti^{4+} by Cr^{3+}, creating an extra energy level between the VB and the CB of TiO_2, which permits those photons which have lower energy to accomplish the photocatalytic activity in the visible light range [218]. Because of the narrowing of the bandgap between valence and acceptor, the electron movement is better even at a lower temperature. In addition, such substitution restrains the crystal growth of TiO_2 as well as reducing TiO_2 crystallization, which may improve the absorption of light derived from the size effect [219]. Peng et al. [220] studied the influence of modification with Cr on the photocatalytic activity of TiO_2 and observed a shift in absorption edges of TiO_2 towards high wavelength region with the increasing Cr content. Various approaches are being employed to fabricate Cr-TiO_2 such as the spray pyrolysis [221], sol–gel method [220], and sputtering [45]. Table 9 presents the summary of recent progress on Cr-TiO_2 photocatalysts for organic pollutants degradation.

Table 9. Summary of recent progress on Cr-TiO$_2$ photocatalysts for organic pollutants degradation.

Materials (TiO$_2$ Phase Transition)	Optimum	Catalyst Dosage	Synthetic Methods	Pollutants	Light Source	Unmodified	Modified	Ref.
Cr-TiO$_2$ nanoparticles (anatase phases)	0.5 wt% Cr-TiO$_2$	1.5 g/L	Sol–gel method	10 mg/L MB (100 mL)	Hg vapor lamp	62% within 120 min for pure TiO$_2$	58% within 120 min	[84]
Cr-TiO$_2$ nanoparticles (anatase phase)	1 mol% Cr	0.1 g	Sol–gel method	15 mg/L MB (50 mL)	UV	33.43% for pure anatase within 24 h	50.01% within 24 h	[222]
Cr-TiO$_2$ nanoparticles (anatase phase)	4 mol% Cr	0.1 g	Sol–gel method	100 ppm CR (50 mL)	UV	0.73% for pure anatase within 24 h	17.78% within 24 h	[222]
Cr-TiO$_2$ nanoparticles (anatase phase)	10% Cr-TiO$_2$	0.025 g	Sol–gel method	10^{-5} mol/L MO (50 mL)	UV/Visible light	95.6 and 16.35% under UV and visible light irradiation, respectively within 120 min	0.00276 min^{-1} (3.7 larger than that of the unmodified TiO$_2$ (0.00075 min^{-1}) within 120 min	[92]
Cr-TiO$_2$ nanoparticles (anatase phase)	1 wt% Cr-TiO$_2$	0.1 g	Sol–gel method	5 mg/L MO, MB (100 mL)	Visible light	44.18 and 26.80% for MB and MO, respectively for unmodified TiO$_2$. 45% for MB within 5 h for Degussa P25.	11.47 and 15.48% for MB and MO, respectively within 5 h.	[94]
Cr-TiO$_2$ nanoparticles (anatase phase)	0.5% Cr-TiO$_2$	0.008 g	Sol–gel method	10 mg/L 4-CP (100 mL)	Visible light	76.5% within 390 min	90.7% within 390 min	[223]
Cr-TiO$_2$ nanoparticles (anatase phase)	-	0.4 g	FSP, coprecipitation, and sol–gel synthesis techniques	50 μM 4-CP (50 mL)	Visible light	2% within 4 h	61% within 4 h.	[224]
Cr-TiO$_2$ nanoparticles (mixed anatase and brookite phases)	0.5 mol% Cr-TiO$_2$	1 g/L	Sol–gel method	10 mg/L PNP (100 mL)	UV/Visible light	50 and 20% under UV/Visible and visible light, respectively for Degussa P25 within 8 h.	38 and 27% under UV/Visible and visible light, respectively within 8 h.	[127]

4-CP: 4-chlorophenol; FSP: flame spray pyrolysis; MO: methyl orange; PNP: *p*-nitrophenol; MB: Methyl blue; CR: Congo red.

4.1.8. Modification with Molybdenum (Mo)

Modification of TiO_2 using metals with a higher oxidation state (e.g., Mo^{6+} and Mo^{5+}) increases the photocatalytic activity due to improved transfer and separation of photogenerated holes and electrons [225]. Moreover, Mo^{6+} is also a suitable transition metal to be introduced into the lattice of TiO_2 due to similarity in the ionic radii of Ti^{4+} and Mo^{6+} [226], so Mo can easily be incorporated into TiO_2 crystal structure, producing the impurity levels, which as a consequence narrows the bandgap of TiO_2 [77]. In addition, Mo^{6+} has no electron in the d orbital and can also be reduced to lower oxidation states (Mo^{4+}, Mo^{5+}), implying its several oxidation states in the TiO_2 matrix can act as a superficial potential trap for the photoinduced e^- to h^+ pairs, thus lengthening the lifetime of carriers and increasing the photocatalytic activity. Furthermore, the redox potential of Mo^{6+}/Mo^{5+} (vs. NHE) is 0.4 V, allowing Mo^{6+} to capture photoinduced electrons, inhibiting the recombination of charge carriers [227]. Mo-TiO_2 photocatalysts can be synthesized using evaporation-induced self-assembly, hydrothermal method, and sol–gel process [228–233]. Table 10 presents the summary of recent progress on Mo-TiO_2 photocatalysts for organic pollutants degradation.

Table 10. Summary of recent progress on Mo-TiO$_2$ photocatalysts for organic pollutants degradation

Materials (TiO$_2$ Phase Transition)	Optimum	Catalyst Dosage	Synthetic Methods	Pollutants (Volume)	Light Source	Unmodified	Modified	Ref.
Mo-TiO$_2$ nanocrystals (anatase phase)	5% Mo-TiO$_2$	0.03 g	Facile hydrothermal method	25 ppm Benzene (-)	UV	13.6% within 4 h	79.1% (0.0065 min^{-1}, which was 4.81 times higher than the unmodified TiO$_2$) within 4 h. Furthermore, the degradation ratio of benzene at the sixth run was 76.4%.	[234]
Mo-TiO$_2$ layer (rutile to stable anatase phase)	6.0% Mo-Ti O$_2$	15 mm × 10 mm	PEOx	10 mg/L MB (100 mL)	660-nm Tungsten-halogen	55% within 180 min for pure TiO$_2$	86% within 180 min	[76]
Mo-TiO$_2$ nanoparticles (anatase phase)	1 wt% Mo-TiO$_2$	0.2 g/L	EISA method	0.156 mmol L^{-1} 4-CP (1.5 L)	UV	32% within 100 min	95% (three times faster than Degussa P25) within 100 min	[233]
Mo-TiO$_2$ nanoparticles (anatase to brookite and rutile phases)	0.125 mol% Mo-TiO$_2$	0.1 g/L	MWASG	85 mg/L MB, SMX (100 mL)	UV	0.031 min^{-1} for MB within 64 min	0.04 and 0.0318 min^{-1} for MB and SMX, respectively within 64 min	[77]
MoO$_3$/P25 nanoparticles (anatase phase)	0.25% MoO$_3$/P25	0.1 g	Impregnation method	15 mg/L MB (100 mL)	High pressure sodium lamp	8% within 150 min	38% within 150 min	[235]

MB: Methylene blue; SMX: sulfamethoxazole; PEOx: plasma electrolytic oxidation; EISA: evaporation induced self-assembly; MWASG: microwave-assisted sol–gel method; 4-CP: 4-chlorophenol.

4.1.9. Modification with Cobalt (Co)

Co^{2+} has a similar radius as Ti^{4+}, which easily enters into lattice interstitial sites or replaces Ti^{4+} to broaden its photocatalytic activity [236,237]. Co-TiO$_2$ is a capable candidate owing to its excellent properties such as stability, optically active nature, transparency, low cost and high n-type carrier mobility [238,239]. Furthermore, the presence of cobalt (Co^{2+} or Co^{3+}) enhances crystallization due to the increased amounts of oxygen vacancies in the lattice of TiO$_2$, created by replacing the Ti^{4+} sites of the TiO$_2$ lattice [182,240,241]. Ebrahimian et al. [242] prepared Co-TiO$_2$ NPs with a great absorption range in the visible light range. Iwasaki et al. [243] synthesized Co-TiO$_2$ and observed that Co^{2+} could shift the edge of light absorption of TiO$_2$ to the visible light range and enhance photocatalytic activity in both visible and UV regions. Additionally, [92,240] reported that modifying TiO$_2$ lattice with Co enhances the photocatalytic activity of MO and carbamazepine under both visible and UV-A irradiations in comparison with unmodified TiO$_2$.

Some studies have greatly emphasized the contradictory influence of cobalt: some authors have reported its incorporation as detrimental for photocatalytic activity, while some have observed a slight improvement in photodegradation or selectively for some organic compounds. Studies by [244,245] show that that the photocatalytic activity of Co-TiO$_2$ is lower than unmodified TiO$_2$ in the presence of UV light. Meanwhile, 0.5% Co-TiO$_2$ presents the highest activity in the presence of visible light. Generally, most authors have concluded on the following facts (i) Co is present as the divalent form; (ii) Co (II) states are located within the bandgap; (iii) cobalt can be found in interstitial positions of TiO$_2$ [246]. Table 11 presents the summary of recent progress on Co-TiO$_2$ photocatalysts for organic pollutants degradation.

Table 11. Summary of recent progress on Co-TiO$_2$ photocatalysts for organic pollutants degradation.

Materials (TiO$_2$ Phase Transition)	Optimum	Catalyst Dosage	Synthetic Methods	Pollutants (Volume)	Light Source	Unmodified	Modified	Ref.
Co-TiO$_2$ nanosheets (anatase phase)	2.81% Co-TiO$_2$	100 mg	Hydrothermal route	30 mg/L TC (100 mL)	Visible light	51.56% within min	50.19% within 140 min.	[247]
Co-TiO$_2$ nanoparticles (anatase phase)	1 wt% Co-TiO$_2$	0.5 g/L	Sol–gel and precipitation methods	10 mg/L MO (250 mL)	White compact fluorescent lamp	16.3% within 360 min.	34.7% within 360 min	[248]
Cobalt phthalocyanine complex sensitized TiO$_2$ nanoparticles (anatase phase)	-	0.3 g/L	Hydrothermal methods	40 mg/L 4-CP (200 mL)	Visible light	25% within 90 min.	50% within 90 min.	[249]
Co-TiO$_2$ film (anatase phase)	8% Co-TiO$_2$	-	MBE methods	20 mg/L MB, Azo (100 mL)	Visible light	38 and ~37% for MB and AZO dyes, respectively within 70 min.	91 and 88% for MB and Azo dye, respectively within 70 min	[239]
Co-TiO$_2$ nanosheets (Co-TNT) (anatase phase)	0.152% Co-TNT/rGO	0.152 g	Hydrothermal methods	30 mg/L TC (100 mL)	Visible light	48.57% within 180 min.	~60% within 180 min. Reusing the optimal photocatalyst after five successive cycles showed ~7% decline in its activity for degrading of TC.	[250]
Co-TiO$_2$ nanoparticles (anatase phase)	0.06% Co/TiO$_2$	0.1 g	Sol–gel using cobalt resinate as both template and cobalt source.	10 mg/L MB, RhB (100 mL)	Visible light	Unmodified TiO$_2$ and unmodified Degussa P25 titania (P25) was 55 and 4.7%, respectively within 4 h.	82 and 55% for MB and RhB, respectively within 4 h	[251]
Co-TiO$_2$ nanoparticles (anatase phase)	0.060% Co/TiO$_2$	0.1 g	Sol–gel using resin acids as both template and cobalt source.	10 mg/L MB, RhB (100 mL)	Visible light	Unmodified TiO$_2$ and unmodified Degussa P25 titania (P25) were 5.2 and 4.7%, respectively within 4 h.	86 and 94% for MB and RhB, respectively within 4 h	[251]
Co-TiO$_2$ nanoparticles (anatase phase)	1 wt% Co-TiO$_2$ NPs	0.5 g	Sol gel method	40 mg/L 2, 4-DCP (100 mL)	Visible light	43.65% within 120 min	68.03% within 120 min	[252]
Co-TiO$_2$ flim (anatase phase)	1 wt% Co-TiO$_2$	0.5 g	Phase inversion technique	40 mg/L 2, 4-DCP (100 mL)	UV/Visible light	-	61.6 and 63.74% in the presence of UV and visible light, respectively within 120 min. Furthermore, the membrane flux was increased by 53%.	[252]

Table 11. *Cont.*

Materials (TiO$_2$ Phase Transition)	Optimum	Catalyst Dosage	Synthetic Methods	Pollutants (Volume)	Light Source	Unmodified	Modified	Ref.
Co-TiO$_2$ nanoparticles (anatase phase)	2 wt% Co-TiO$_2$ NPs	0.38 g/L	Photochemical deposition-assisted sol–gel technique.	10 mg/L Phenol (120 mL)	UV/Visible light	~95 and ~58% in the presence of UV and visible light, respectively for neat TiO$_2$ within 180 min. Moreover, the neat P25 shows ~85 and ~80% in the presence of UV and visible light, respectively.	~98 and ~67% in the presence of UV and visible light, respectively within 180 min	[121]
Co-TiO$_2$ nanopowders (anatase phase)	1 wt% Co	0.1 g/L	Sol–gel method	25 mg/L NB (-)	Medium-pressure mercury lamp	-	~81% within 180 min	[253]
Co-TiO$_2$ nanopowders (anatase phase)	2 wt% Co- TiO$_2$	0.01 g	Conventional solid-state reaction	20 mg/L MB (100 mL)	Xenon arc lamp	90.80% within 210 min.	90.92% within 210 min	[182]
Co-TiO$_2$ nanoparticles (anatase phase)	1% Co-TiO$_2$	0.1 g	Sol–gel method	5 mg/L MO, MB (100 mL)	Visible light	44.18 and 26.80% degradation rates for MB and MO, respectively for unmodified TiO$_2$ within 5 h. 45% for MB for Degussa P25	66.17 and 38.14% for MB and MO, respectively within 5 h.	[94]
Co-TiO$_2$ nanoparticles (anatase phase)	0.05% Co-TiO$_2$	2 g/L	Sol–gel method	75 μM Crystal violet (100 mL)	UV	60% within 120 min	~100% within 120 min	[254]
CoO-RGO-TiO$_2$ nanoparticles (anatase phase)	0.5% TiO$_2$–RGO–CoO	0.05 g	Sol–gel method	10 mg/L 2-CP (100 mL)	Visible light	35.7% within 12 h.	58.9% within 12 h	[255]
Co-TiO$_2$ nanoparticles (anatase phase) c	1% Co-TiO$_2$	0.01 g	Sol–gel method	10 mg/L RhB (10 mL)	Visible light	~86% within 40 min	99% within 40 min	[237]
Co-TiO$_2$ nanopowders (anatase phase)	1% Co-TiO$_2$	0.1 g/L	Sol–gel method	2.5×10^{-4} M NB (-)	UV	57.13% within 2 h	81.03% within 2 h	[256]
Co-TiO$_2$ nanopowders (anatase phase)	2% Co-TiO$_2$	0.1 g/L	Sol–gel method	2.5×10^{-4} M NB (-)	UV	57.13% within 2 h	67.17% within 2 h	[256]
Co-TiO$_2$/(GO) inverse opal photonic crystal (IO PC) (anatase phase)	-	0.1 g	Simple casting and calcination process using polystyrene opal as the template	0.013 M 4-CP (100 mL)	LT50 lamp	60% within 120 min.	75% within 120 min	[257]

Table 11. *Cont.*

Materials (TiO$_2$ Phase Transition)	Optimum	Catalyst Dosage	Synthetic Methods	Pollutants (Volume)	Light Source	Unmodified	Modified	Ref.
Co-TiO$_2$ nanopowders (anatase phase)	0.05 mol% Co-TiO$_2$	1 g L^{-1}	Sol–gel method (non-aqueous)	10 mg L^{-1} MB (500 mL)	UV	88.0% within 120 min	97.7% within 120 min	[91]
Co-TiO$_2$ nanoparticles (anatase phase)	1.75% Co-TiO$_2$	0.03 g/L	Nanosol/dip-coating method.	30 mg/L MB (50 mL)	UV	-	69% within 2 h	[217]
Co-TiO$_2$ nanoparticles (anatase phase)	1% Co-TiO$_2$	0.025 g	Sol–gel method	10^{-5} mol/L MO (50 mL)	Visible light	0.00075 and 0.002631 min^{-1} for visible and UV irradiation, respectively. 16.3 and 95.6% for visible and 95.6 for visible and UV light, irradiation within 120 min	0.00149 and 0.00280 min^{-1} (2 times larger than that of the unmodified TiO$_2$) for visible and UV irradiation, respectively.	[92]
Co-TiO$_2$ nanoparticles (anatase phase)	5% Co-TiO$_2$	0.1 g	Sol–gel method	5×10^{-5} mol/L MB, MO (100 mL)	UV/Visible light	65.3 and 72.4% for MO and MB, respectively within 60 min under UV irradiation. 4.1 and 6.2% for MO and MB, respectively within 240 min under visible irradiation.	78.2 and 86.4% for MO and MB, respectively within 60 min under UV irradiation. 53.2 and 64.3% for MO and MB, respectively within 240 min under visible irradiation.	[38]
Co-TiO$_2$ nanoparticles (mixed anatase and brookite phases)	0.5 mol% Co-TiO$_2$	1 g/L	Sol–gel method	10 mg/L PNP (100 mL)	UV/Visible light	50 and 20% under UV/Visible and visible light, respectively for Degussa P25 within 8 h.	32 and 15% under UV/Visible and visible light, respectively within 8 h.	[127]

2,4-DCP: 2,4-dichlorophenol; Co-TiO$_2$: cobalt modified TiO$_2$; PNP: *p*-nitrophenol; MO: methyl orange; RhB: rhodamine B; MB: methyl blue; NB: nitrobenzene; 4-CP: 4-chlorophenol; 2-CP: 2-chlorophenol; TC: tetracycline.

4.1.10. Modification with Niobium (Nb)

The incorporation of niobium (Nb) can act as electrons sink as well as minimize the recombination of e^- to h^+ pairs, and thus make more carriers available for reduction or oxidation processes on TiO_2 surface [258]. Modifying with Nb^{5+} enables the release of one electron for every Nb introduced: the Fermi level of TiO_2 shifts upward into the CB and results in a typical n-type metallic characteristic in the electronic structure [259]. Furubayashi et al. [260] prepared an Nb^{5+}-TiO_2 film and their results show a room temperature resistivity of 2 to 3×10^{-4} Ω cm when the Nb concentration was >3%. Modifying of Nb5+ into TiO_2 lattice can extend the absorption that spans from UV to visible region as well as to the mid-infrared region. This allows TiO_2 to be active in the presence of both visible and UV light [261]. Some studies have also shown that charge transfer can be improved upon implantation with small Nb^{5+} content. Upon modifying with Nb, Nb^{5+} replaces Ti^{4+} and the donor is formed at the CB of TiO_2, providing electron for Ti^{4+} as well as obtaining a high concentration of carrier [260]. Su et al. [262] have showed that modifying with Nb increases the electrical conductivity, decreases bandgap, and increases optoelectronic property. Khan et al. [263] also demonstrated that charge-compensating $(NbTi-VTi)^{3-}$ complexes serve as the dominant defect in Nb-TiO_2 composite enabling the improvement in the photocatalytic activity via the formation of shallow defect level. Table 12 presents the summary of recent progress on Nb-TiO_2 photocatalysts for organic pollutants degradation.

Table 12. Summary of recent progress on Nb-TiO$_2$ photocatalysts for organic pollutants degradation.

Materials (TiO$_2$ Phase Transition)	Optimum	Catalyst Dosage	Synthetic Methods	Pollutants (Volume)	Light Source	Unmodified	Modified	Ref.
Nb-TiO$_2$ Nanoparticles (Anatase phase)	0.5 mol%Nb-TiO$_2$	1 g/L	Sol–gel method	100 uM 4-CP (-)	Visible light	8% within 120 min	The degradation of Nb-TiO$_2$ was only slightly enhanced from the bare TiO$_2$ case.39% within120 min	[264]
Nb-TiO$_2$ nanoparticles (anatase phase)	0.5 at% Nb-TiO$_2$	0.5 g/L	Sol–gel method	100 uM 4-CP (30 mL)	Visible light	~90% within 4 h	~100% within 4 h	[265]
Nb$_2$O$_5$/TiO$_2$ hexagonal (anatase phase)	60 wt% or 0.6 of Nb$_2$O$_5$	1 g/L	Sol–gel method	50 mg/L MB (100 mL)	Visible light	~14% within 150 in	~23% within 150 in	[266]
Nb-TiO$_2$ microspheres microspheres (anatase phase)	-	0.1 g	Ultrasonic spray pyrolysis method combined with impregnation method	10 mg/L MB (100 mL)	Visible light irradiation	5% within 60 min	Nb-TiO$_2$ microspheres show higher activity as compared to unmodified TiO$_2$, 26% within 60 min	[267]
Nb$_2$O$_5$/TiO$_2$ nanoparticles (anatase phase)	0.5 mol% Nb$_2$O$_5$/TiO$_2$	50 mg	Coprecipitation	10 µmol/L MB (300 mL)	UV	P25 showed the highest photocatalytic activity within 1 h.	Degradation rate for 0.5 mol% Nb$_2$O$_5$-TiO$_2$ was slightly higher than the unmodified TiO$_2$ within 1 h	[268]
Nb-TiO$_2$ nanoparticles (anatase phase)	2 mol% Nb-TiO$_2$	-	Hydrothermal method	10 ppm MB (-)	Solar light	~40% within 100 min	~40% within 100 min	[262]
Nb–TiO$_2$ films (mixture of anatase and rutile phases)	0.58 mol% Nb–TiO$_2$	-	Spin coating technology	10 ppm MB (-)	UV	~10% (1.07×10^{-3} min^{-1}) within 120 min	~60% (4.97×10^{-3} min^{-1}) within 120 min	[269]

XC: carbon xerogel; 4-CP: 4-chlorophenol; MB: methyl blue.

4.1.11. Modification with Tungsten (W)

Tungsten (W) can easily replace Ti in the TiO_2 matrix due to the similarities in ionic radii of Ti^{4+} and W^{6+}. W in its high oxidation state (+6) can act as an electron trap center and the substitutional modification of Ti^{4+} with W^{6+} can impart an almost small change in the TiO_2 matrix [270]. Modifying with W can only reduce the recombination in the TiO_2 bulk, whereas the defects present on the TiO_2 surface can act as recombination centers [271]. Furthermore, modifying with W can lead to the placement of electrons in a state below the CB or donor state [272]. These electrons can receive energy from visible light and be transferred to the CB. Finally, these excited electrons can generate $O^2\bullet^-$, OH$\bullet$, and OH$\bullet$ which are responsible for the heterogeneous photocatalytic treatment of organic pollutants [273]. When the anatase TiO_2 is modified with WO_3, separation of charge is improved as a result of the coupling of both materials [274]. Moreover, the presence of WO_3 can increase the TiO_2 acidity, modifying the substrate's affinity for TiO_2 surface and thus affects the adsorption equilibrium and photooxidation activity of the catalyst [275,276]. Three major advantages of WO_3 include the thermodynamically favorable position of VB edge for the oxidation of H_2O (3 V vs. NHE), visible light response with a bandgap energy of 2.6–2.8 eV, and photochemical stability in acidic media [277]. Superior photocorrosion resistance and chemical stability are the other advantages provided when TiO_2 is modified with WO_3. Various techniques including sol–gel, chemical vapor deposition, impregnation, mechanical blending, and liquid phase plasma (LPP) method have been also applied to the modification of host photocatalyst with transition metals [278,279]. Table 13 presents the summary of recent progress on W-TiO_2 photocatalysts for organic pollutants degradation.

Table 13. Summary of recent progress on W-TiO$_2$ photocatalysts for organic pollutants degradation.

Materials (TiO$_2$ Phase Transition)	Optimum	Catalyst Dosage	Synthetic Methods	Pollutant	Light Source	Unmodified	Modified	Ref.
W-TiO$_2$ nanoparticles (anatase phase)	5% W-TiO$_2$	0.5 g	Liquid phase plasma	10 mg/L DEP (600 mL)	UV/Blue light	1.22×10^{-2} min^{-1} and 4.72×10^{-2} min^{-1} for UV light and blue light, respectively within 180 min	0.92×10^{-2} min^{-1} and 29.37×10^{-2} min^{-1} for UV light and blue light, respectively within 180 min	[280]
W-TiO$_2$ nanoparticles (anatase phase)	2.5 wt% W-TiO$_2$	2 g/L	Sol–gel method	600 mg/L COD (150 mL)	Fluorescent light	-	50% within 34 h	[281]
W-TiO$_2$/reduced graphene oxide nanoparticles (anatase phase)	1% W-TiO$_2$	0.01 g	Sol–gel method	10 mg/L PNP (50 mL)	UV	30% within 180 min	62% within 180 min	[271]
W-TiO$_2$ nanoparticles (anatase phase to stable rutile phase)	TiO$_2$/W$_{50\ ppm}$	0.1 g	Hydrothermal method	20 mg/L RhB, MB, MO (100 mL)	Visible light	~81% of MO within 15 min. 0.0031 min^{-1}, 0.01612 min^{-1} and 0.1441 min^{-1} for RhB, MB and MO, respectively	Degradation rate is 10 times the unmodified TiO$_2$. 0.03181 min^{-1}, 0.04148 min^{-1}, 0.2730 min^{-1} for RhB, MB and MO, respectively. ~99.4% of MO within 15 min. Furthermore, 93.1 and 87.1% of MB and RhB were degraded, respectively, within 60 min, while 99.61% of MO within 20 min.	[282]
W-TiO$_2$ nanoparticles (anatase phase)	0.5 mol% W-TiO$_2$	0.5 g	Sol–gel method	50 mg/L CR (250 mL)	Visible light	1.25 min^{-1} for Degussa P25 within 180 min	2.62 min^{-1} within 180 min	[283]
WO$_3$/TiO$_2$ nanotube (anatase phase)	-	1 cm $\times$ 2 cm	Electrochemical approach	100 ppm Toluene (-)	Xenon lamp	-	65% within 60 min	[284]
Colloidal W- TiO$_2$ nanocrystals (anatase phase)	2% W–TiO$_2$	1 g/L	Hydrothermal method	10 mg/L Phenol (-)	UV	48.9% (0.1092 h^{-1}) within 6 h	80.0% (0.2694 h^{-1}) within 6 h	[285]
W-TiO$_2$ layer (rutile to stable anatase phase)	6 wt% W-TiO$_2$	15 mm $\times$ 10 mm	PEOx method	10 mg/L MB (100 mL)	660-nm Tungsten-halogen	55% within 180 min for pure TiO$_2$	95% within 180 min	[76]
W-TiO$_2$ nanoparticles (anatase phase)	1 wt% W-TiO$_2$	0.2 g/L	EISA method	0.156 mol L^{-1} 4-CP (70 mL)	UV	32% within 100 min	88% within 100 min	[233]
WO$_3$/TiO$_2$ nanoparticles (anatase phase)	10% WO$_3$/TiO$_2$	0.05 g	combination of hydrothermal and calcination method	10 mg/L MB (50 mL)	Visible light	40.7 and 55.3% using pure TiO$_2$ and WO$_3$, respectively for MB within 2 h. 41.6 and 54.8% using pure TiO$_2$ and WO$_3$, respectively for MET within 2 h.	87.8 and 67.1% for MB and MET, respectively within 2 h. After three cycles, 10% WO$_3$/TiO$_2$ samples could still remove 63.2% of MET and 79.8% of MB.	[286]

Table 13. *Cont*.

Materials (TiO$_2$ Phase Transition)	Optimum	Catalyst Dosage	Synthetic Methods	Pollutant	Light Source	Unmodified	Modified	Ref.
W-TiO$_2$ nanoparticles (anatase phase)	-	0.5 g/L	Sol–gel method	30 mg/L SMZ (200 mL)	Metal-halide lamps	80% within 30 min	The extended reuse of the photocatalysts for five consecutive runs obtained an SMZ degradation of 97.7, 97.6, 96.2, 95.1, and 90.34% in the same order.	[287]
W-TiO$_2$ nanoparticles (anatase phase)	1.5 wt% W-TiO$_2$	-	Sol–gel method	10 mg/L Thymol (100 mL)	Solar light	9.65% (0.085×10^{-2} min^{-1}) within 120 min	48.76% (0.582×10^{-2} min^{-1}) within 120 min	[288]
W-TiO$_2$ nanosheets (anatase phase)	-	64 m^2	Spray pyrolysis method	1 mM oxalic acid 2.5 $\times 10^{-4}$ M NB (-)	Sunlight	42% within 320 min	~83% within 180 min	[289]
W-TiO$_2$ coupons (rutile to stable anatase phase)	6 wt% W-TiO$_2$	15 mm × 10 mm	PEOx method	10 mg/L MB (100 mL)	660-nm Tungsten-halogen	55% within 180 min for pure TiO$_2$	95% within 180 min	[76]

PNP: *p*-nitrophenol; SMZ: sulfamethazine; MB: methyl blue; PEOx: plasma electrolytic oxidation; 4-CP: 4-chlorophenol; RhB: rhodamine B; CR: Congo red; MO: methyl orange; COD: chemical oxygen demand; DEP: diethyl phthalate.

4.1.12. Modification with Zinc (Zn)

Zn^{2+} ion can easily substitute Ti^{4+} ion in TiO_2 lattice without destroying the crystal structure, thereby stabilizing the anatase phase. Zn-TiO_2 powder can be synthesized using various preparative methods such as sol-hydrothermal, homogeneous hydrolysis, sol–gel and solid-phase reaction, electrospinning, controlled hydrolysis of titanium (IV) butoxide, assembly process based on a Ligand exchange reaction; micro-emulsion and sol–gel method. Table 14 presents the summary of recent progress on Zn-TiO_2 photocatalysts for organic pollutants degradation.

Table 14. Summary of recent progress on Zn-TiO$_2$ photocatalysts for organic pollutants degradation.

Materials (TiO$_2$ Phase Transition)	Optimum	Catalyst Dosage	Synthetic Methods	Pollutants (Volume)	Light Source	Unmodified	Modified	Ref.
Zn-TiO$_2$ nanoparticles (anatase phase)	1 wt% Zn-TiO$_2$	0.1 g	Single step of sonochemical method	10 mg/L RhB (100 mL)	UV	18% within 90 min	35% within 90 min	[290]
Zn-TiO$_2$ nanoparticles (mixed anatase and rutile phases)	0.01% Zn-TiO$_2$	0.1 g	Sol–gel method	20 mg/L MB (50 mL)	Visible light	89.69% within 60 min	99.64% within 60 min	[128]
Zn-TiO$_2$ nanoparticles (mixed anatase and brookite phases)	0.5 mol% Zn-TiO$_2$	1 g/L	Sol–gel method	10 mg/L PNP (100 mL)	UV/Visible light	50 and 20% under UV/Visible and visible light, respectively for Degussa P25 within 8 h.	75 and 32% for UV/Visible and visible light, respectively within 8 h	[127]
Zn-TiO$_2$ nanoparticles (anatase phase)	5 wt% Zn-TiO$_2$	0.007 g	Sol–gel method	5 mg/L MB (50 mL)	Visible light	50% within 150 min	28.75 and 50% within 35 min and 47 min, respectively	[291]
Zn-TiO$_2$ nanoparticles (anatase phase)	0.2 wt% Zn-TiO$_2$	-	Sol–gel method	50 mg/L MO (50 mL)	Visible light	27% (0.45 min^{-1}) and 3% (0.40 min^{-1}) under UV irradiation and visible irradiation, respectively within 30 min	62% (1.54 min^{-1}) and 40% (0.92 min^{-1}) under UV irradiation and visible irradiation, respectively within 30 min	[113]
Zn-TiO$_2$ nanoparticles (anatase phase)	5% Zn-TiO$_2$	0.1 g	Oil-in-water microemulsions, (O/W) microemulsion method	30 mg/L Phenol (200 mL)	UV	84% within 5 h	93% within 5 h	[292]

MB: methylene blue; MO: methyl orange; PNP: *p*-nitrophenol; RhB: rhodamine B.

4.2. Modification with Noble Metals

4.2.1. Modification with Gold (Au)

Gold (Au) can act as an electron acceptor since the energy gap (Eg) of Au (5.1–5.47 eV) is greater than TiO_2 (~4.7 eV) [293]. Owing to its plasmon resonance effect, modifying TiO_2 with Au will allow the achievement of visible light-driven photocatalyst [294,295]. Au-TiO_2 can also enhance the functional abilities of the material, causing alteration of the chemical or photocatalytic properties. Thus, the interaction between the photogenerated active species and the substrate of the Au-TiO_2 interface is increased and easily distinguished [296–298]. The collective oscillating motion of CB electrons on the Au nanoparticles (NPs) surface is mainly responsible for the reductive properties of the NPs and originates from a well-known surface plasmon resonance (SPR) [299]. Furthermore, modifying with Au promotes the gradual injection of hot electrons into TiO_2, and as a consequence increases the life span of the hole–electron pair and improve the photocatalytic activity [300]. The presence of Au in TiO_2 lattice structure may cause the switching of Ti^{4+}/Ti^{3+} in defects, which effectively minimizes the wide bandgap of TiO_2. The presence of Ti^{4+}/Ti^{3+} states inside the nanostructure enhances the electron-transfer mechanism inside the crystal lattice of TiO_2, increasing the photocatalysis efficiency [301]. This property can overcome the limitations of using unmodified TiO_2 photocatalyst due to its low recycling capability and complications of recovery from H2O.

The key parameters for the Au-TiO_2 activity are the Au particle size and the crystal phase of TiO_2. Additionally, Au-TiO_2 possesses a high performance coupled with a longer life span [302]. On the other hand, the dependence Au-TiO_2 activity is also influenced by the particle size of Au in the action mechanisms, which can be classified into the electron–hole transfer mechanism [303]. Deposition of Au occurred without changing the TiO_2 crystal structure and also achieved effective separation of photogenerated electron–hole in the UV–visible (UV-vis) light conditions, due to the smaller Au particle size of 15 nm. Table 15 presents the summary of recent progress on Au-TiO_2 photocatalysts for organic pollutants degradation.

Table 15. Summary of recent progress on Au-TiO$_2$ photocatalysts for organic pollutants degradation.

Materials (TiO$_2$ Phase Transition)	Optimum	Catalyst Dosage	Synthetic Methods	Pollutant	Light Source	Unmodified	Modified	Ref.
Au-TiO$_2$ nanoparticles (anatase phase)	1% Au-TiO$_2$	0.005 g	Photodeposition method	10 mg/L MB, CBN, MNZ (10 mL)	UV	73.9 and 88.7% for CBN and MNZ, respectively	35.7 and 46.8% for CBN and MNZ, respectively	[304]
Au-P25 nanoparticles (mixed anatase rutile phase)	1% Au-P25	0.005 g	Precipitation–deposition method	10 mg/L BPA (10 mL)	UV	35% within 24 h	76% within 24 h	[305]
Au-TiO$_2$ nanoparticles (mixed anatase rutile phase)	1% Au-TiO$_2$	0.005 g	Sol–gel method	10 mg/L BPA (10 mL)	UV	35% within 24 h	~57% within 24h	[305]
Au-TiO$_2$ nanoparticles (mixed anatase rutile phase)	1% Au-TiO$_2$ NPs	0.005 g	Sol–gel method	10 mg/L BPA (10 mL)	UV	35% within 24 h	~56% within 24 h	[305]
Au-meso-TiO$_2$ nanoparticles (mixed anatase rutile phase)	1% Au-meso-TiO$_2$	0.005 g	Sol–gel method	10 mg/L BPA (10 mL)	UV	35% within 24 h	37% within 24 h	[305]
TiO$_2$ hollow microspheres impregnated with biogenic Au nanoparticles (stable anatase phase)	5% Au-TiO$_2$ NPs	0.005 g	Sol–gel method	2.5×10^{-4} mol/L Phenol (10 mL)	Visible light	21% within 1 h	95% within 1 h	[306]
Au-TiO$_2$ nanoparticles (anatase phase)	0.154 wt% Au-TiO$_2$	0.004 g	Simple synthesis route	3.125×10^{-5} mol/L MB (-)	Visible LED light	25% within 150 min	97% within 150 min	[307]
Au-TiO$_2$ yolk-shell (anatase phase)	0.14 at% Au-TiO$_2$	0.005 g	Seed-growth method	300 ppm gaseous toluene (-)	Visible light	20% within 3 h	57.3% within 3 h	[308]
Au-TiO$_2$ nanoparticles (anatase phase)	-	-	Sol–gel, wet chemical synthesis, hydrothermal, and plasma oxidative pyrolysis	20 mg/L CR, MO (100 mL)	UV	-	40.1 and 19.7 for MO and CR, respectively within 210 min.	[309]
Ag-TiO$_2$ nanoparticles (anatase phase)	0.005 wt% Ag-TiO$_2$	1.005 g	Sol–gel, wet chemical synthesis, hydrothermal, and plasma oxidative pyrolysis	20 mg/L CR, MO (100 mL)	UV	-	52.3 and 34.4% for MO and CR, respectively within 3.5 h	[309]

Table 15. *Cont.*

Materials (TiO$_2$ Phase Transition)	Optimum	Catalyst Dosage	Synthetic Methods	Pollutant	Light Source	Unmodified	Modified	Ref.
Au-TiO$_2$ nanoparticles (anatase phase)	0.1% Au-TiO$_2$	0.5 g	Hydrothermal method	10 mg/L Resorcinol (500 mL)	UVA	72.36% (0.0044 min^{-1}) within 5 h	95.34% (0.0102 min^{-1}) within 5 h (1.5 times of magnitude higher than pure TiO$_2$ NPs while the rate constant was 2.5 times greater than that for pure TiO$_2$). Furthermore, it shows 95% after five repeating experiments	[310]
Au-TiO$_2$ films (anatase phase)	0.02 wt% Au/TiO$_2$ meso-porous thin films	-	Sol–gel method	5 mg/L TC (100 mL)	UVA	27% within 2 h	After 6 cycles, the percentage removal of TC is decreased from 58.51% to 57.89% only (i.e., a 0.62% decrease)	[311]
Au-TiO$_2$ plasmonic nanohybrids (anatase phase)	-	0.005 g	Wet chemical method	10 mg/L MB, MO (100 mL)	Sunlight	25% within 20 min	94% for MB, 85% for MO, and 87% for the mixture of MO and MB within 20 min (3.3 times greater than that of the unmodified TiO$_2$)	[312]
Au-TiO$_2$ nanoparticles (Mixed anatase rutile phase)	2 wt% Au-TiO$_2$	1.3 g/L	Deposition–precipitation method	50 mg/L CFS (100 mL)	UV/Visible light	<5% within 2 h under visible light irradiation	95 and 65% within 2 h under UV–visible and visible light irradiation, respectively	[313]
Au-TiO$_2$ photoanode on carbon cloth (anatase phase)	0.1 wt% Au-TiO$_2$	2 cm^2	Sol–gel method	78.5 mg/L paracetamol (100 mL)	PEC/Sunlight	-	62 and 66% under PEC process and sunlight radiation in solar PEC, respectively within 180 min	[314]
Au-TiO$_2$ film (anatase phase)	3 at% Au-TiO$_2$ film	10 cm × 10 cm	Chemical spray pyrolysis technique	1 mmol/L benzoic acid (-)	UV	37% within 400 min	49% within 400 min	[29]

CBN: carbofuran; MNZ: metronidazole; MO: methyl orange; CFS: ceftiofur sodium; MB: methylene blue; CR: Congo red; TC: tetracycline; BPA: bisphenol A.

4.2.2. Modification with Silver (Ag)

Compared to gold and platinum, silver (Ag) is the cheapest coinage metal having a high charge carrier density [315]. It also has other advantages such as higher antibacterial activity, lower cost, and toxicity [316]. Modifying with Ag ions can create a new impurity band about 0.7 eV below the CB of titania which will thus narrow the energy bandgap of titania [317]; subsequently, Ag enhances the electron–hole separation by acting as an electron trapper to capture the electrons while reacting with the contaminants [318]. Hence, Ag assists in charge separation via the formation of a Schottky barrier between the metal and TiO_2 [319,320]. The incorporation of silver ion also extends the absorption of TiO_2 under visible light due to SPR effect, excited by visible light [321–324]. The presence of Ag ion can also contribute in two ways: (i) reinforcement of the photoinduced charge carriers as well as enhancing the electromagnetic field at the interfaces, (ii) promotion of interfacial charge-transfer process which limits the recombination rates. The electronic band-alignment at the Ag-clusters-TiO_2 interface favors the migrations of photogenerated electrons to metallic particles.

This process increases the lifespan of holes leading to redox reactions required for the photodegradation of the organic pollutants [119]. There are many approaches to synthesize Ag modified TiO_2, including solvothermal [325,326], reduction using UV irradiation [327], hydrothermal [328], electrochemical [329], microwave [330], deposition–precipitation [331,332], sonochemical [333], and sol–gel methods [334,335].

Zhou et al. [336] reported Ag decorated Ti^{3+} self-doped porous black TiO_2 pillar using a combined oil bath and wet impregnation approach. They claimed that the synergistic effect between Ti^{3+} self-doping and Ag decoration enhances photocatalytic activity. Liu et al. [337] presented the formation of Ag impurity band above the VB and observed the presence of AgO on the TiO_2 surface as well as the presence of Ag in the bulk. They noted that this Ag system will fail to show the energy level matching concept as the presence of Ag-ions is required on the TiO_2 surface. Contrary to various conventional reports, some reports have also confirmed the formation of impurity bands starting from 0.7 eV below CB [338]. Xiong et al. [339] also introduced 0.25 wt% Ag NPs into mesoporous TiO_2 and observed enhanced degradation of RhB in the presence of UV light irradiation. In addition, the Ag-TiO_2 catalysts present a higher photocatalytic efficiency for indigo carmine in the presence of visible light which was higher than the commercial P25 titania or unmodified TiO_2 [339]. Table 16 presents the summary of recent progress on Ag-TiO_2 photocatalysts for organic pollutants degradation.

Table 16. Summary of recent progress on Ag-TiO$_2$ photocatalysts for organic pollutants degradation.

Materials (TiO$_2$ Phase Transition)	Optimum	Catalyst Dosage	Synthetic Methods	Pollutant (Volume)	Light Source	Unmodified	Modified	Ref.
Ag-TiO$_2$ nanoparticles (anatase phase)	5% Ag-TiO$_2$	0.0113 mg	Sol–gel method	8 mg/L 2-CP (300 mL)	UV	16% within 150 min	30.4% within 150 min	[340]
Ag-TiO$_2$ thin films (anatase phase)	5%Ag-TiO$_2$	2.5 cm × 2.5 cm	Sol–gel method	5 mg/L MO, MB (25 mL)	Visible light	40.10% for MB within 240 min	98.86% for MB within 240 min, 96.34% for MO within 180 min. After ten consecutive cycles, approximately 98.85% MB dye were removed.	[341]
Ag-TiO$_2$ Films (anatase phase)	Ag-TiO$_2$ films	-	Sol–gel method	10 mg/L RB (-)	Solar light/Visible light/UV	45% within 70 min	98, 78, and 50% under solar light, visible and UV within 70 min. After four consecutive cycles, approximately 96.5% RB dye was removed.	[342]
Ag-TiO$_2$ nanopowders (anatase phase)	10% Ag-TiO$_2$	0.05 g	Sol–gel method	0.03 mg/L MB (50 mL)	UV	96% within 2 h, 97% within 35 min	97% within 35 min, 96% within 2 h	[343]
Ag-TiO$_2$ nanoparticles (anatase phase)	10 wt% Ag-TiO$_2$	0.3 g/L	Polyol method	1000 mg/L DCA (100 mL)	UV	65.4% within 480 min	79.3% within 480 min	[344]
Ag-TiO$_2$ nanoparticles (anatase phase)	10 wt% Ag-TiO$_2$	0.05 g	Sol–gel method	0.01 mmol/L MB (-)	Visible light	~30% within 50 h	Almost 100% within 50 h	[317]
Ag-TiO$_2$ nanoparticles (anatase phase)	1.4 wt% Ag-TiO$_2$	0.05 g	Photoreduction method	10 mg/L 4-CP (50 mL)	UV	-	After 8 times of reaction, the degradation effect of 4-CP decreased to 65%.	[345]
Ag-TiO$_2$ nanoparticles (anatase phase)	4.0 mol% Ag-TiO$_2$	0.18 g	Sol–gel method	10 mg/L MB (180 mL)	Visible light irradiation	30% within 60 min	96% within 60 min. After five consecutive cycles, approximately 89% MB dye was removed.	[318]
Ag TiO$_2$ nanopowders (anatase phase)	Ag 3% TiO$_2$	0.125 mol/L	Sol–gel method	2.10^{-5} mol./L MB (-)	UV	0.08124 min^{-1} within 120 min	0.11319 min^{-1} within 120 min	[119]
Ag/TiO$_2$ photoanode (anatase phase)	-	-	Photoreduction method	30 mg/L RhB (250 mL)	UV	97.3% (0.0301 min^{-1}) within 120 min	99.5% (0.0451 min^{-1}) within 120 min	[346]
Ag/TiO$_2$ nanoparticles (mixture of anatase and rutile phases)	1.06 wt% Ag-TiO$_2$	1.5 g/L	Photodeposition method	5 mg/L DXM (600 mL)	UV/VIS	2% within 240 min	77.6 and 63.8% for UV and visible light irradiation, respectively	[347]

Table 16. *Cont*.

Materials (TiO$_2$ Phase Transition)	Optimum	Catalyst Dosage	Synthetic Methods	Pollutant (Volume)	Light Source	Unmodified	Modified	Ref.
Ag/TiO$_2$ nanoparticles (mixture of anatase and rutile phases)	0.03 wt% Ag-TiO$_2$	1.0 g/L	LP followed by wet impregnation and reduction methods	125 µM MO (130 mL)	UV	6.54×10^{-3} min^{-1} and 0.19 $\times$ 10^{-3} min^{-1} for UV and visible light irradiation within 120 min, respectively	28.74×10^{-3} min^{-1} and 16.78 $\times$ 10^{-3} min^{-1} for UV and visible light irradiation within 120 min, respectively	[348]
Ag/TiO$_2$ nanoparticles (anatase phase)	0.25 wt% Ag-TiO$_2$	1 g/dm^3	MWASG	20 mg/L MO (100 mL)	UV	57% within 70 min	99.5% within 70 min	[349]
Ag-TiO$_2$ nanoparticles (mixture of anatase and rutile phases)	0.15 wt% Ag-TiO$_2$	0.5 g	Sol–gel method	8 mg/L MB (100 mL)	Visible light	40 and 42% for unmodified TiO$_2$ and P25, respectively within 7 h	~68% within 7 h	[350]
Ag^{2+}/TiO$_2$ nanoparticles (anatase-brookite TiO$_2$ nanoparticles with a spherical shape)	2 mol% Ag^{2+}/TiO$_2$	1 g/L	Sol–gel method	10 mg/L PNP (100 mL)	UV/Visible light	50 and 20% for Degussa P25 under UV/Visible light and visible light, respectively within 8 h	60 and 31% under UV/Visible light and visible light, respectively within 8 h	[127]
Ag-TiO$_2$ nanopowders (anatase phase)	3% Ag-TiO$_2$	0.125 molL^{-1}	Sol–gel method	20 mg/L MB (100 mL)	UV	0.08124 min^{-1} within 6 h	0.11319 min^{-1} within 6 h	[119]
Ag-TiO$_2$ nanoparticles (anatase phase)	10% Ag-TiO$_2$	0.5 g	Sol–gel, mechanothermal decomposition method	5×10^{-5} M MO (500 mL)	UV/Solar	69% within 60 min under UV, 8% within 80 min under solar irradiation	98.9% within 60 min under UV, 99.3% within 80 min under solar irradiation	[351]
Ag-TiO$_2$ Nanoparticles (anatase phase)	1.75% Ag-TiO$_2$	0.03 g/L	Nanosol/dip-coating method	30 mg/L MB (50 mL)	UV	-	74% within 2 h	[217]

MWASG: microwave-assisted sol–gel method; RB: rose Bengal; DXM: dexamethasone; 4-CP: *p*-chlorophenol; DCA: dichloroacetic acid; 2CP: 2-chlorophenol; PNP: *p*-nitrophenol; LP: laser pyrolysis; MO: methyl orange; RhB: rhodamine B; MB: methylene blue; 4-CP: 4-chlorophenol.

4.2.3. Modification with Platinum (Pt)

Platinum (Pt) is a shiny silvery metal with low chemical activity. It is stable in air and a humid environment. The oxidation state of platinum is +2 to +6, which easily forms coordination compounds and has good ductility, thermal conductivity, and electrical conductivity. Pt is a noble metal that can increase the TiO_2 photoefficiency [352]. The energy level of Pt is lower than the one of the TiO_2 CB, so the energy required for the electron transition is lower and may be induced by the light with higher wavelengths. Therefore, the absorption spectrum can be broadened from the UV towards the VIS region. In the presence of UV light, the photogenerated electrons quickly transfer from the TiO_2 surface to the Pt particles, leading to effective separation of electron–hole, and as a consequence improving the photocatalytic activity [353]. The deposition of Pt nanoclusters onto TiO_2 surface serves as an electron sink, consequently slowing down charge–pair recombination as well as changing reaction pathways by providing catalytic sites where active intermediates can be stabilized [121]. Table 17 presents the summary of recent progress on Pt-TiO_2 photocatalysts for organic pollutants degradation.

Table 17. Summary of recent progress on Pt-TiO$_2$ photocatalysts for organic pollutants degradation.

Materials (TiO$_2$ Phase Transition)	Optimum	Catalyst Dosage	Synthetic Methods	Pollutant (Volume)	Light Source	Unmodified	Modified	Ref.
Pt-TiO$_2$ nanoparticles (mixed rutile and anatase phase)	5 wt% Pt-TiO$_2$	1 g/L	hydrothermal method	10 mg/L RhB (100mL)	Visible light	Amount of RhB degraded in 90 min reaction time 0.326 $\pm$ 0.011 $\times$ 10^{-9} moles/min/mg.	99.5% within 90 min (4.5-fold better than pristine TiO$_2$)	[354]
Pt-TiO$_2$ nanocrystals (mixed anatase and brookite phases)	0.1wt% Pt-TiO$_2$	1g/L	Sol–gel method	10 mg/L PNP (10mL)	Halogen lamp	20 and 12% for TiO$_2$ and P25, respectively within 24 h under visible light. 47 and 84% for TiO$_2$ and P25, respectively within 24 h under UV/Visible light.	~46% within 24 h under visible light. ~78% within 24 h under UV/Visible light.	[114]
Pt-TiO$_2$ film (mixed anatase and brookite phases)	0.1% Pt-TiO$_2$	size of 100 mm $\times$ 120 mm	Immersion and reduction method	100 ppb/500 ppb Ethenzamide (-)	V-UV	50 and 42% for 500 ppb and 100 ppb, respectively.	94.52 and 100% for 500 ppb and 100 ppb, respectively. The rate constant (0.180 min^{-1}) was 1.86 times as compared to unmodified nanoporous TiO$_2$ film (0.097 min^{-1})	[355]
Pt-TiO$_2$ nanoparticles (mixed rutile and anatase phase)	10 wt% Pt-TiO$_2$	0.3 g/L	Polyol method	1000 mg/L DCA (100 mL)	UV	34.6% within 420 min	Almost 100% within 420 min	[344]
Pt-P25 nanoparticles (mixed rutile and anatase phase)	/	0.5 g L^{-1}	Sol–gel method	20 mg/L MG (250 mL)	UV	70% within 30 min for P25	100% within 30 min	[356]
Pt-MTiO$_2$ nanoparticles (mixed rutile and anatase phase)	1.5 wt% Pt-MTiO$_2$	1.5 g/L	facile synthesis procedure	CIP (-)	Visible light	~5% within 120 min	100% within 120 min. After five cycles, approximately 100% was still maintained.	[357]
Pt/P25 and Pt/TiO$_2$ nanoparticles (mix ed rutile and anatase phase)	0.14 wt% Pt/TiO$_2$ and Pt/P25	1.0 g/L	laser pyrolysis (LP) followed by wet impregnation and reduction methods;	125 μM MO (-)	UV/Visible light	6.54 $\times$ 10^{-3} and 9.6 $\times$ 10^{-3} min^{-1} for pure P25 and TiO$_2$ (LP), respectively in the presence of UV light. 0.19 $\times$ 10^{-3} and 1.8 $\times$ 10^{-3} min^{-1} for pure P25 and TiO$_2$ (LP), respectively in the presence of VIS lamp	In the presence of UV lamp, the rate constant of Pt/P25 and Pt/TiO$_2$ was 9.78 $\times$ 10^{-3} min^{-1} and 10.16 $\times$ 10^{-3} min^{-1}. In the presence of VIS lamp, the rate constant of Pt/P25 and Pt/TiO$_2$ were 5.47 $\times$ 10^{-3} min^{-1} and 4.1 $\times$ 10^{-3} min^{-1}.	[348]

Table 17. *Cont*.

Materials (TiO$_2$ Phase Transition)	Optimum	Catalyst Dosage	Synthetic Methods	Pollutant (Volume)	Light Source	Unmodified	Modified	Ref.
Pt-TiO$_2$ nanoparticles (mixed anatase and brookite phases)	0.8 wt% Pt-TiO$_2$	0.2 g/L	Sol–gel method	6 mg/L MB(50 mL)	UVC	-	57% within 60 min	[358]
Pt-TiO$_2$ nanoparticles (mixed anatase and brookite phases)	0.5 mol% Pt-TiO$_2$	1 g/L	Sol–gel method	10 mg/L PNP (100 mL)	UV/Visible light	50 and 20% for UV/Visible light and visible light, respectively for Degussa P25 within 8 h	80 and 45% for UV/Visible light and visible light, respectively within 8 h	[127]
Pt-TiO$_2$ nanoparticles (mixed anatase and brookite phases)	3 wt% Pt-HPT	0.3 g/L	Hydrothermal method	10 mg/L RhB (100 mL)	UV/Visible light	0.0013 min^{-1} for core(metal)-shell (TiO$_2$) within 180 min	63% (0.0053 min^{-1}) within 180 min	[359]
Pt-TiO$_2$ nanoparticles (mixed anatase and brookite phases)	10 wt% Pt-TiO$_2$	0.3 g/L	Polyol method	1000 mg/L DCA (100 mL)	UV	34.6% within 420 min	100% within 420 min	[344]

CIP: ciprofloxacin; LP: laser pyrolysis; HPT: highly porous TiO$_2$; DCA: dichloroacetic acid; MG: malachite green; MO: methyl orange; MB: *p*-nitrophenol; methylene blue; PNP: RhB: rhodamine B.

4.2.4. Modification with Ruthenium (Ru)

Modifying with ruthenium (Ru) can reduce the Egap of TiO_2, allowing the visible light-driven photocatalysts, and acts as an electron acceptor/donor, which efficiently minimizes the recombination due to acceleration of electron transfer [360,361]. Ru-TiO_2 nanotubes have been widely used for the photocatalytic degradation of organic pollutants under visible or UV light [362,363]. Table 18 presents the summary of recent progress on Ru-TiO_2 photocatalysts for organic pollutants degradation.

Table 18. Summary of recent progress on Ru-TiO$_2$ photocatalysts for organic pollutants degradation.

Materials (TiO$_2$ Phase Transition)	Optimum	Catalyst Dosage	Synthetic Methods	Pollutants (Volume)	Light Source	Unmodified	Modified	Ref.
Ru-TiO$_2$ nanotube arrays (anatase phase)	0.15 wt%Ru-TiO$_2$	-	Anodic oxidation	0.11 M TB (20 mL)	UV/Visible light	84 and 26% under UV and visible light, respectively within 120 min	82 and 28% under UV and visible light, respectively within 120 min.	[364]
[Ru(4,4′-dicarboxy-2,2′-bipyridine)$_3$]Cl$_2$ (RuC)-TiO$_2$ (anatase phase)	-	0.2 g	Hydrothermal method	20 mg/L Bromophenol blue (500 mL)	UV	0.0018 min^{-1} within 120 min	0.0038 min^{-1} within 120 min	[365]
Ru-TiO$_2$ nanoparticles (mixed anatase and brookite phases)	0.2 wt% Ru-TiO$_2$	0.002/L	Incipient wet impregnation method	100 mg/L 2-CP (500 mL)	UV/Visible light	45 and 40% for UV and visible light, respectively within 60 min for pure TiO$_2$.	61 and 53% for UV and visible light, respectively within 60 min.	[366]
RuO$_2$/TiO$_2$ composite nanotube arrays (anatase phase)	0.0030 mol/L Ru-TiO$_2$	-	Anodic oxidation method combined with dipping	8 mg/L MB (12 mL)	Fluorescent lamp	37.8% within 2 h	69% within 2 h	[362]
Ru-TiO$_2$ nanotube arrays (mixed anatase and brookite phases)	0.16 wt% Ru-TiO$_2$	0.01 mol L^{-1}	Electrochemical anodization	4 ppm TB (-)	UV	0.0150 min^{-1}; 81.4% color removal within 120 min	1.33 higher activity than the unmodified TiO$_2$	[363]

2-CP: 2-chlorophenol; PNP: *p*-nitrophenol; MB: Methyl blue; TB: Terasil blue.

4.2.5. Modification with Palladium (Pd)

Modification of TiO_2 with Palladium (Pd) has also received some attention due to their good stability coupled with high effectivity [367]. Pd is one of the most active elements for interacting with the surface of oxides as support. It has been revealed that the absorbability in the visible light region notably increases with the Pd incorporation; moreover, this metal can act as trapping sites for electrons and hence increase the photocatalytic activity of TiO_2. Table 19 presents the summary of recent progress on Pd-TiO_2 photocatalysts for organic pollutants degradation.

Table 19. Summary of recent progress on Pd-TiO$_2$ photocatalysts for organic pollutants degradation.

Materials (TiO$_2$ Phase Transition)	Optimum	Catalyst Dosage	Synthetic Methods	Pollutants (Volume)	Light Source	Unmodified	Modified	Ref.
Pd-TiO$_2$ nanoparticles (anatase phase)	0.5 wt% Pd-TiO$_2$	0.01 g	Sol–gel methods	20 mg/L MB, MO (1 L)	UV	96.7% (0.024 min^{-1}) and 82.5% (0.012 min^{-1}) for MB and MO, respectively within 120 min.	92.6% (0.018 min^{-1}) and 99.4% (0.044 min^{-1}) for MO and MB, respectively within 120 min. The catalytic performance remained nearly unchanged and the degradation of MB was maintained at 95.9% after 10 continuous cycles.	[368]
Pd-TiO$_2$ flower-like structures (anatase phase)	2 wt% Pd-TiO$_2$	0.01 g	UV light-induced method	10 mg/L BPA (500 mL)	UV/Visible light	100% within 45 min.	100% within 45 min, 50% within 10 min under UV light; 100% within 240 min under visible light. The rate constants were 2.92, and 3.88 times higher than the P25 TiO$_2$. Furthermore, they were 1.65 and 1.91 times higher than those of unmodified TiO$_2$ under visible and UV lights, respectively.	[369]
Pd-TiO$_2$ nanoparticles (mixed anatase and brookite phases)	1.3 wt% Pd-TiO$_2$	0.01 g/L	Photodeposition	20 mg/L MB (100 m)	Xenon Lamp	0.008 min^{-1} within 45 min.	0.023 min^{-1} within 45 min.	[370]
Pd-TiO$_2$ nanoparticles (anatase phase)	1 wt% Pd-TiO$_2$	1 g/L	Hydrothermal	5 mM Oxalic acid (100 mL)	Fluorescent lamps	50, 54, and 87% for bare Aldrich rutile, bare P25 and P25 (cubical), respectively within 2 h,	96, 70, 72% for AA-Pd(spherical), AA-Pd(cubical), P25-Pd(spherical), respectively within 120 min. ~100 for AR-Pd(cubical) within 100 min	[371]
Pd-TiO$_2$ nanoparticles (anatase phase)	1 wt% Pd-TiO$_2$	1 g/L	Hydrothermal	0.5 mM Phenol	Fluorescent lamps	87, 63, 41% for P25, AA and bare Aldrich rutile, respectively within 2 h	72, 66, 98, 90, 75, and 71% for P25-Pd (spherical), P25-Pd(cubical), AA-Pd(spherical), AA-Pd(cubical), AR-Pd(spherical)), and AR-Pd(cubical), respectively within 2 h.	[371]

AA: Aldrich anatase; AR: Aldrich rutile; P25: Evonik AEROXIDE P25; BPA: bisphenol A; MB: methyl blue; MO: methyl orange.

4.3. Modification with Rare Earth Metals

Modifying with yttrium (Y) was found to be successful for improving the photocatalytic response of TiO_2 under visible light irradiations [372,373]. Y-TiO_2 can be synthesized using different techniques such as deposition–precipitation with urea, sol–gel, impregnation and chemical coprecipitation method. It has been reported that Y-TiO_2 gives improved photocatalytic response attributed to the visible light absorption, electron–hole pairs separation, higher interfacial charge transfer, lower crystallite size, and high specific surface area. Niu et al. [372] found that introducing yttrium shifted the absorption edge of TiO_2 towards visible light, reduced the crystallite size, inhibited anatase to rutile phase transformation and decreased the photogenerated electron–hole pair recombination. Table 20 presents the summary of recent progress on Y-TiO_2 photocatalysts for organic pollutants degradation.

Table 20. Summary of recent progress on Y-TiO_2 photocatalysts for organic pollutants degradation.

Materials (TiO_2 Phase Transition)	Optimum	Catalyst Dosage	Synthetic Methods	Pollutants (Volume)	Light Source	Unmodified	Modified	Ref.
Y-TiO_2 nanoparticles (Anatase phase)	-	4 cm^2	Electrochemical method	0.21 mM Toluene (200 µL)	Visible light	9% within 60 min	21% within 60 min	[374]
Y^{3+}/TiO_2 nanoparticles (Anatase phase)	0.25 mol% Y^{3+}/TiO_2	0.125 g	Hydrothermal methods	0.21 mM Phenol (100 mL)	UV/Visible light	2.40 h^{-1} within 60 min	3.85 h^{-1} within 60 min	[375]
Y^{3+}/TiO_2 nanoparticles (Anatase phase)	0.25 mol% Y^{3+}/TiO_2	0.125 g	Sol–gel methods	0.21 mM Phenol (-)	UV/Visible light	2.40 h^{-1} within 60 min	1.43 h^{-1} within 60 min	[375]

Modification with lanthanide ions can form complexes with various Lewis bases such as thiols amines, alcohols due to the interaction of their f-orbitals with different functional groups. Adding lanthanides in TiO_2 lattice suppresses e^- to h^+ recombination and also increases the adsorptive capacity of the model pollutants [376]. It also stabilizes the mesoporous structure, prevents agglomeration, and increases thermal stability [53,377]. The common lanthanides include lanthanum (La), erbium (Er), neodymium (Nd), gadolinium (Gd), thulium (Tm), ytterbium (Yb), holmium (Ho), terbium (Tb), praseodymium (Pr), samarium (Sm), and europium (Eu).

Among the lanthanide ions, modifying TiO_2 with cerium (Ce) has received considerable attention due to the following: (1) it forms labile oxygen vacancies easily with the relatively high mobility of bulk oxygen species (2) the redox couple $Ce^{3}+/Ce^{4+}$ with the ability of ceria to shift between Ce_2O_3 and CeO_2 under reducing and oxidizing conditions [378–380]. This enables Ce to reduce e- to h^+ recombination within TiO_2 via the trapping of an electron. The cerium ions (Ce^{3+}/Ce^{4+}) have variable valence states with multi-electron energy levels [381]. CeO_2 has a strong absorption ability to UV light with a small bandgap [382], its electrons are easy to jump and the 5d and 4f orbitals of Ce^{4+} are without electrons, which leads to large deformation and strong polarization which allows for effective separation of photoinduced carriers and the improvement of the photocatalytic activity of TiO_2 [383]. Ce-TiO_2 materials can be prepared by hydrothermal and sol–gel methods [380,384–386].

Xie et al. [387] prepared the monodisperse Ce-TiO_2 microspheres via a facile solvothermal process. Their results showed that the photocatalytic activity of TiO_2 was improved activity for MB under visible light irradiation upon introduction with Ce. Aman et al. [388] presented a 5% Ce-TiO_2 and their results show an improved activity for MB (50 ppm) with photodegradation of MB of ~100% within 60 min in the presence of visible light. Table 21 presents the summary of recent progress on lanthanides modified TiO_2 photocatalysts for organic pollutants degradation.

Table 21. Summary of recent progress on lanthanides modified TiO_2 photocatalysts for organic pollutants degradation.

Material (TiO_2 Phase Transition)	Optimum	Catalyst Dosage	Synthetic Methods	Pollutants (Volume)	Light source	Unmodified	Modified	Ref.
Er-TiO_2 mesoporous spheres (anatase phase)	1 mM of Er-TiO_2	1 g	Solvothermal method	10 ppm RhB (50 mL)	Visible light	84.27% (0.0428 min^{-1}) within 60 min	98.78% (0.1544 min^{-1}) within 60 min	[389]
Ce-TiO_2 nanoparticles (mixture of anatase and rutile phases)	1% Ce-TiO_2	0.5 g/L	Facile EDTA-citrate method	10 mg/L CIP, NOR (200 mL)	Sunlight	69.29 and 75% for CIP and NOR, respectively within 180 min	90–93% for both CIP and NOR within180 min	[390]
Ce-TiO_2 nanoparticles (anatase phase)	0.5% Ce-TiO_2	0.5 g	Facile hydrothermal method	MEK (200 mL)	Visible light	-	76% for 0.5% Ce-TiO_2	[391]
Ce-TiO_2 nanoparticles (anatase phase)	0.5% Ce-TiO_2	0.5 g	Facile hydrothermal method	MEK (200 mL)	UV	-	62% for 0.5% Ce-TiO_2	[391]
Ce-TiO_2 nanoparticles (anatase phase)	0.41% Ce-TiO_2	10 mg/cm^2	Sol–gel method	25 mg/L DB15	Visible light	3.3% within 1 h	33% within 1 h	[216]
Ce-TiO_2 mesoporous (mixture of anatase and rutile phases)	2.5% Ce-TiO_2	0.001 g	EISA approach	20 mg/L Phenol (100 mL)	UV	-	95–99% within 4 h	[392]
Ce-TiO_2 nanocrystalline films (anatase phase)	2.5% Ce-TiO_2	-	EISA approach	20 mg/L Phenol (100 mL)	Solar light	99% within 4 h for the mesoporous TiO_2	55-68% within 4 h	[392]
Ce-TiO_2 nanocrystalline films (anatase phase)	10% Ce-TiO_2	0.05 g	Sol–gel method	2.5×10^{-5} M BB-41 (80 mL)	UV	16.8×10^{-3} min^{-1} within 180 min	15.9×10^{-3} min^{-1} within 180 min	[393]
Ce-TiO_2 nanocrystalline films (anatase phase)	12% Ce-TiO_2	0.05 g	Sol–gel method	2.5×10^{-5} M BB-41 (80 mL)	Visible light	11.2×10^{-3} min^{-1} within 180 min	16.1×10^{-3} min^{-1} within 180 min	[393]
CeO_2/TiO_2 core-shell nanoparticles (anatase phase)	-	0.04 g	Hydrothermal route assisted with the Stöber method	1×10^{-5} M RhB (40 mL)	Xe arc-lamp	0.004 min^{-1} for CeO_2 nanocubes and 0.003 min^{-1} for unmodified TiO_2 within 120 min	0.012 min^{-1} within 120 min	[394]
CeO_2/TiO_2 nanoparticles (mixture of anatase and rutile phases)	0.25% CeO_2/TiO_2	0.1 g	Sol–gel method	40 ppm MB (100 mL)	Visible light	96.43% within 150 min	97.86% within 150 min	[395]
Ho-TiO_2 nanotubes (anatase phase)	-	4 cm^2	Electrochemical method	0.21 mM Toluene (200 μL)	Visible light	9% within 60 min	30% within 60 min	[374]
Er-TiO_2 nanotubes (anatase phase)	-	4 cm^2	Electrochemical method	0.21 mM Toluene (200 μL)	Visible light	9% within 60 min	22% within 60 min	[374]

<div align="center">**Table 21.** *Cont*.</div>

Material (TiO$_2$ Phase Transition)	Optimum	Catalyst Dosage	Synthetic Methods	Pollutants (Volume)	Light source	Unmodified	Modified	Ref.
Gd-TiO$_2$ nanotubes (anatase phase)	-/	4 cm^2	Electrochemical method	0.21 mM Toluene (200 μL)	Visible light	9% within 60 min	28% within 60 min	[374]
Tb-TiO$_2$ nanotubes (anatase phase)	-	4 cm^2	Electrochemical method	0.21 mM Toluene (200 μL)	Visible light	9% within 60 min	28% within 60 min	[374]
Nd^{3+}/TiO$_2$ nanosphere (anatase phase)	1.0 mol% Nd^{3+}/TiO$_2$	0.05 g	template-free method (recombined coprecipitation with hydrothermal method	20 mg/L MB (50 mL)	Visible light	91.83% (0.46 h^{-1}) within 120 min	99.14% (2.3 h^{-1}) within 120 min	[396]
Nd^{3+}/TiO$_2$ nanosphere (anatase phase)	1.0 mol% Nd^{3+}/TiO$_2$	0.05 g	template-free method (recombined coprecipitation with hydrothermal method	20 mg/L MB (50 mL)	Sunlight	60.09% of dyes degraded without catalyst	almost completely degradation within 80 min.	[396]
Nd-TiO$_2$ nanoparticles (anatase phase)	2.0 mM Nd-TiO$_2$	0.02 g	Sol–gel method	40 mg/L CR (100 mL)	UV	64% within 30 min	86% within 30 min, the photocatalytic efficiency after utilizing five times was more than 92%.	[397]
Nd-TiO$_2$ nanoparticles (anatase phase)	2.0 mM Nd- TiO$_2$	0.02 g	Sol–gel method	40 mg/L MB (100 mL)	UV	74% within 45 min	92% within 45 min, the photocatalytic efficiency after utilizing five times was more than 92%.	[397]
Yb^{3+}/TiO$_2$ nanoparticles (anatase phase)	1% Yb^{3+}/TiO$_2$	0.05 g	Sol–gel method	0.21 mM phenol (5 mL)	Visible light	45% within 180 min	89% within 180 min	[398]
Er^{3+}/TiO$_2$ nanoparticles (anatase phase)	0.5% Er^{3+}/TiO$_2$	0.05 g	Sol–gel method	0.21 mM Phenol (5 mL)	Visible light	-	75% within 180 min	[398]
Er^{3+}/TiO$_2$ nanoparticles (anatase phase)	2 mol% Er^{3+}/TiO$_2$	0.025 g	Electrospinning	10 mg/L MO (25 mL)	Solar light	78% within 60 min	43% within 60 min	[399]
Er^{3+}/TiO$_2$ nanoparticles (anatase phase)	0.5 mo% Er^{3+}/TiO$_2$	0.05 g	Electrospinning	10^{-5} mol/L RhB (25 mL)	Solar light	71.3% within 10 h	91.3% within 10 h	[399]
Er^{3+}/TiO$_2$ nanoparticles (anatase phase)	0.5 mol% Er^{3+}/TiO$_2$	0.05 g	Electrospinning	20 mg/L Phenol (25 mL)	Solar light	23.9% within 72 h	46.1% within 72 h	[399]
Yb-TiO$_2$ nanoparticles (anatase phase)	10% Yb-TiO$_2$	1 g/L	Hydrothermal process	10 ppm Phenol (100 mL)	Solar light	~Initial Rate with 31.9 mol/L/h	~Initial Rate with 54 mol/L/h	[400]

Table 21. *Cont.*

Material (TiO$_2$ Phase Transition)	Optimum	Catalyst Dosage	Synthetic Methods	Pollutants (Volume)	Light source	Unmodified	Modified	Ref.
Er-TiO$_2$ nanoparticles (anatase phase)	2% Er-TiO$_2$	1 g/L	Hydrothermal process	10 ppm Phenol (100 mL)	Solar light	~Initial Rate with 31.9 mol/L/h	~Initial Rate with 144 mol/L/h	[400]
Gd-TiO$_2$ nanoparticles (anatase phase)	1.8 at% Gd- TiO$_2$	0.1 g	Sol–gel method sintering at 550 °C	20 mg/L CR (100 mL)	UV	42% within 1 h	76% within 1 h	[401]
Gd-TiO$_2$ nanoparticles (anatase phase)	1.8 at% Gd- TiO$_2$	0.1 g	Sol–gel method sintering at 700 °C	20 mg/L CR (100 mL)	UV	35% within 1 h	84% within 1 h	[401]
Sm-TiO$_2$ nanoparticles (anatase phase)	1.8 at% Sm-TiO$_2$	0.1 g	Sol–gel method sintering at 700 °C	20 mg/L CR (100 mL)	UV	35% within 1 h	74% within 1 h	[401]
Sm-TiO$_2$ nanoparticles (anatase phase)	1.8 at% Sm-TiO$_2$	0.1 g	Sol–gel method sintering at 550 °C	20 mg/L CR (100 mL)	UV	42% within 1 h	70% within 1 h	[401]
Er-TiO$_2$ nanotube arrays (anatase phase)	10 wt% Er-TiO$_2$	-	Electrochemical anodization	0.5 mM Toluene (8 mL)	Visible light	-	2.85×10^{-3} µmol·min^{-1} within 60 min	[402]
Ho-TiO$_2$ nanotube arrays (anatase phase)	10 wt% Ho-TiO$_2$	-	Electrochemical anodization	0.5 mM Toluene (8 mL)	Visible light	-	2.87×10^{-3} µmol·min^{-1} within 60 min	[402]
Gd-TiO$_2$ nanoparticles (anatase phase)	0.3% Gd-TiO$_2$	0.01 g	Sol–gel method	10 mg/L RhB (10 mL)	Visible light	75% within 240 min	93% within 240 min	[403]
La-TiO$_2$ nanoparticles (mixture of anatase and rutile phases)	0.05 La-TiO$_2$	1 g/L	Ultrasound-assisted wet impregnation method	10 mg/L MB (1 L)	UV	0.1372 ± 0.0038 min^{-1} and 0.1332 ± 0.0051 min^{-1} for pristine TiO$_2$ and P25-TiO$_2$, respectively within 30 min	0.1528 ± 0.0017 min^{-1} within 30 min	[404]
Gd-TiO$_2$ nanoparticles (anatase phase)	3% Gd^{3+}/TiO$_2$	0.05 g	Impregnation method	20 mg/L RhB (60 mL)	Mercury lamp	75% within 50 min	81–96% within 50 min	[405]
Ce^{3+}/TiO$_2$ nanoparticles (mixture of anatase and rutile phases)	1 mol% Ce^{3+}/TiO$_2$	0.2 g/L	Combustion synthesis method	20 mg/L MB (100 mL)	Visible light	41% within 120 min	72% within 120 min	[406]
La-TiO$_2$ nanoparticles (anatase phase)	1.0% La–TiO$_2$	0.05 g	Sol–gel method	10 mg/L RhB (100 mL)	562-nm Xenon Lamp	21.56% within 300 min	11.09% within 300 min	[74]
Ce-TiO$_2$ nanoparticles (anatase phase)	1.0% Ce–TiO$_2$	0.05 g	Sol–gel method	10 mg/L RhB (100 mL)	562-nm Xenon Lamp	21.56% within 300 min	83.43% within 300 min	[74]
Eu-TiO$_2$ nanopowders (anatase phase)	3% Eu-TiO$_2$	0.125 molL^{-1}	Sol–gel method	20 mg/L MB (250 mL)	Xenon Lamp	0.08124 min^{-1} within 6 h	0.03719 min^{-1} within 6 h	[119]
Gd-TiO$_2$ nanopowders (anatase phase)	1 wt% Gd-TiO$_2$	0.1 g	Sol–gel method	10 mg/L MO (100 mL)	Visible light	31% within 180 min	78% within 180 min	[205]

Table 21. *Cont.*

Material (TiO$_2$ Phase Transition)	Optimum	Catalyst Dosage	Synthetic Methods	Pollutants (Volume)	Light source	Unmodified	Modified	Ref.
Gd-TiO$_2$ nanopowders (anatase phase)	1 wt% Gd-TiO$_2$	0.1 g	Sol–gel method	10 mg/L 4-CP (100 mL)	Visible light	28% within 180 min	69% within 180 min	[205]
Eu-TiO$_2$ nanoparticles (anatase phase)	10% Eu-TiO$_2$	0.3 g	LPP process	50 mg/L ASA (250 mL)	Blue light	0.685×10^{-3} min^{-1} within 24 h	1.475×10^{-3} min^{-1} within 24 h	[407]
Eu-TiO$_2$ nanoparticles (anatase phase)	10% Eu-TiO$_2$	0.3 g	LPP process	50 ppm ASA (250 mL)	UV	9.37×10^{-3} min^{-1} within 24 h	10.65×10^{-3} min^{-1} within 24 h	[407]

at. %: atomic %; NOR: norfloxacin; MEK: methyl ethyl ketone; EE2: 17-α-ethinylestradiol; DB15; direct blue 15; BB-41: basic blue 41; RhB: rhodamine B; LPP: liquid phase plasma; MB: methylene blue; ASA: acetylsalicylic acid; RB: reactive blue; Cr: Congo red; MO: methyl orange; CIP: ciprofloxacin; 4-CP: 4-chlorophenol; EISA: evaporation-induced self-assembly.

4.4. Modification with Other Metal Ions

The other metal ions are also introduced in TiO_2 crystal lattices to replace Ti ions, thus improving the transferring rate of interfacial electrons, lowering the recombination between e^- and h^+, and adjusting the energy band structure [408]. Simultaneously, the energy level is introduced into the bandgap of TiO_2 to broaden the absorption band edge to the visible light range, and finally, improve the activity of TiO_2 under visible light [408,409].

Indium (In)-TiO_2 has been observed to increase the photoelectron chemical responses and photocatalytic activity of TiO_2 by enhancing the transfer of electrons and reduction in recombination rate of photoinduced charge carriers due to its CB/VB potential difference from TiO_2 [410,411]. Indium has lower toxicity, is relatively cheap, and has multiple oxidation states (In°, In^{+1}, In^{+3}), which can help to improve charge mobility and electron trapping over the surface of TiO_2 [412]. The result by [413] shows an enhanced photocatalytic activity for 2,4-dichlorophenoxyacetic acid in the presence of UV light irradiation. Pozynak et al. [414] reported an efficient separation of photogenerated charges in nanocrystalline In_2O_3/TiO_2 photocatalyst during the degradation of 2-CP.

The presence of transition metal such as Gallium ion (Ga^{3+}) at the Ti^{4+} sites can induce oxygen vacancies gaps [415,416] and build deficiencies near the CB in TiO_2, which function as electron traps and increase the isolation of e- to h^+ pairs [417,418]. Simultaneously, modifying with Ga shift the absorption edge towards visible regime as well as improving the separation between photoexcited charge carriers [419]. The synthesis of Ga–TiO_2 can be achieved by laser pyrolysis [420], sol–gel method [417], traditional solid-state reaction [421,422], and hydrothermal method [419,423–425]. However, these methods often require either a high experimental temperature to promote the reactions [420] or post heat treatment for crystallization [417,423]. Generally, a higher heating temperature always leads to grain growth and agglomeration, which decreases the specific surface area and is detrimental to photocatalytic activity. Table 22 presents the summary of recent progress on other metals modified TiO_2 photocatalysts for organic pollutants degradation.

Table 22. Summary of recent progress on other metals modified TiO_2 photocatalysts for organic pollutants degradation.

Materials (TiO_2 Phase Transition)	Optimum	Catalyst Dosage	Synthetic Methods	Pollutants (Volume)	Light Source	Unmodified	Modified	Ref.
Ga^{3+}-TiO_2 nanoparticles (anatase phase)	0.5 wt% Ga^{3+}-TiO_2	0.1 g	Ultrasonic irradiation	20 mg/L MB (100 mL)	Solar light	70.6% (0.0096 min^{-1}) in 150 min	86.4% (0.021 min^{-1}) in 150 min	[418]
In_2O_3-TiO_2 nanopowders (anatase phase)	5 mol% In_2O_3/TiO_2	0.5 g	Sol–gel method	200 mg/L CR (-)	UV	0.15 h^{-1} in 4 h	0.86 h^{-1} in 4 h	[426]
In_2O_3-TiO_2 nanorods (anatase phase)	0.4 wt% In_2O_3/TiO_2	1 × 1.5 cm^2	Hydrothermal method	10 uM MO (-)	Sunlight	86% in 6 h	94% in 6 h	[427]
In_2O_3-TiO_2 nanorods (anatase phase)	0.4 wt% In_2O_3/TiO_2	1 × 1.5 cm^2	Hydrothermal method	2.5 uM BPA (-)	Sunlight	65% in 6 h	68% in 6 h	[427]
In_2O_3-TiO_2 nanoparticles (mixture of anatase and rutile phases)	0.15 mol% In_2O_3/TiO_2	0.5 g	Sol–gel method	8 mg/L MB (100 mL)	high-voltage Mercury lamp	40 and 42% in 7 h for pure TiO_2 and P25, respectively.	~80% in 7 h	[350]
TiO_2-In_2O_3 porous structure and spherical morphology (anatase phase)	1 mol% In_2O_3/TiO_2	0.02 g	UAS assisted method	10 ppm MO (20 mL)	Visible light	26% in 5 h for pure In_2O_3	~98% within 5 h	[411]
TiO_2-In_2O_3 porous structure and spherical morphology (anatase phase)	1 mol% In_2O_3/TiO_2	0.02 g	UAS assisted method	10 ppm RhB (20 mL)	Visible light	18% in 3 h for pure In_2O_3	95% within 3 h	[411]
Ga^{3+}-TiO_2 nanoparticles (anatase phase)	0.5 wt% Ga^{3+}-TiO_2	-	Ultrasonic irradiation	20 ppm Phenol (100 mL)	Solar	0.0052 $min-1$ in 180 min	0.021 min^{-1} and ~4 times higher activity than unmodified TiO_2	[418]
Ga-TiO_2/rGO nanoparticles (mixed anatase and rutile phases)	1.0 wt% Ga-TiO_2/rGO	0.01 g	Simple synthesis process	10 mg/L RB dye (-)	Visible light	0.0015 min^{-1} in 180 min	0.0029 min^{-1} in 180 min	[428]
Ga_2O_3-TiO_2 nanoparticles (anatase phase)	0.1% Ga_2O_3-TiO_2	0.05 g	Sol–gel method	0.08 mmol/L Imazapyr (100 mL)	UV	19% in 180 min for mesoporous Ga_2O_3.	98% within 180 min (10 times higher than the mesoporous Ga_2O_3). The photodegradation efficiency of imazapyr continues to maintain over 95% after five cycles.	[429]
Al-TiO_2 nanoparticles (anatase to rutile phase)	0.25% Al-TiO_2	2 g/L	Impregnation method	10^{-6} M MB (100 mL)	LED lamp	75% within 60 min for P-25	-	[430]

Table 22. *Cont.*

Materials (TiO$_2$ Phase Transition)	Optimum	Catalyst Dosage	Synthetic Methods	Pollutants (Volume)	Light Source	Unmodified	Modified	Ref.
Al-TiO$_2$ nanoparticles (anatase to rutile)	0.25% Al-TiO$_2$	0.5 g/L	Impregnation method	10^{-6} M MB (100 mL)	LED lamp	-	80% in 60 min	[430]
Al-TiO$_2$ nanoparticles (anatase to rutile)	0.25% Al-TiO$_2$	1 g/L	Impregnation method	MB (100 mL)	LED lamp	-	85% in 60 min	[430]
Sn-TiO$_2$ nanoparticles (anatase to rutile)	1% Sn-TiO$_2$	0.2 g	Sol–gel method	600 ppm DES (-)	Solar light	38% in 90 min, 48% in 180 min	~100% in 90 min, 75% in 150 min	[431]
Sn-TiO$_2$ nanoparticles (anatase to rutile phase)	5 mol% Sn-TiO$_2$	0.005 g	Sol–gel method	10 mg/L MB (25 mL)	Solar lamp	98% within 60 min for TiO$_2$-NTs, 94% within 60 min for TiO$_2$–P25	98% (reaction rate of 0.1215 min^{-1} which is 1.8 and 2.7 times as much as those of TiO$_2$-NTs and TiO$_2^-$P, respectively) within 30 min	[432]
Sn-TiO$_2$ nanoparticles (anatase to rutile phase)	1 mol% Sn-TiO$_2$	0.3 g	Sol−gel method	10 mg/L RhB (300 mL)	UV	46.2% within 180 min	99.5% (0.02732 min^{-1}) within 180 min	[433]
Sn-TiO$_2$ Hollow Spheres	1 mol% Sn-TiO$_2$	0.025 g	Sol−gel method templated by polystyrene spheres	0.00385 g/L MO (50 mL)	UV	~55% within 240 min	~72% within 240 min	[434]
SnO$_2$-TiO$_2$ nanoparticles (anatase to rutile phase)	1% Sn-TiO$_2$	1 g/L	Sonication–impregnation method	10 mg/L TC (-)	Visible light	-	95% within 15 min, 81–95% within 20 min	[435]
Sn-TiO$_2$ nanoparticles (anatase phase)	0.20 ± 0.03% Sn-TiO$_2$	-	Washcoating method	ERY (1 L)	UV-A	~18% within 240 min	67% within 240 min, 50% within 2280 min	[436]
Sn-TiO$_2$ nanoparticles	5% Sn-TiO$_2$	0.8 g/L	Hydrothermal method	10 mg/L DCF (-)	UV	~62% within 300 min	89% within 300 min 53% after 4 cycles (1200 min)	[437]
Sn-TiO$_2$ nanoparticles	1 mol% Sn-TiO$_2$	0.2 g	Sol−gel method	40 ppm 2,4-DCA (-)	UV	77% within 180 min	93% (16.8 × 10^{-3} min^{-1}) within 180 min	[438]
Al^{3+}/TiO$_2$ nanoparticles (mixed anatase and brookite phases)	0.5 mol% Al^{3+}/TiO$_2$	1 g/L	Sol−gel method	10^{-4} M PNP (100 mL)	UV/Visible light	50 and 20% under UV/Visible and visible light, respectively for Degussa P25 within 8 h,	64 and 24% under UV/Visible and visible light, respectively within 8 h	[127]

PNP: *p*-nitrophenol; CR: Congo red; UAS: Ultrasonic aerosol spray; MB: methylene blue; RhB: rhodamine B; DCA: dichloroacetic acid; DCF: diclofenac; ERY: erythromycin; TC: tetracycline; MO: methyl orange; BPA: bisphenol A; RB: reactive blue.

5. Conclusions and Future Outlooks

TiO_2 is the most widely used photocatalyst for the photodegradation of organic pollutants. This paper presents the recent development of metal ion modified TiO_2 for the photodegradation of organic pollutants. Among the metal ions, metal such as Ni, Fe, Co, Cu, Au, Ag, Zr, W, and Mn have been widely explored and found to show beneficial influence on photocatalytic activity. However, the application of metal ion modified TiO_2 photocatalyst for organic pollutants continues to be limited due to several obstacles (preparation method, security, cost, commercial use, and efficiency). Some of the recommendations drawn from this review are listed as follows:

The activity of TiO_2 photocatalyst has a lot to do with its preparation method. The preparation methods are different, and the shape and size, surface, and structural properties of the catalyst are different. The main methods for preparing metal ion modified TiO_2 include sol–gel, precipitation, immersion, and hydrothermal method. It was found that the samples prepared by sol–gel and hydrothermal methods produce better results. Its photocatalytic performance is much higher than that of photocatalysts prepared by other methods. This is mainly because the reaction process of these two methods is simple, the operation is controllable, and the prepared powder has a relatively small particle size, high purity, and good chemical uniformity. However, there is a limitation in the long preparation cycle. Therefore, future research should be devoted to new ways to find simple and effective ways to improve some defects of metal ions modified TiO_2.

There is a need for continuous in-depth study on the use of sunlight irradiation, and the economical applicability of this approach for removing organic pollutants. To date, various metal ion modified TiO_2 photocatalysts have been developed and reported. However, their preparations consume considerable chemicals which are expensive, time-consuming and complex. Traditional TiO_2 is generally a massive particle, and the control of the morphology of TiO_2 is an effective way to increase their contact with pollutants. For example, the preparation of hollow, porous, or larger specific surface area TiO_2 nanoscale particles can effectively solve the traditional small contact surface of TiO_2 and pollutants. In addition, TiO_2 itself can be modified to add its hydrophilic functional groups. It can increase the compatibility of TiO_2 with H_2O, thereby promoting the working process of TiO_2. Therefore, it is a necessity to develop a relatively scalable, inexpensive, environmentally friendly, and easy synthesis route.

There are also many defects in the application of TiO_2 in daily life. The limiting factor for its development is the photocatalytic performance problem. In addition, if the traditional photocatalyst is unmodified, it cannot adapt to the change to other light sources (e.g., sunlight). The water body purified by TiO_2 in daily life will take away part of the TiO_2, and at the same time, the photocatalytic degradation of organic pollutants often produces some intermediate products. However, in most cases, the toxicity of the intermediate products tends to be stronger than the initial organic pollutants, and as a consequence poses greater harm to the environment and human beings. Therefore, there is a need for an extensive toxicological study of these intermediate products. Therefore, in terms of these issues, how to improve the flexibility of particles in practical applications and how to improve the safety of TiO_2 also needs to be considered in future research.

The applicability of this method requires additional engineering amplification testing. However, it is hoped that through rapid and continuous evaluation of the pilot plant configuration, a large-scale solar-driven photocatalytic activity treatment process with low site area requirements and high efficacy can be realized in near future. Furthermore, the majority of the studies use artificial organic pollutants and studying the performance of TiO_2 photocatalysts under real situations should be the focus of future work.

Finally, we hope that this paper can assist researchers to better understand the recent trend in the removal of organic pollutants using metal ion modified TiO_2 photocatalysts and also hope that this field can flourish in the future.

Author Contributions: Conceptualization, D.J., T.A.O.; methodology, T.A.O., D.J.; software, N.F.S.; resources, S.L., T.A.O., D.J.; writing—original draft preparation, T.A.O., D.J., Y.O.; writing—review and editing, T.A.O., D.J., Y.O., N.F.S.; project administration, S.L., T.A.O.; funding acquisition, S.L.; supervision, S.L., T.A.O., S.W., A.Z. All authors have read and agreed to the published version of the manuscript.

Conflicts of Interest: The authors declare no conflict of interest.

Abbreviations

$^{\bullet}$OH: hydroxyl radicals; 2,4-CP: 2,4-dichlorophenol; 2-CP: 2-chlorophenol; 4-CP: 4-chlorophenol; AA: Aldrich anatase; Ag: silver; AO7: acid orange 7; AOPs: advanced oxidation processes; AR: Aldrich rutile; AR-27: acid red 27; ASA: acetylsalicylic acid; at. %: atomic %; Au: gold; BB-41: basic blue 41; BO2: basic orange 2; BPA: bisphenol A; CB: conduction band; CBN: carbofuran; CFS: ceftiofur sodium; CIP: ciprofloxacin; Co: cobalt; Cr: chromium; CR: Congo red; Cu: copper; CV: crystal violet; CVD: chemical vapor deposition; DB15: direct blue 15; DCA: dichloroacetic acid; DCF: diclofenac; DEP: diethyl phthalate; DES: diethyl sulfide; DXM: dexamethasone; E131 VF: food colorant; EB: eosin blue; ECR: Eriochrome cyanine red; EE2: 17-α-ethinylestradiol; EISA: evaporation induced self-assembly; ERY: erythromycin; Fe: iron; FSP: flame spray pyrolysis; h$^+$: hole; HPT: highly porous TiO$_2$; IBP: ibuprofen; LPP: liquid phase plasma; LP: laser pyrolysis; MB: methylene blue; MBE: molecular beam epitaxy technique; MEK: methyl ethyl ketone; MG: malachite green; Mn: manganese; MNZ: metronidazole; MO: methyl orange; Mo: molybdenum; MWASG: microwave-assisted sol–gel method; Nb: niobium; NB: nitrobenzene; NHE: normal hydrogen electrode; Ni: nickel; NOR: norfloxacin; NPs: nanoparticles; NPX: naproxen; O$_2$$^{\bullet-}$: superoxide anion radicals; OG: orange G; OH$^{\bullet}$: hydroxyl radicals; OOH$^{\bullet}$: hydroperoxyl radicals; P25: Evonik AEROXIDE P25; Pd: palladium; PEC: photoelectrocatalysis with UVA light; PEOx: plasma electrolytic oxidation; Pt: platinum; PNP: p-nitrophenol; RB: reactive blue; RB5: reactive black 5; RhB: rhodamine B; RR 198: reactive red 198; Ru: ruthenium; SMX: sulfamethoxazole; SMZ: sulfamethazine; TB: Terasil blue; TC: tetracycline; TNT: titania nanotubes; TiO$_2$: titanium dioxide; TNAs: titanium nanotube arrays; UAS: ultrasonic aerosol spray; V: vanadium; VB: valence band; W: tungsten; wt.%: mass percent; Zn: zinc; Zr: zirconium.

References

1. Otitoju, T.A.; Ooi, B.S.; Ahmad, A.L. Synthesis of 3-aminopropyltriethoxysilane-silica modified polyethersulfone hollow fiber membrane for oil-in-water emulsion separation. *React. Funct. Polym.* **2019**, *136*, 107–121. [CrossRef]
2. Shoparwe, N.F.; Otitoju, T.A.; Ahmad, A.L. Fouling evaluation of polyethersulfone (PES)/sulfonated cation exchange resin (SCER) membrane for BSA separation. *J. Appl. Polym. Sci.* **2018**, *135*, 45854. [CrossRef]
3. Zhong, Q.; Lan, H.; Zhang, M.; Zhu, H.; Bu, M. Preparation of heterostructure g-C$_3$N$_4$/ZnO nanorods for high photocatalytic activity on different pollutants (MB, RhB, Cr(VI) and eosin). *Ceram. Int.* **2020**, *46*, 12192–12199. [CrossRef]
4. Wang, Y.; Li, J.; Wang, Q. The performance of daylight photocatalytic activity towards degradation of MB by the flower-like and approximate flower-like complexes of graphene with ZnO and Cerium doped ZnO. *Optik* **2019**, *204*, 164131. [CrossRef]
5. Pirgholi Givi, G.; Farjami Shayesteh, S.; Azizian, Y. Investigation of The influence of irradiation intensity and stirring rate on the photocatalytic activity of titanium dioxide nanostructures prepared by the microwave-assisted method for photodegradation of MB from water. *Phys. B Condens. Matter* **2019**, *578*, 411886. [CrossRef]
6. Lalliansanga; Tiwari, D.; Tiwari, A.; Shukla, A.; Shim, M.; Lee, S.-M. Facile synthesis and characterization of Ag(NP)/TiO$_2$ nanocomposite: Photocatalytic efficiency of catalyst for oxidative removal of Alizarin Yellow. *Catal. Today*. [CrossRef]
7. Dong, S.; Lee, G.J.; Zhou, R.; Wu, J. Synthesis of g-C$_3$N$_4$/BiVO$_4$ Heterojunction Composites for Photocatalytic Degradation of Nonylphenol Ethoxylate. *Sep. Purif. Technol.* **2020**, *250*, 117202. [CrossRef]
8. Tian, J.; Zhu, Z.; Liu, B. Novel Bi$_2$MoO$_6$/Bi$_2$WO$_6$/MWCNTs photocatalyst with enhanced photocatalytic activity towards degradation of RB-19 under visible light irradiation. *Colloids Surf. A Physicochem. Eng. Asp.* **2019**, *581*, 123798. [CrossRef]
9. Rodrigues, J.; Hatami, T.; Rosa, J.; Tambourgi, E.; Innocentini-Mei, L. Photocatalytic degradation using ZnO for the treatment of RB 19 and RB 21 dyes in industrial effluents and mathematical modeling of the process. *Chem. Eng. Res. Des.* **2020**, *153*, 294–305. [CrossRef]

10. Natesan, K.; Sinthiya, M.; Ramamurthi, K.; Ramraj, R.; Raman, S. Visible light driven photocatalytic activity of ZnO/CuO nanocomposites coupled with rGO heterostructures synthesized by solid-state method for RhB dye degradation. *Arab. J. Chem.* **2019**, *13*, 3910–3928. [CrossRef]

11. Akpan, U.G.; Hameed, B.H. Parameters affecting the photocatalytic degradation of dyes using TiO_2-based photocatalysts: A review. *J. Hazard. Mater.* **2009**, *170*, 520–529. [CrossRef] [PubMed]

12. Kang, W.; Yu, H.; Xu, T.; Wu, S.; Wang, X.; Lu, N.; Quan, X.; Liang, H. Photocatalytic ozonation of organic pollutants in wastewater using a flowing through reactor. *J. Hazard. Mater.* **2020**, *405*, 124277. [CrossRef]

13. Liao, X.; Wang, F.; Wang, Y.; Cai, Y.; Liu, H.; Wang, X.; Zhu, Y.; Chen, L.; Yao, Y.; Qinglan, H. Constructing Fe-based bi-MOFs for photo-catalytic ozonation of organic pollutants in Fischer-Tropsch waste water. *Appl. Surf. Sci.* **2020**, *509*, 145378. [CrossRef]

14. Žener, B.; Matoh, L.; Carraro, G.; Miljevic, B.; Cerc Korošec, R. Sulfur-, nitrogen- and platinum-doped titania thin films with high catalytic efficiency under visible-light illumination. *Beilstein J. Nanotechnol.* **2018**, *9*, 1629–1640. [CrossRef]

15. Hasanpour, M.; Hatami, M. Photocatalytic performance of aerogels for organic dyes removal from wastewaters: Review study. *J. Mol. Liq.* **2020**, *309*, 113094. [CrossRef]

16. Otitoju, T.A.; Jiang, D.; Ouyang, Y.; Elamin, M.A.M.; Li, S. Photocatalytic degradation of Rhodamine B using $CaCu_3Ti_4O_{12}$ embedded polyethersulfone hollow fiber membrane. *J. Ind. Eng. Chem.* **2020**, *83*. [CrossRef]

17. Diao, Y.; Yan, Z.; Guo, M.; Wang, X. Magnetic multi-metal co-doped magnesium ferrite nanoparticles: An efficient visible light-assisted heterogeneous Fenton-like catalyst synthesized from saprolite laterite ore. *J. Hazard. Mater.* **2017**, *344*, 829–838. [CrossRef]

18. Ensaldo-Rentería, M.K.; Ramírez-Robledo, G.; Sandoval-González, A.; Arellano, C.; Alvarez-Gallegos, A.; Zamudio-Lara, Á.; Silva Martínez, S. Photoelectrocatalytic oxidation of acid green 50 dye in aqueous solution using Ti/TiO_2-NT electrode. *J. Environ. Chem. Eng.* **2018**, *6*, 1182–1188. [CrossRef]

19. Alijani, M.; Kaleji, B.; Rezaee, S. Highly visible-light active with Co/Sn co-doping of TiO_2 nanoparticles for degradation of methylene blue. *J. Mater. Sci. Mater. Electron.* **2017**, *28*, 15345–15353. [CrossRef]

20. Wei, Z.; Liu, D.; Wei, W.; Chen, X.; Han, Q.; Yao, W.-Q.; Ma, X. Ultrathin $TiO_2(B)$ Nanosheets as the Inductive Agent for Transfering H_2O_2 into Superoxide Radicals. *ACS Appl. Mater. Interfaces* **2017**, *9*, 15533–15540. [CrossRef]

21. Ayode Otitoju, T.; Ugochukwu Okoye, P.; Chen, G.; Li, Y.; Onyeka Okoye, M.; Li, S. Advanced ceramic components: Materials, Fabrication, and Applications. *J. Ind. Eng. Chem.* **2020**, *85*, 34–65. [CrossRef]

22. Sangchay, W.; Kaewjang, S. SnO_2-doped TiO_2 nanostructured thin films with antibacterial properties. *AIP Conf. Proc.* **2016**, *1775*, 030023.

23. Fujishima, A.; Honda, K. Electrochemical Photolysis of Water at a Semiconductor Electrode. *Nature* **1972**, *238*, 37–38. [CrossRef] [PubMed]

24. Negishi, N.; Iyoda, T.; Hashimoto, K.; Fujishima, A. Preparation of Transparent TiO_2 Thin Film Photocatalyst and Its Photocatalytic Activity. *Chem. Lett.* **1995**, *9*, 841–842. [CrossRef]

25. Patil, N.; Uphade, B.; Jana, P.; Sonawane, R.; Bhargava, S.; Choudhary, V. Epoxidation of Styrene by Anhydrous t-Butyl Hydroperoxide over Au/TiO_2 Catalysts. *Catal. Lett.* **2004**, *94*, 89–93. [CrossRef]

26. Baran, W.; Makowski, A.; Wardas, W. The effect of UV radiation absorption of cationic and anionic dye solutions on their photocatalytic degradation in the presence TiO_2. *Dye. Pigment.* **2008**, *76*, 226–230. [CrossRef]

27. Poulopoulos, S.; Philippopoulos, C. Photo-assisted Oxidation of Chlorophenols in Aqueous Solutions Using Hydrogen Peroxide and Titanium Dioxide. *J. Environ. Sci. Health. A Tox. Hazard. Subst. Environ. Eng.* **2004**, *39*, 1385–1397. [CrossRef]

28. Ahmad, R.; Ahmad, Z.; Khan, A.; Mastoi, N.; Aslam, M.; Kim, J. Photocatalytic Systems as an Advanced Environmental Remediation: Recent Developments, Limitations and new Avenues for Applications. *J. Environ. Chem. Eng.* **2016**, *4*, 4143–4164. [CrossRef]

29. Mohite, V.S.; Mahadik, M.; Kumbhar, S.S.; Hunge, Y.; Kim, J.-H.; Moholkar, A.; Rajpure, K.; Bhosale, C. Photoelectrocatalytic degradation of benzoic acid using Au doped TiO_2 thin films. *J. Photochem. Photobiol. B* **2014**, *142C*, 204–211. [CrossRef]

30. Shinde, S.S.; Shinde, P.S.; Bhosale, C.H.; Rajpure, K.Y. Zinc oxide mediated heterogeneous photocatalytic degradation of organic species under solar radiation. *J. Photochem. Photobiol. B Biol.* **2011**, *104*, 425–433. [CrossRef] [PubMed]

31. Murtaza, G.; Ahmad, R.; Rashid, M.S.; Hassan, M.; Hussnain, A.; Khan, M.A.; Ehsan ul Haq, M.; Shafique, M.A.; Riaz, S. Structural and magnetic studies on Zr doped ZnO diluted magnetic semiconductor. *Curr. Appl. Phys.* **2014**, *14*, 176–181. [CrossRef]

32. Inturi, S.; Boningari, T.; Suidan, M.; Smirniotis, P. Visible-light-induced photodegradation of gas phase acetonitrile using aerosol-made transition metal (V, Cr, Fe, Co, Mn, Mo, Ni, Cu, Y, Ce, and Zr) doped TiO_2. *Appl. Catal. B Environ.* **2014**, *144*, 333–342. [CrossRef]

33. Choina, J.; Fischer, C.; Flechsig, G.-U.; Kosslick, H.; Tuan, V.; Nguyen, T.; Tuyen, N.A.; Schulz, A. Photocatalytic properties of Zr-doped titania in the degradation of the pharmaceutical ibuprofen. *J. Photochem. Photobiol. A Chem.* **2014**, *274*, 108–116. [CrossRef]

34. Kim, T.-H.; Lee, Y.; Han, S.-H.; Hwang, S.-J. The effects of wavelength and wavelength mixing ratios on microalgae growth and nitrogen, phosphorus removal using Scenedesmus sp. for wastewater treatment. *Bioresour. Technol.* **2013**, *130*, 75–80. [CrossRef] [PubMed]

35. Saravanan, R.; Sacari, E.; Gracia, F.; Khan, M.M.; Mosquera, E.; Gupta, V.K. Conducting PANI stimulated ZnO system for visible light photocatalytic degradation of coloured dyes. *J. Mol. Liq.* **2016**, *221*, 1029–1033. [CrossRef]

36. Saravanan, R.; Gupta, V.K.; Mosquera, E.; Gracia, F.; Narayanan, V.; Stephen, A. Visible light induced degradation of methyl orange using β-$Ag_{0.333}V_2O_5$ nanorod catalysts by facile thermal decomposition method. *J. Saudi Chem. Soc.* **2015**, *19*, 521–527. [CrossRef]

37. Saravanan, R.; Gracia, F.; Khan, M.M.; Poornima, V.; Gupta, V.K.; Narayanan, V.; Stephen, A. ZnO/CdO nanocomposites for textile effluent degradation and electrochemical detection. *J. Mol. Liq.* **2015**, *209*, 374–380. [CrossRef]

38. Gnanasekaran, L.; Hemamalini, R.; R, S.; Ravichandran, K.; Gracia, F.; Gupta, V. Intermediate state created by dopant ions (Mn, Co and Zr) into TiO2 nanoparticles for degradation of dyes under visible light. *J. Mol. Liq.* **2016**, *223*, 652–659. [CrossRef]

39. Choi, W.; Termin, A.; Hoffmann, M. The Role of Metal Ion Dopants in Quantum-Sized TiO2: Correlation Between Photoreactivity and Charge Carrier Recombination Dynamics. *J. Phys. Chem.* **1994**, *98*, 13669–13679. [CrossRef]

40. Zhang, H.; Chen, G.; Bahnemann, D. Photoelectrocatalytic Materials for Environmental Applications. *J. Mater. Chem.* **2009**, *19*, 5089–5121. [CrossRef]

41. Graetzel, M.; Howe, R. Electron paramagnetic resonance studies of doped titanium dioxide colloids. *J. Phys. Chem.* **1990**, *94*, 2566–2572. [CrossRef]

42. Schneider, J.; Matsuoka, M.; Takeuchi, M.; Zhang, J.; Horiuchi, Y.; Anpo, M.; Bahnemann, D. Understanding TiO2 Photocatalysis: Mechanisms and Materials. *Chem. Rev.* **2014**, *114*, 919–9986. [CrossRef]

43. Dvoranová, D.; Brezová, V.; Mazúr, M.; Malati, M. Investigations of Meta-Doped Titanium Dioxide Photocatalysis. *Appl. Catal. B Environ.* **2002**, *37*, 91–105. [CrossRef]

44. Wang, Y.; Zhang, R.; Li, J.; Li, L.; Lin, S. First-principles study on transition metal-doped anatase TiO2. *Nanoscale Res. Lett.* **2014**, *9*, 46. [CrossRef] [PubMed]

45. Jun, T.; Lee, K.-S. Cr-doped TiO2 thin films deposited by RF-sputtering. *Mater. Lett.* **2010**, *64*, 2287–2289. [CrossRef]

46. Qin, L.Z.; Liang, H.; Liao, B.; Liu, A.D.; Wu, X.Y.; Sun, J. Photocatalytic performance of Fe-, Ni-, or Cu-ion implanted TiO2 films under UV light, visible light and sunlight irradiation. *Nucl. Instrum. Methods Phys. Res. Sect. B Beam Interact. Mater. At.* **2013**, *307*, 385–390. [CrossRef]

47. Leyland, N.; Carroll (Podporska), J.; Browne, J.; Hinder, S.; Quilty, B.; Pillai, S. Highly Efficient F, Cu doped TiO2 anti-bacterial visible light active photocatalytic coatings to combat hospital-acquired infections. *Sci. Rep.* **2016**, *6*, 24770. [CrossRef] [PubMed]

48. Mathew, S.; Ganguly, P.; Rhatigan, S.; Vignesh, K.; Byrne, C.; Hinder, S.; Bartlett, J.; Nolan, M.; Pillai, S. Cu-Doped TiO2: Visible Light Assisted Photocatalytic Antimicrobial Activity. *Appl. Sci.* **2018**, *8*, 2067. [CrossRef]

49. Ibram, G.; Polkampally, P.; Annapoorna, I.; Sumliner, J.; Ramakrishna, M.; Hebalkar, N.; Padmanabham, G.; Sundararajan, G. Preparation and characterization of Cu-doped TiO2 materials for electrochemical, photoelectrochemical, and photocatalytic applications. *Appl. Surf. Sci.* **2014**, *293*, 229–247. [CrossRef]

50. Choi, J.; Park, H.; Hoffmann, M. Effects of Single Metal-Ion Doping on the Visible-Light Photoreactivity of TiO2. *J. Phys. Chem. C* **2009**, *114*, 783–792. [CrossRef]

51. Murakami, N.; Chiyoya, T.; Tsubota, T.; Ohno, T. Switching redox site of photocatalytic reaction on titanium (IV) oxide particles modified with transition-metal ion controlled by irradiation wavelength. *Appl. Catal. A Gen.* **2008**, *348*, 148–152. [CrossRef]

52. Rauf, M.A.; Meetani, M.A.; Hisaindee, S. An overview on the photocatalytic degradation of azo dyes in the presence of TiO2 doped with selective transition metals. *Desalination* **2011**, *276*, 13–27. [CrossRef]

53. Nešić, J.; Manojlović, D.; Andelković, I.; Dojcinovic, B.; Vulić, P.; Krstic, J.; Roglic, G. Preparation, characterization and photocatalytic activity of lanthanum and vanadium co-doped mesoporous TiO2 for azo-dye degradation. *J. Mol. Catal. A Chem.* **2013**, *378*, 67–75. [CrossRef]

54. Ni, M.; Leung, M.K.H.; Leung, D.; Sumathy, K. A Review and Recent Developments in Photocatalytic Water-Splitting Using TiO2 for Hydrogen Production. *Renew. Sustain. Energy Rev.* **2007**, *11*, 401–425. [CrossRef]

55. Chang, S.-M.; Liu, W. Surface doping is more beneficial than bulk doping to the photocatalytic activity of vanadium-doped TiO2. *Appl. Catal. B Environ.* **2011**, *101*, 333–342. [CrossRef]

56. Marschall, R. Photocatalysis: Semiconductor Composites: Strategies for Enhancing Charge Carrier Separation to Improve Photocatalytic Activity. *Adv. Funct. Mater.* **2014**, *24*, 2421–2440. [CrossRef]

57. Dong, H.; Zeng, G.; Tang, L.; Fan, C.; Zhang, C.; He, X.; He, Y. An overview on limitations of TiO2-based particles for photocatalytic degradation of organic pollutants and the corresponding countermeasures. *Water Res.* **2015**, *79*, 128–146. [CrossRef]

58. Mutlu, E.; Cristy, T.; Graves, S.; Hooth, M.; Waidyanatha, S. Characterization of aqueous formulations of tetra- and pentavalent forms of vanadium in support of test article selection in toxicology studies. *Environ. Sci. Pollut. Res.* **2017**, *24*, 405–416. [CrossRef]

59. Ntobeng, M.; Imoisili, P.; Jen, T.-C. Facile fabrication of vanadium sensitized silver titanium oxides (V–Ag/TiO2) photocatalyst nanocomposite for pollutants removal in river water. *Mater. Sci. Semicond. Process.* **2020**, *123*, 105569. [CrossRef]

60. Mitoraj, D.; Kisch, H. Surface Modified Titania Visible Light Photocatalyst Powders. *Solid State Phenom.* **2010**, *162*, 49–75. [CrossRef]

61. Phung, H.; Truong, N.; Lâm, N.T.; Phan Thi, K.L.; Duong, P.; Le, H. Enhancement of the visible light photocatalytic activity of vanadium and nitrogen co-doped TiO2 thin film. *J. Nonlinear Opt. Phys. Mater.* **2015**, *25*, 1550052. [CrossRef]

62. Weng, K.-W.; Han, S. Photocatalytic performance of TiVOx/TiO2 thin films prepared by bipolar pulsed magnetron sputter deposition. *J. Vac. Sci. Technol. B Nanotechnol. Microelectron.* **2017**, *35*, 41201–41207. [CrossRef]

63. Shao, G.; Imran, S.; Jeon, S.J.; Kang, S.J.; Haider, M.; Kim, H.T. Sol–gel synthesis of vanadium doped titania: Effect of the synthetic routes and investigation of their photocatalytic properties in the presence of natural sunlight. *Appl. Surf. Sci.* **2015**, *351*, 1213–1223. [CrossRef]

64. Zhou, J.; Takeuchi, M.; Ray, A.; Anpo, M.; Zhao, X.S. Enhancement of photocatalytic activity of P25 TiO2 by vanadium-ion implantation under visible light irradiation. *J. Colloid Interface Sci.* **2007**, *311*, 497–501. [CrossRef]

65. Bettinelli, M.; Dallacasa, V.; Falcomer, D.; Fornasiero, P.; Gombac, V.; Montini, T.; Romanò, L.; Speghini, A. Photocatalytic activity of TiO₂ doped with boron and vanadium. *J. Hazard. Mater.* **2007**, *146*, 529–534. [CrossRef]

66. Kubacka, A.; Fuerte, A.; Martínez-Arias, A.; Fernández-García, M. Nanosized Ti–V mixed oxides: Effect of doping level in the photo-catalytic degradation of toluene using sunlight-type excitation. *Appl. Catal. B Environ.* **2007**, *74*, 26–33. [CrossRef]

67. Patel, S.; Gajbhiye, N. Intrinsic room-temperature ferromagnetism of V-doped TiO₂ (B) nanotubes synthesized by the hydrothermal method. *Solid State Commun.* **2011**, *151*, 1500–1503. [CrossRef]

68. Khan, M.; Song, Y.; Chen, N.; Cao, W. Effect of V doping concentration on the electronic structure, optical and photocatalytic properties of nano-sized V-doped anatase TiO₂. *Mater. Chem. Phys.* **2013**, *142*, 148–153. [CrossRef]

69. Gu, D.-E.; Yang, B.-C.; Hu, Y.-D. A Novel Method for Preparing V-doped Titanium Dioxide Thin Film Photocatalysts with High Photocatalytic Activity Under Visible Light Irradiation. *Catal. Lett.* **2007**, *118*, 254–259. [CrossRef]

70. Iketani, K.; Sun, R.-D.; Toki, M.; Hirota, K.; Yamaguchi, O. Sol–gel-derived VXTi₁₋XO₂ films and their photocatalytic activities under visible light irradiation. *Mater. Sci. Eng. B* **2004**, *108*, 187–193. [CrossRef]

71. Lu, D.; Zhao, B.; Fang, P.; Zhai, S.; Li, D.; Chen, Z.; Wu, W.; Chai, W.; Wu, Y.; Qi, N. Facile one-pot fabrication and high photocatalytic performance of vanadium doped TiO₂-based nanosheets for visible-light-driven degradation of RhB or Cr(VI). *Appl. Surf. Sci.* **2015**, *359*, 435–448. [CrossRef]

72. Camposeco, R.; Castillo, S.; Hinojosa Reyes, M.; Mejía-Centeno, I.; Zanella, R. Effect of incorporating vanadium oxide to TiO₂, Zeolite-ZM5, SBA and P25 supports on the photocatalytic activity under visible light. *J. Photochem. Photobiol. A Chem.* **2018**, *367*, 178–187. [CrossRef]

73. Vasilic, R.; Stojadinović, S.; Radic, N.; Stefanov, P.; Dohčević-Mitrović, Z.; Grbic, B. One-step preparation and photocatalytic performance of vanadium doped TiO₂ coatings. *Mater. Chem. Phys.* **2015**, *151*, 337. [CrossRef]

74. Wang, B.; Zhang, G.; Sun, Z.; Zheng, S. A comparative study about the influence of metal ions (Ce, La and V) doping on the solar-light-induced photodegradation toward rhodamine B. *J. Environ. Chem. Eng.* **2015**, *3*. [CrossRef]

75. Sinirtas, E.; Isleyen, M.; Pozan, G. Photocatalytic degradation of 2,4-dichlorophenol with V₂O₅-TiO₂ catalysts: Effect of catalyst support and surfactant additives. *Chinese J. Catal.* **2016**, *37*, 607–615. [CrossRef]

76. Palanivel, M.; Lokeshkumar, E.; Amruthaluru, S.; Govardhanan, B.; Mahalingam, A.; Rameshbabu, N. Visible light photocatalytic activity of metal (Mo/V/W) doped porous TiO₂ coating fabricated on Cp-Ti by plasma electrolytic oxidation. *J. Alloys Compd.* **2020**, *825*, 154092. [CrossRef]

77. Khan, H.; Berk, D. Characterization and mechanistic study of Mo⁺⁶ and V⁺⁵ codoped TiO₂ as a photocatalyst. *J. Photochem. Photobiol. A Chem.* **2014**, *294*, 96–109. [CrossRef]

78. Murakami, E.; Mizoguchi, R.; Yoshida, Y.; Kitashoji, A.; Nakashima, N.; Yatsuhashi, T. Multiple strong field ionization of metallocenes: Applicability of ADK rates to the production of multiply charged transition metal (Cr, Fe, Ni, Ru, Os) cations. *J. Photochem. Photobiol. A Chem.* **2018**, *369*, 16–24. [CrossRef]

79. Elahifard, M.; Ahmadvand, S.; Mirzanejad, A. Effects of Ni-doping on the photo-catalytic activity of TiO₂ anatase and rutile: Simulation and experiment. *Mater. Sci. Semicond. Process.* **2018**, *84*, 10–16. [CrossRef]

80. Kwak, B.; Vignesh, K.; Park, N.-K.; Ryu, H.-J.; Baek, J.-I.; Kang, M. Methane formation from photoreduction of CO₂ with water using TiO₂ including Ni ingredient. *Fuel* **2015**, *143*, 570–576. [CrossRef]

81. Ranjitha, A.; Muthukumarasamy, N.; Thambidurai, M.; Velauthapillai, D.; Balasundaraprabhu, R.; Agilan, S. Fabrication of Ni-doped TiO₂ thin film photoelectrode for solar cells. *Sol. Energy* **2014**, *106*, 159–165. [CrossRef]

82. Devi, L.; Kottam, N.; Murthy, B.; Kumar, S. Enhanced photocatalytic activity of transition metal ions Mn²⁺, Ni²⁺ and Zn²⁺ doped polycrystalline titania for the degradation of Aniline Blue under UV/solar light. *J. Mol. Catal. A Chem.* **2010**, *328*, 44–52. [CrossRef]

83. Shaban, M.; Ahmed, A.; Shehata, N.; Betiha, M.; Rabie, A. Ni-doped and Ni/Cr co-doped TiO₂ nanotubes for enhancement of photocatalytic degradation of methylene blue. *J. Colloid Interface Sci.* **2019**, *555*, 31–41. [CrossRef]

84. Chaudhari, S.; Gawal, P.; Sane, P.; Sontakke, S.; Nemade, P. Solar light-assisted photocatalytic degradation of methylene blue with Mo/TiO₂: A comparison with Cr- and Ni-doped TiO₂. *Res. Chem. Intermed.* **2018**, *44*, 3115–3134. [CrossRef]

85. Anju, K.R.; Radhik, T.; Raja, J.; Al-Lohedan, H. Hydrothermal synthesis of nanosized (Fe, Co, Ni)-TiO₂ for enhanced visible light photosensitive applications. *Optik* **2018**, *165*. In Press. [CrossRef]

86. Li, X.; Wu, Y.; Shen, Y.; Sun, Y.; Yang, Y.; Xie, A. A novel bifunctional Ni-doped TiO₂ inverse opal with enhanced SERS performance and excellent photocatalytic activity. *Appl. Surf. Sci.* **2017**, *427*, 739–744. [CrossRef]

87. Blanco-Vega, M.P.; Guzmán Mar, J.; Villanueva, M.; Maya-Treviño, L.; Garza-Tovar, L.L.; Hernandez-Ramírez, A.; Reyes, L. Photocatalytic elimination of bisphenol A under visible light using Ni-doped TiO₂ synthesized by microwave assisted sol-gel method. *Mater. Sci. Semicond. Process.* **2017**, *71*, 275–282. [CrossRef]

88. Bhatia, V.; Dhir, A. Transition metal doped TiO₂ mediated Photocatalytic degradation of anti-inflammatory drug under solar irradiations. *J. Environ. Chem. Eng.* **2016**, *4*, 1267–1273. [CrossRef]

89. Manjakuppam, M.; Rao, C.; Das, R.; Giri, A.; Golder, A. Evaluation of bimetal doped TiO₂ in dye fragmentation and its comparison to mono-metal doped and bare catalysts. *Appl. Surf. Sci.* **2016**, *368*, 316–324. [CrossRef]

90. Baygi, N.J.; Saghir, A.V.; Beidokhti, S.M.; Khaki, J.V. Modified auto-combustion synthesis of mixed-oxides TiO₂/NiO nanoparticles: Physical properties and photocatalytic performance. *Ceram. Int.* **2020**, *46*, 15417–15437. [CrossRef]

91. Mohseni-Salehi, M.; Taheri-Nassaj, E.; Zori, M. Effect of dopant (Co, Ni) concentration and hydroxyapatite compositing on photocatalytic activity of titania towards dye degradation. *J. Photochem. Photobiol. A Chem.* **2017**, *356*, 57–70. [CrossRef]

92. Elmragui, A.; Zegaoui, O.; Daou, I. Synthesis, characterization and photocatalytic properties under visible light of doped and co-doped TiO$_2$-based nanoparticles. *Mater. Today Proc.* **2019**, *13*, 857–865. [CrossRef]

93. Hinojosa Reyes, M.; Solis, R.; Ruiz, F.; Glez, V.; Moctezuma, E. Promotional effect of metal doping on nanostructured TiO$_2$ during the photocatalytic degradation of 4-chlorophenol and naproxen sodium as pollutants. *Mater. Sci. Semicond. Process.* **2019**, *100*, 130–139. [CrossRef]

94. Kerkez, Ö.; Kibar, E.; Dayıoğlu, K.; Gedik, F.; Akin, A.; Özkara-Aydınoğlu, A.P.Ş. A comparative study for removal of different dyes over M/TiO$_2$ (M=Cu, Ni, Co, Fe, Mn and Cr) photocatalysts under visible light irradiation. *J. Photochem. Photobiol. A Chem.* **2015**, *311*, 176–185. [CrossRef]

95. Yang, X.-J.; Wang, S.; Sun, H.; Wang, X.-B.; Lian, J.-S. Preparation and photocatalytic performance of Cu-doped TiO$_2$ nanoparticles. *Trans. Nonferrous Met. Soc. China* **2015**, *25*, 504–509. [CrossRef]

96. Tsai, C.-Y.; Hsi, H.-C.; Kuo, T.-H.; Chang, Y.-M.; Liou, J.-H. Preparation of Cu-Doped TiO$_2$ Photocatalyst with Thermal Plasma Torch for Low-Concentration Mercury Removal. *Aerosol Air Qual. Res.* **2013**, *13*, 639–648. [CrossRef]

97. Yang, J.; Ganesan, P.; Teuscher, J.; Moehl, T.; Kim, Y.J.; Yi, C.; Comte, P.; Pei, K.; Holcombe, T.; Nazeeruddin, M.; et al. Influence of the Donor Size in D−π–A Organic Dyes for Dye-Sensitized Solar Cells. *J. Am. Chem. Soc.* **2014**, *136*, 5722–5730. [CrossRef]

98. Pava-Gómez, B.; Vargas-Ramírez, X.; Díaz-Uribe, C. Physicochemical study of adsorption and photodegradation processes of methylene blue on copper-doped TiO$_2$ films. *J. Photochem. Photobiol. A Chem.* **2018**, *360*, 13–25. [CrossRef]

99. Yusoff, R.; Shamiri, A.; Aroua, M.; Ahmady, A.; Shafeeyan, M.S.; Lee, W.; Lim, S.; Burhanuddin, S.N.M. Physical properties of aqueous mixtures of N-methyldiethanolamine (MDEA) and ionic liquids. *J. Ind. Eng. Chem.* **2014**, *20*, 3349–3355. [CrossRef]

100. Mohan, R.; Krishnamoorthy, K.; Kim, S.-J. Enhanced photocatalytic activity of Cu-doped ZnO nanorods. *Solid State Commun.* **2012**, *152*, 375–380. [CrossRef]

101. Hanaor, D.; Sorrell, C. Review of the Anatase to Rutile Phase Transformation. *J. Mater. Sci.* **2011**, *46*, 855–874. [CrossRef]

102. López, R.; Gomez, R.; Llanos, M. Photophysical and photocatalytic properties of nanosized copper-doped titania sol–gel catalysts. *Catal. Today* **2009**, *148*, 103–108. [CrossRef]

103. Xia, X.H.; Gao, Y.; Wang, Z.; Jia, Z.J. Structure and photocatalytic properties of copper-doped rutile TiO$_2$ prepared by a low-temperature process. *J. Phys. Chem. Solids* **2008**, *69*, 2888–2893. [CrossRef]

104. Li, G.; Dimitrijevic, N.; Chen, L.; Rajh, T.; Gray, K. Role of Surface/Interfacial Cu^{2+} Sites in the Photocatalytic Activity of Coupled CuO-TiO$_2$ Nanocomposites. *J. Phys. Chem. C* **2008**, *112*, 19040–19044. [CrossRef]

105. Morikawa, T.; Irokawa, Y.; Ohwaki, T. Enhanced photocatalytic activity of TiO$_2$−xNx loaded with copper ions under visible light irradiation. *Appl. Catal. A Gen.* **2006**, *314*, 123–127. [CrossRef]

106. Colón, G.; Maicu, M.; Hidalgo, M.C.; Navio, J.A. Cu-doped TiO2 systems with improved photocatalytic activity. *Appl. Catal. B Environ.* **2006**, *67*, 41. [CrossRef]

107. Jiang, Y.; Yang, Y.; Qiang, L.; Fan, R.; Ning, H.; Li, L.; Ye, T.; Yang, B.; Cao, W. Based on Cu(II) silicotungstate modified photoanode with long electron lifetime and enhanced performance in dye sensitized solar cells. *J. Power Sources* **2015**, *278*, 527–533. [CrossRef]

108. Kim, C.-S.; Shin, J.-W.; Cho, Y.-H.; Jang, H.D.; Byun, H.-S.; Kim, T. Synthesis and characterization of Cu/N-doped mesoporous TiO$_2$ visible light photocatalysts. *Appl. Catal. A Gen.* **2013**, *455*, 211–218. [CrossRef]

109. Habibi, M.; Karimi, B.; Zendehdel, M.; Habibi, M. Fabrication, characterization of two nano-composite CuO-ZnO working electrodes for dye-sensitized solar cell. *Spectrochim. Acta. A Mol. Biomol. Spectrosc.* **2013**, *116C*, 374–380. [CrossRef]

110. Liu, M.; Qiu, X.; Miyauchi, M.; Hashimoto, K. Cu(II) Oxide Amorphous Nanoclusters Grafted Ti^{3+} Self-Doped TiO$_2$: An Efficient Visible Light Photocatalyst. *Chem. Mater.* **2011**, *23*, 5282–5286. [CrossRef]

111. Hu, Q.; Huang, J.; Li, G.; Chen, J.; Zhaojun, Z.; Deng, Z.; Jiang, Y.; Guo, W.; Cao, Y. Effective water splitting using CuO$_x$/TiO$_2$ composite films: Role of Cu species and content in hydrogen generation. *Appl. Surf. Sci.* **2016**, *369*, 201–206. [CrossRef]

112. Ravichandra, D.; Rao, T.; Kim, H.-S.; Pammi, S.V.N.; Prabhakarrao, N.; Imandi, M.R. Hybrid copper doped titania/polythiophene nanorods as efficient visible light-driven photocatalyst for degradation of organic pollutants. *J. Asian Ceram. Soc.* **2017**, *5*, 436–443. [CrossRef]

113. Khairy, M.; Zakaria, W. Effect of metal-doping of TiO$_2$ nanoparticles on their photocatalytic activities toward removal of organic dyes. *Egypt. J. Pet.* **2014**, *23*, 419–426. [CrossRef]

114. Mahy, J.; Tilkin, R.; Douven, S.; Lambert, S. TiO$_2$ nanocrystallites photocatalysts modified with metallic species: Comparison between Cu and Pt doping. *Surfaces Interfaces* **2019**, *66*, 100366. [CrossRef]

115. Jaiswal, R.; Bharambe, J.; Patel, N.; Dashora, A.; Kothari, D.C.; Miotello, A. Copper and Nitrogen co-doped TiO$_2$ photocatalyst with enhanced optical absorption and catalytic activity. *Appl. Catal. B Environ.* **2015**, *168–169*, 333–341. [CrossRef]

116. Makki, F.; El Hajj Hassan, M.; El Jamal, M.; Tabatabai-Yazdi, F.-S.; Ebrahimian, A. Kinetic evaluation of photocatalytic degradation of food colorant E 131 VF by copper doped TiO$_2$ nanophotocatalysts prepared at different calcination temperatures. *Environ. Technol. Innov.* **2020**, *19*, 100981. [CrossRef]

117. Qian, S.; Zhang, Y.; Wang, P.; Bai, Y.; Lai, B. New insights on the enhanced non-hydroxyl radical contribution under copper promoted TiO2/GO for the photodegradation of tetracycline hydrochloride. *J. Environ. Sci.* **2021**, *100*, 99–109. [CrossRef]

118. Medina Ramirez, I.; Rodil, S.; Pedroza-Herrera, G.; Lozano-Alvarez, J. Evaluation of the Photocatalytic Activity of Copper Doped TiO$_2$ nanoparticles for the Purification and/or Disinfection of Industrial Effluents. *Catal. Today* **2019**, *341*, 37–48. [CrossRef]

119. Hernández, J.; Coste, S.; García Murillo, A.; Carrillo-Romo, F.; Kassiba, A. Effects of metal doping (Cu, Ag, Eu) on the electronic and optical behavior of nanostructured TiO$_2$. *J. Alloys Compd.* **2017**, *710*, 355–363. [CrossRef]

120. Reda, S.M.; Khairy, M.; Mousa, M. Photocatalytic Activity of Nitrogen and Copper Doped TiO$_2$ Nanoparticles Prepared by Microwave-Assisted Sol-Gel Process. *Arab. J. Chem.* **2017**, *13*, 86–95. [CrossRef]

121. Hamadanian, M.; Karimzadeh, S.; Jabbari, V.; Villagran, D. Synthesis of cysteine, cobalt and copper-doped TiO$_2$ nanophotocatalysts with excellent visible-light-induced photocatalytic activity. *Mater. Sci. Semicond. Process.* **2016**, *41*, 168–176. [CrossRef]

122. Lin, J.; Sopajaree, K.; Jitjanesuwan, T.; Lu, M.-C. Application of visible light on copper-doped titanium dioxide catalyzing degradation of chlorophenols. *Sep. Purif. Technol.* **2017**, *191*, 233–243. [CrossRef]

123. Ahmad, S.; Yasin, A. Photocatalytic degradation of deltamethrin by using Cu/TiO$_2$/bentonite composite. *Arab. J. Chem.* **2020**, *13*, 8481–8488. [CrossRef]

124. Dorraj, M.; Alizadeh, M.; Sairi, A.; Basirun, W.; Goh, B.T.; Woi, P.; Alias, Y. Enhanced Visible Light Photocatalytic Activity of Copper-doped Titanium Oxide–Zinc Oxide Heterojunction for Methyl Orange Degradation. *Appl. Surf. Sci.* **2017**, *414*, 251–261. [CrossRef]

125. Bensouici, F.; Bououdina, M.; Tala-Ighil, R.; Tounane, M.; Iratni, A.; Souier, M.; Shengwen, L.; Cai, W. Optical, Structural and Photocatalysis Properties of Cu-Doped TiO$_2$ Thin Films. *Appl. Surf. Sci.* **2016**, *395*, 110–116. [CrossRef]

126. Reddam, H.; Elmail, R.; Lloria, S.; Monros, G.; Reddam, Z.; Coloma-Pascual, F. Synthesis of Fe, Mn and Cu modified TiO$_2$ photocatalysts for photodegradation of Orange II. *Boletín la Soc. Española Cerámica y Vidr.* **2019**, *59*, 138–148. [CrossRef]

127. Mahy, J.; Lambert, S.; Leonard, G.; Zubiaur, A.; Olu, P.-Y.; Mahmoud, A.; Boschini, F.; Heinrichs, B. Towards a large scale aqueous sol-gel synthesis of doped TiO$_2$: Study of various metallic dopings for the photocatalytic degradation of p-nitrophenol. *J. Photochem. Photobiol. A Chem.* **2016**, *329*, 189–202. [CrossRef]

128. Periyakaruppan, K.; Nisha, N.; Pugazhendhi, A.; Kandasamy, S.; Pitchaimuthu, S. An investigation of transition metal doped TiO$_2$ photocatalysts for the enhanced photocatalytic decoloration of methylene blue dye under visible light irradiation. *J. Environ. Chem. Eng.* **2021**, *9*, 105254. [CrossRef]

129. Paul, S.; Chetri, P.; Choudhury, A. Effect of manganese doping on the optical property and photocatalytic activity of nanocrystalline titania: Experimental and theoretical investigation. *J. Alloys Compd.* **2014**, *583*, 578–586. [CrossRef]

130. Duan, J.; Wang, H.; Wang, H.; Zhang, J.; Wu, S.; Wang, Y. Mn-doped ZnO nanotubes: From facile solution synthesis to room temperature ferromagnetism. *CrystEngComm* **2012**, *14*, 1330–1336. [CrossRef]

131. Deng, Q.; Xia, X.; Guo, M.; Gao, Y. Mn-doped TiO$_2$ nanopowders with remarkable visible light photocatalytic activity. *Mater. Lett.* **2011**, *65*, 2051–2054. [CrossRef]

132. Liu, M.; Du, Y.; Ma, L.; Jing, D.; Guo, L. Manganese doped cadmium sulfide nanocrystal for hydrogen production from water under visible light. *Int. J. Hydrogen Energy* **2012**, *37*, 730. [CrossRef]

133. Pérez Larios, A.; Lartundo, L.; Mantilla, A.; Mendoza, G.; Gomez, R.; Hernández-Gordillo, L. Enhancing the H$_2$ evolution from water-methanol solution using Mn^{2+}–Mn^{+3}–Mn^{4+} redox species of Mn-doped TiO$_2$ sol-gel photocatalysts. *Catal. Today* **2016**. [CrossRef]

134. Shu, Y.; Xu, Y.; Huang, H.; Ji, J.; Liang, S.; Wu, M.; Leung, D. Catalytic oxidation of VOCs over Mn/TiO$_2$/activated carbon under 185 nm VUV irradiation. *Chemosphere* **2018**, *208*, 550–558. [CrossRef] [PubMed]

135. Devi, L.; Kumar, S.; Murthy, B.; Kottam, N. Influence of Mn^{2+} and Mo^{6+} dopants on the phase transformations of TiO$_2$ lattice and its photo catalytic activity under solar illumination. *Catal. Commun.* **2009**, *10*, 794–798. [CrossRef]

136. Faouzi, A.; Corbel, S.; Balan, L.; Mozet, K.; Girot, E.; Medjahdi, G.; Ben Said, M.; Ghrabi, A.; Schneider, R. Porous Mn-doped ZnO nanoparticles for enhanced solar and visible light photocatalysis. *Mater. Des.* **2016**, *101*, 309–316. [CrossRef]

137. Reddy, C.; Reddy, I.; Akkinepally, B.; Harish, V.; Reddy, R.; Jaesool, S. Mn-doped ZrO$_2$ nanoparticles prepared by a template-free method for electrochemical energy storage and abatement of dye degradation. *Ceram. Int.* **2019**, *45*, 15298–15306. [CrossRef]

138. Bharati, B.; Mishra, N.C.; Sinha, A.S.K.; Rath, C. Unusual Structural Transformation and Photocatalytic Activity of Mn Doped TiO$_2$ Nanoparticles under Sunlight. *Mater. Res. Bull.* **2019**, *123*, 110710. [CrossRef]

139. Xu, Z.; Li, C.; Fu, N.; Li, W.; Zhang, G. Facile synthesis of Mn-doped TiO$_2$ nanotubes with enhanced visible light photocatalytic activity. *J. Appl. Electrochem.* **2018**, *48*, 1197–1203. [CrossRef]

140. Choudhury, B.; Paul, S.; Ahmed, G.; Choudhury, A. Adverse effect of Mn doping on the magnetic ordering in Mn doped TiO$_2$ nanoparticles. *Mater. Res. Express* **2015**, *2*, 96104. [CrossRef]

141. Shu, Y.; Ji, J.; Xu, Y.; Deng, J.; Huang, H.; He, M.; Leung, D.; Wu, M.; Liu, S.; Liu, S.; et al. Promotional role of Mn doping on catalytic oxidation of VOCs over mesoporous TiO$_2$ under Vacuum Ultraviolet (VUV) irradiation. *Appl. Catal. B Environ.* **2017**, *220*, 78–87. [CrossRef]

142. Islam, M.; Bredow, T. Rutile Band-Gap States Induced by Doping with Manganese in Various Oxidation States. *J. Phys. Chem. C* **2015**, *119*, 5534–5541. [CrossRef]

143. Zhang, L.; Zhang, Y.; Ma, Z. Effect of manganese on photocatalysis. *China Acad. J.* **2011**, *4–6*, 15.

144. Binas, V.; Sambani, K.; Maggos, T.; Katsanaki, A.; Kiriakidis, G. Synthesis and photocatalytic activity of Mn-doped TiO$_2$ nanostructured powders under UV and visible light. *Appl. Catal. B Environ.* **2012**, *113–114*, 79–86. [CrossRef]

145. Esparza, P.; Hernández, T.; Borges, M.E.; Alvarez-Galvan, M.; Ruiz-Morales, J.C.; Fierro, J.L.G. TiO$_2$ modifications by hydrothermal treatment and doping to improve its photocatalytic behaviour under visible light. *Catal. Today* **2013**, *210*, 135–141. [CrossRef]

146. Feng, H.; Yu, L.; Zhang, M.-H. Ultrasonic synthesis and photocatalytic performance of metal-ions doped TiO$_2$ catalysts under solar light irradiation. *Mater. Res. Bull.* **2013**, *48*, 672–681. [CrossRef]

147. Park, J.; Anh Le, H.; Kim, Y.-S.; Chin, S.-M.; Bae, G.-N.; Jurng, J. Synthesis and enhanced photocatalytic activity of Mn/TiO$_2$ mesoporous materials using the impregnation method through CVC process. *J. Porous Mater.* **2012**, *19*, 877–881. [CrossRef]

148. Khraisheh, M.; Wu, L.; Al-Muhtaseb, A.; Albadarin, A.; Walker, G. Phenol degradation by powdered metal ion modified titanium dioxide photocatalysts. *Chem. Eng. J.* **2012**, *213*, 125–134. [CrossRef]

149. Zou, X.; Li, G.-D.; Guo, M.; Li, X.-H.; Liu, D.-P.; Su, J.; Chen, J. Heterometal Alkoxides as Precursors for the Preparation of Porous Fe- and Mn-TiO$_2$ Photocatalysts with High Efficiencies. *Chemistry* **2008**, *14*, 11123–11131. [CrossRef] [PubMed]

150. Kamble, R.; Sabale, S.; Chikode, P.; Puri, V.; Mahajan, S. Corrigendum: Structural and photocatalytic studies of hydrothermally synthesized Mn^{2+}–TiO$_2$ nanoparticles under UV and visible light irradiation (2016 *Mater. Res. Express* **3** 115005). *Mater. Res. Express* **2018**, *5*, 129502. [CrossRef]

151. Tbessi, I.; Benito, M.; Molins, E.; LIorca, J.; Touati, A.; Sayadi, S.; Najjar, W. Effect of Ce and Mn co-doping on photocatalytic performance of sol-gel TiO$_2$. *Solid State Sci.* **2018**, *88*, 20–28. [CrossRef]

152. Binas, V.; Stefanopoulos, V.; Kiriakidis, G.; Papagiannakopoulos, P. Photocatalytic oxidation of gaseous benzene, toluene and xylene under UV and visible irradiation over Mn-doped TiO$_2$ nanoparticles. *J. Mater.* **2018**, *5*, 56–65. [CrossRef]

153. Sudrajat, H.; Babel, S.; Ta, A.; Nguyen, T.K. Mn-doped TiO$_2$ photocatalysts: Role, chemical identity, and local structure of dopant. *J. Phys. Chem. Solids* **2020**, *144*, 109517. [CrossRef]

154. Wu, M.; Leung, D.; Zhang, Y.; Huang, H.; Xie, R.; Szeto, W.; Li, F. Toluene degradation over Mn-TiO$_2$/CeO$_2$ composite catalyst under vacuum ultraviolet (VUV) irradiation. *Chem. Eng. Sci.* **2018**, *195*, 985–994. [CrossRef]

155. Pirzada, B.; Mir, N.; Qutub, N.; Mehraj, O.; Sabir, S.; Muneer, M. Synthesis, characterization and optimization of photocatalytic activity of TiO$_2$/ZrO$_2$ nanocomposite heterostructures. *Mater. Sci. Eng. B* **2014**, *193*, 137–145. [CrossRef]

156. Ranjbar, S.; Saberyan, K.; Parsayan, F. A new process for preparation of Zr doped TiO$_2$ nanopowders using APCVS method. *Mater. Chem. Phys.* **2018**, *214*, 337–344. [CrossRef]

157. Kambur, A.; Pozan, G.; Boz, I. Preparation, characterization and photocatalytic activity of TiO$_2$–ZrO$_2$ binary oxide nanoparticles. *Appl. Catal. B Environ.* **2012**, *115–116*, 149–158. [CrossRef]

158. Mohammadi, M.R.; Fray, D. Synthesis and characterization of nanosized TiO$_2$-ZrO$_2$ binary system prepared by an aqueous sol-gel process: Physical and sensing properties. *Sensors Actuators B Chem.* **2011**, *155*, 568–576. [CrossRef]

159. T V L, T.; Deivasigamani, P.; Maheswari, M.A. Synthesis of mesoporous worm-like ZrO$_2$–TiO$_2$ monoliths and their photocatalytic applications towards organic dye degradation. *J. Photochem. Photobiol. A Chem.* **2017**, *344*, 212–222. [CrossRef]

160. Goswami, P.; Ganguli, J. Tuning the band gap of mesoporous Zr-doped TiO$_2$ for effective degradation of pesticide quinalphos. *Dalton Trans.* **2013**, *42*, 14480–14490. [CrossRef] [PubMed]

161. Loganathan, K.; Azhagapillai, P.; Palanichamy, M.; Arumugam, E.; Murugesan, V. Synthesis and characterization of Zr^{4+}, La^{3+} and Ce^{3+} doped mesoporous TiO$_2$: Evaluation of their photocatalytic activity. *J. Hazard Mater.* **2011**, *186*, 1183–1192. [CrossRef]

162. Babaei, M.; Dehghanian, C.; Taheri, P.; Babaei, M. Effect of duty cycle and electrolyte additive on photocatalytic performance of TiO$_2$-ZrO$_2$ composite layers prepared on CP Ti by micro arc oxidation method. *Surf. Coatings Technol.* **2016**, *307*, 554–564. [CrossRef]

163. Pantelides, S. The electronic structure of impurities and other point defects in semiconductors. *Rev. Mod. Phys.* **1978**, *50*, 797–858. [CrossRef]

164. Hamukwaya, S.L.; Zhao, Z.; Wang, N.; Liu, H.; Umar, A.; Zhang, J.; Wu, T.; Guo, Z. Enhanced Photocatalytic Activity of B, N-Codoped TiO$_2$ by a New Molten Nitrate Process. *J. Nanosci. Nanotechnol.* **2019**, *19*, 839–849. [CrossRef]

165. Li, M.; Li, X.; JIANG, G.; He, G. Hierarchically macro-mesoporous ZrO$_2$-TiO$_2$ composites with Enhanced photocatalytic activity. *Ceram. Int.* **2015**, *41*, 5749–5757. [CrossRef]

166. Huang, Q.; Ma, W.; Yan, X.; Chen, Y.; Zhu, S.; Shen, S. Photocatalytic decomposition of gaseous HCHO by Zr$_x$Ti$_{1-x}$O$_2$ catalysts under UV–vis light irradiation with an energy-saving lamp. *J. Mol. Catal. A Chem.* **2013**, *366*, 261–265. [CrossRef]

167. Mbiri, A.; Taffa, D.; Gatebe, E.; Wark, M. Zirconium doped mesoporous TiO$_2$ multilayer thin films: Influence of the zirconium content on the photodegradation of organic pollutants. *Catal. Today* **2019**, *328*, 71–78. [CrossRef]

168. Huang, C.; Ding, Y.; Chen, Y.; Li, P.; Zhu, S.; Shen, S. Highly efficient Zr doped-TiO$_2$/glass fiber photocatalyst and its performance in formaldehyde removal under visible light. *J. Environ. Sci.* **2017**, *60*, 61–69. [CrossRef]

169. Mahy, J.; Lambert, S.; Tilkin, R.; Wolfs, C.; Poelman, D.; Devred, F.; Gaigneaux, E.; Douven, S. Ambient temperature ZrO$_2$-doped TiO$_2$ crystalline photocatalysts: Highly efficient powders and films for water depollution. *Mater. Today Energy* **2019**, *13*, 312–322. [CrossRef]

170. Belver, C.; Bedia, J.; Rodriguez, J.J. Zr-doped TiO$_2$ supported on delaminated clay materials for solar photocatalytic treatment of emerging pollutants. *J. Hazard Mater.* **2016**, *322*, 233–242. [CrossRef]

171. Zhao, J.; Ge, S.; Pan, D.; Shao, Q.; Lin, J.; Wang, Z.; Hu, Z.; Wu, T.; Guo, Z. Solvothermal Synthesis, Characterization and Photocatalytic Property of Zirconium Dioxide Doped Titanium Dioxide Spinous Hollow Microspheres with Sunflower Pollen as Bio-templates. *J. Colloid Interface Sci.* **2018**, *529*, 111–121. [CrossRef]

172. Prabhakarrao, N.; Ravichandra, D.; Rao, T. Synthesis of Zr doped TiO$_2$/reduced Graphene Oxide (rGO) nanocomposite material for efficient photocatalytic degradation of dyes under visible light irradiation. *J. Alloys Compd.* **2016**, *694*, 596–606. [CrossRef]

173. Yasin, S.A.; Obaid, M.; El-Newehy, M.; Al-Deyab, S.; Barakat, N. Influence of Ti$_x$Zr$_{(1-x)}$O$_2$ nanofibers composition on the photocatalytic activity toward organic pollutants degradation and water splitting. *Ceram. Int.* **2015**, *41*, 11876–11885. [CrossRef]

174. Ali, T.; Tripathi, P.; Azam, A.; Raza, W.; Shareef Ahmed, A.; Ahmed, A.; Muneer, M. Photocatalytic performance of Fe-doped TiO$_2$ nanoparticles under visible-light irradiation. *Mater. Res. Express* **2017**, *4*, 15022. [CrossRef]

175. Khan, H.; Swati, I. Fe³⁺-doped Anatase TiO₂ with d-d Transition, Oxygen Vacancies and Ti³⁺ Centers: Synthesis, Characterization, UV-vis Photocatalytic and Mechanistic Studies. *Ind. Eng. Chem. Res.* **2016**, *55*, 6619–6633. [CrossRef]

176. Sayyar, Z.; Babaluo, A.; Rahbar Shahrouzi, J. Kinetic Study of Formic Acid Degradation by Fe³⁺ doped TiO₂ Self-Cleaning Nanostructure Surfaces Prepared by Cold Spray. *Appl. Surf. Sci.* **2015**, *335*, 1–10. [CrossRef]

177. Naghibi, S.; Gharagozlou, M. Solvothermal Synthesis of M-doped TiO₂ Nanoparticles for Sonocatalysis of Methylene Blue and Methyl Orange (M = Cd, Ag, Fe, Ce, and Cu): Sonocatalytic Performance of M-doped TiO₂ NPs. *J. Chin. Chem. Soc.* **2017**, *64*, 640–650. [CrossRef]

178. Li, J.; Ren, D.; Wu, Z.; Xu, J.; Bao, Y.; He, S.; Chen, Y. Flame retardant and visible light-activated Fe-doped TiO₂ thin films anchored to wood surfaces for the photocatalytic degradation of gaseous formaldehyde. *J. Colloid Interface Sci.* **2018**, *530*, 78–87. [CrossRef] [PubMed]

179. Craciun, E.; Predoana, L.; Atkinson, I.; Jitaru, I.; Anghel, E.M.; Bratan, V.; Gifu, C.; Anastasescu, C.; Rusu, A.; Raditoiu, V.; et al. Fe³⁺-doped TiO₂ nanopowders for photocatalytic mineralization of oxalic acid under solar light irradiation. *J. Photochem. Photobiol. A Chem.* **2018**, *356*, 18–28. [CrossRef]

180. Liu, M.; Qiu, X.; Miyauchi, M.; Hashimoto, K. Energy-Level Matching of Fe(III) Ions Grafted at Surface and Doped in Bulk for Efficient Visible-Light Photocatalysts. *J. Am. Chem. Soc.* **2013**, *135*, 10064–10072. [CrossRef]

181. Han, F.; Kambala, V.; Srinivasan, M.; Dharmarajan, R.; Naidu, R. Tailored Titanium Dioxide Photocatalysts for the Degradation of Organic Dyes in Wastewater Treatment: A Review. *Appl. Catal. A General* **2009**, *359*, 25–40. [CrossRef]

182. Jaihindh, D.; Verma, A.; Chen, C.-C.; Huang, Y.-c.; Dong, C.; Fu, Y. Study of oxidation states of Fe- and Co-doped TiO₂ photocatalytic energy materials and their visible-light-driven photocatalytic behavior. *Int. J. Hydrog. Energy* **2018**, *44*, 15892–15906. [CrossRef]

183. Ismael, M. Enhanced photocatalytic hydrogen production and degradation of organic pollutants from Fe (III) doped TiO₂ nanoparticles. *J. Environ. Chem. Eng.* **2020**, *8*, 103676. [CrossRef]

184. Mancuso, A.; Sacco, O.; Sannino, D.; Pragliola, S.; Vaiano, V. Enhanced visible-light-driven photodegradation of Acid Orange 7 azo dye in aqueous solution using Fe-N co-doped TiO₂. *Arab. J. Chem.* **2020**, *13*, 8347–8360. [CrossRef]

185. Moradi, V.; Ahmed, F.; Jun, M.; Blackburn, A.; Herring, R. Acid-treated Fe-doped TiO₂ as a high performance photocatalyst used for degradation of phenol under visible light irradiation. *J. Environ. Sci.* **2019**, *83*, 183–194. [CrossRef] [PubMed]

186. Rodríguez, P.; Pecchi, G.; Casuscelli, S.; Elías, V.; Eimer, G. A simple synthesis way to obtain iron-doped TiO₂ Nanoparticles as photocatalytic surfaces. *Chem. Phys. Lett.* **2019**, *732*, 136643. [CrossRef]

187. Sood, S.; Umar, A.; Mehta, S.; Kansal, S. Highly effective Fe-doped TiO₂ nanoparticles photocatalysts for visible-light driven photocatalytic degradation of toxic organic compounds. *J. Colloid Interface Sci.* **2015**, *450*, 213–223. [CrossRef] [PubMed]

188. Komaraiah, D.; Radha, E.; Sivakumar, J.; Reddy, M.V.R.; Sayanna, R. Influence of Fe3+ ion doping on the luminescence emission behavior and photocatalytic activity of Fe³⁺, Eu³⁺-codoped TiO₂ thin films. *J. Alloys Compd.* **2021**, *868*, 159109. [CrossRef]

189. Kanakaraju, D.; Ya, M.; Jasni, M.; Endra, M.; Lim, Y.C. Fe Doped Titania Photocatalyst for Degradation of Methyl Orange. *Mater. Today Proc.* **2019**, *19*, 1657–1662. [CrossRef]

190. Crişan, M.; Mardare, D.; Ianculescu, A.; Drăgan, N.; Niţoi, I.; Crişan, D.; Voicescu, M.; Todan, L.; Oancea, P.; Adomniţei, C.; et al. Iron doped TiO₂ films and their photoactivity in nitrobenzene removal from water. *Appl. Surf. Sci.* **2018**, *455*, 201–215. [CrossRef]

191. Ahadi, S.; Moalej, N.; Sheibani, S. Characteristics and photocatalytic behavior of Fe and Cu doped TiO₂ prepared by combined sol-gel and mechanical alloying. *Solid State Sci.* **2019**, *96*, 105975. [CrossRef]

192. Li, G.; Yi, L.; Wang, J.; Song, Y. Hydrodynamic cavitation degradation of Rhodamine B assisted by Fe³⁺-doped TiO₂: Mechanisms, geometric and operation parameters. *Ultrason. Sonochem.* **2019**, *60*, 104806. [CrossRef] [PubMed]

193. Velázquez-Martínez, S.; Silva Martínez, S.; Arellano, C.; González, A.; Salgado, I.; Morales-Pérez, A.A.; Peña-Cruz, M. Modified sol-gel/hydrothermal method for the synthesis of microsized TiO₂ and iron-doped TiO₂, its characterization and solar photocatalytic activity for an azo dye degradation. *J. Photochem. Photobiol. A Chem.* **2018**, *359*, 93–101. [CrossRef]

194. Indah Anwar, D.; Mulyadi, D. Synthesis of Fe-TiO₂ Composite as a Photocatalyst for Degradation of Methylene Blue. *Procedia Chem.* **2015**, *17*, 49–54. [CrossRef]

195. Ambati, R.; Gogate, P. Photocatalytic degradation of Acid Blue 80 using iron doped TiO₂ catalyst: Understanding the effect of operating parameters and combinations for synergism. *J. Water Process Eng.* **2017**, *20*, 217–225. [CrossRef]

196. Tabasideh, S.; Maleki, A.; Shahmoradi, B.; Ghahremani, E.; Mckay, G. Sonophotocatalytic degradation of diazinon in aqueous solution using iron-doped TiO₂ nanoparticles. *Sep. Purif. Technol.* **2017**, *189*, 186–192. [CrossRef]

197. Khan, M.; Siwach, R.; Kumar, S.; Alhazaa, A. Role of Fe doping in tuning photocatalytic and photoelectrochemical properties of TiO₂ for photodegradation of methylene blue. *Opt. Laser Technol.* **2019**, *118*, 170–178. [CrossRef]

198. Han, F.; Kambala, V.; Dharmarajan, R.; Liu, Y.; Naidu, R. Photocatalytic degradation of azo dye acid orange 7 using different light sources over Fe³⁺ -doped TiO₂ nanocatalysts. *Environ. Technol. Innov.* **2018**, *12*, 27–42. [CrossRef]

199. Zafar, Z.; Kim, J.-O. Optimization of hydrothermal synthesis of Fe-TiO₂ nanotube arrays for enhancement in visible light using an experimental design methodology. *Environ. Res.* **2020**, *189*, 109908. [CrossRef]

200. Bensouici, F.; Mostafa, B.; Tala-Ighil, R.; Bououdina, M.; Tounane, M. Surface, structural and optical properties dependence of Fe-doped TiO₂ films deposited onto soda–lime–glass. *Surf. Interfaces* **2020**, *21*, 100682. [CrossRef]

201. Komaraiah, D.; Radha, E.; Sivakumar, J.; Reddy, M.V.; Sayanna, R. Structural, optical properties and photocatalytic activity of Fe³⁺ doped TiO₂ thin films deposited by sol-gel spin coating. *Surf. Interfaces* **2019**, *17*, 100368. [CrossRef]

202. Moradi, V.; Jun, M.; Blackburn, A.; Herring, R. Significant improvement in visible light photocatalytic activity of Fe doped TiO₂ using an acid treatment process. *Appl. Surf. Sci.* **2017**, *427*, 791–799. [CrossRef]

203. Kakavandi, B.; Jorfi, S.; Fattahi, M.; Isari, A. Photocatalytic degradation of rhodamine B and real textile wastewater using Fe-doped TiO₂ anchored on reduced graphene oxide (Fe-TiO₂/rGO): Characterization and feasibility, mechanism and pathway studies. *Appl. Surf. Sci.* **2018**, *462*, 549–564.

204. Crisan, M.; Răileanu, M.; Drăgan, N.; Crisan, D.; Ianculescu, A.; Nitoi, I.; Oancea, P.; Somacescu, S.; Stanica, N.; Vasile, B.; et al. Sol-gel iron-doped TiO₂ nanopowders with Photocatalytic Activity. *Appl. Catal. A Gen.* **2014**, *504*, 130–142. [CrossRef]

205. Adyani, S.M.; Ghorbani, M. A comparative study of physicochemical and photocatalytic properties of visible light responsive Fe, Gd and P single and tri-doped TiO₂ nanomaterials. *J. Rare Earths* **2017**, *36*, 72–85. [CrossRef]

206. Kaur, T.; Sraw, A.; Toor, A.; Wanchoo, R. Utilization of solar energy for the degradation of carbendazim and propiconazole by Fe doped TiO₂. *Sol. Energy* **2016**, *125*, 65–76. [CrossRef]

207. Wang, Q.; Jin, R.; Zhang, M.; Gao, S. Solvothermal preparation of Fe-doped TiO₂ nanotube arrays for enhancement in visible light induced photoelectrochemical performance. *J. Alloys Compd.* **2017**, *690*, 139–144. [CrossRef]

208. Lian, J.-Z.; Tsai, C.-T.; Chang, S.-H.; Lin, N.-H.; Hsieh, Y.-H. Iron waste as an effective depend on TiO₂ for photocatalytic degradation of dye waste water. *Opt. Int. J. Light Electron Opt.* **2017**, *140*, 197–204. [CrossRef]

209. Lin, H.-J.; Yang, T.-S.; Hsi, C.-S.; Wang, M.-C.; Lee, K.-C. Optical and photocatalytic properties of Fe³⁺-doped TiO₂ thin films prepared by a sol–gel spin coating. *Ceram. Int.* **2014**, *40*, 10633–10640. [CrossRef]

210. May-Lozano, M.; Mendoza-Escamilla, V.; Rojas Garcia, E.; López-Medina, R.; Rivadeneyra-Romero, G.; Delgadillo, S. Sonophoto-catalytic degradation of Orange II dye using low cost photocatalyst. *J. Clean. Prod.* **2017**, *148*, 836–844. [CrossRef]

211. Chen, C.-C.; Hu, S.-H.; Fu, Y.-P. Effects of surface hydroxyl group density on the photocatalytic activity of Fe³⁺-doped TiO₂. *J. Alloys Compd.* **2015**, *632*, 326–334. [CrossRef]

212. Lin, H.-J.; Yang, T.-S.; Moo-Chin, W.; Hsi, C.-S. Structural and photodegradation behaviors of Fe³⁺-doping TiO₂ thin films prepared by a sol–gel spin coating. *J. Alloys Compd.* **2014**, *610*, 478–485. [CrossRef]

213. Nitoi, I.; Oancea, P.; Raileanu, M.; Crisan, M.; Constantin, L.A.; Cristea, I. UV–VIS photocatalytic degradation of nitrobenzene from water using heavy metal doped titania. *J. Ind. Eng. Chem.* **2015**, *21*, 677–682. [CrossRef]

214. Xiang, G.; Yu, Z.; Hou, Y.; Chen, Y.; Peng, Z.; Sun, L.; Sun, L. Simulated solar-light induced photoelectrocatalytic degradation of bisphenol-A using Fe³⁺-doped TiO₂ nanotube arrays as a photoanode with simultaneous aeration. *Sep. Purif. Technol.* **2016**, *161*, 144–151. [CrossRef]

215. Soo, C.W.; Juan, J.C.; Wei Lai, C.; Abd Hamid, S.B.; Yusop, R. Fe-doped mesoporous anatase-brookite titania in the solar-light-induced photodegradation of Reactive Black 5 dye. *J. Taiwan Inst. Chem. Eng.* **2016**, *68*, 153–161. [CrossRef]

216. Maki, L.; Maleki, A.; Rezaee, R.; Daraei, H. LED-activated immobilized Fe-Ce-N tri-doped TiO₂ nanocatalyst on glass bed for photocatalytic degradation organic dye from aqueous solutions. *Environ. Technol. Innov.* **2019**, *15*, 100411. [CrossRef]

217. Hosseini, M.; Ebratkhahan, M.; Shayegan, Z.; Niaei, A.; Salari, D.; Rostami, A.; Raeisipour, J. Investigation of the effective operational parameters of self-cleaning glass surface coating to improve methylene blue removal efficiency; application in solar cells. *Sol. Energy* **2020**, *207*, 398–408. [CrossRef]

218. Choudhury, B.; Choudhury, A. Dopant induced changes in structural and optical properties of Cr³⁺ doped TiO₂ nanoparticles. *Mater. Chem. Phys.* **2012**, *132*, 1112–1118. [CrossRef]

219. Wang, Z.-M.; Yang, G.; Biswas, P.; Bresser, W.; Boolchand, P. Processing of Iron-Doped Titania Powders in Flame Aerosol Reactors. *Powder Technol.* **2001**, *114*, 197–204. [CrossRef]

220. Peng, Y.-H.; Huang, G.; Huang, W.-Q. Visible-light absorption and photocatalytic activity of Cr-doped TiO₂ nanocrystal films. *Adv. Powder Technol.* **2012**, *23*, 8–12. [CrossRef]

221. Mardare, D.; Iacomi, F.; Cornei, N.; Girtan, M.; Luca, D. Undoped and Cr-doped TiO₂ thin films obtained by spray pyrolysis. *Thin Solid Films* **2010**, *518*, 4586–4589. [CrossRef]

222. Pei wen, K.; Mohd Hatta, M.H.; Ong, S.; Yuliati, L.; Lee, S. Photocatalytic degradation of photosensitizing and non-photosensitizing dyes over chromium doped titania photocatalysts under visible light. *J. Photochem. Photobiol. A Chem.* **2017**, *332*, 215–223. [CrossRef]

223. Yamazaki, S.; Fujiwara, Y.; Yabuno, S.; Adachi, K.; Honda, K. Preparation of porous metal-ion-doped titanium dioxide and the photocatalytic degradation of 4-chlorophenol under visible light irradiation. *Appl. Catal. B Environ.* **2012**, *121–122*, 148–153. [CrossRef]

224. Inturi, S.; Suidan, M.; Smirniotis, P. Influence of synthesis method on leaching of the Cr-TiO₂ catalyst for visible light liquid phase photocatalysis and their stability. *Appl. Catal. B Environ.* **2016**, *180*, 351–361. [CrossRef]

225. Park, S.; Joo, H.; Kang, J.-W. Effect of impurities in TiO₂ thin films on trichloroethylene conversion. *Sol. Energy Mater. Sol. Cells* **2004**, *83*, 39–53. [CrossRef]

226. Khan, H.; Jiang, Z.; Berk, D. Molybdenum doped graphene/TiO₂ hybrid photocatalyst for UV/visible photocatalytic applications. *Sol. Energy* **2018**, *162*, 420–430. [CrossRef]

227. Du, Y.; Gan, Y.; Yang, P.; Zhao, F.; Hua, N.; Jiang, L. Improvement in the Heat-Induced Hydrophilicity of TiO₂ Thin Films by Doping Mo(VI) Ions. *Thin Solid Films* **2005**, *491*, 133–136. [CrossRef]

228. Stengl, V.; Bakardjieva, S. Molybdenum-Doped Anatase and Its Extraordinary Photocatalytic Activity in the Degradation of Orange II in the UV and Vis Regions. *J. Phys. Chem. C* **2010**, *114*, 19308–19317. [CrossRef]

229. Shahmoradi, B.; Ibrahim, I.; Sakamoto, N.; Ananda, S.; Row, T.; Soga, K.; Byrappa, K.; Parsons, S.; Shimizu, Y. In situ surface modification of molybdenum-doped organic-inorganic hybrid TiO$_2$ nanoparticles under hydrothermal conditions and treatment of pharmaceutical effluent. *Environ. Technol.* **2010**, *31*, 1213–1220. [CrossRef]

230. Cui, M.; Pan, S.; Tang, Z.; Chen, X.; Qiao, X.; Xu, Q. Physiochemical properties of n-n heterostructured TiO$_2$/Mo-TiO$_2$ composites and their photocatalytic degradation of gaseous toluene. *Chem. Speciat. Bioavailab.* **2017**, *29*, 60–69. [CrossRef]

231. Zhan, C.; Chen, F.; Dai, H.; Yang, J.; Zhong, M. Photocatalytic activity of sulfated Mo-doped TiO$_2$@fumed SiO$_2$ composite: A mesoporous structure for methyl orange degradation. *Chem. Eng. J.* **2013**, *225*, 695–703. [CrossRef]

232. Moghadam, R.; Vankova, S.; Monteverde Videla, A.; Specchia, S. Innovative carbon-free low content Pt catalyst supported on Mo-doped titanium suboxide (Ti$_3$O$_5$-Mo) for stable and durable oxygen reduction reaction. *Appl. Catal. B Environ.* **2016**, *201*, 419. [CrossRef]

233. Avilés, O.; Espino-Valencia, J.; Romero, R.; Rico-Cerda, J.; Arroyo-Albiter, M.; Natividad, R. W and Mo doped TiO$_2$: Synthesis, characterization and photocatalytic activity. *Fuel* **2017**, *198*, 31–41. [CrossRef]

234. Sun, P.; Lu, Q.; Zhang, J.; Xiao, T.; Liu, W.; Ma, J.; Yin, S.; Cao, W. Mo-ion doping evoked visible light response in TiO$_2$ nanocrystals for highly-efficient removal of benzene. *Chem. Eng. J.* **2020**, *397*, 125444. [CrossRef]

235. Yang, H.; Li, X.; Wang, A.; Wang, Y.; Chen, Y. Photocatalytic degradation of methylene blue by MoO$_3$ modified TiO$_2$ under visible light. *Chinese J. Catal.* **2014**, *35*, 140–147. [CrossRef]

236. Liu, S.; Zhao, X.; Wang, Y.; Shao, H.; Qiao, M.; Wang, Y.; Zhao, S. Peroxymonosulfate enhanced photoelectrocatalytic degradation of phenol activated by Co$_3$O$_4$ loaded carbon fiber cathode. *J. Catal.* **2017**, *355*, 167–175. [CrossRef]

237. Yue, X.; Jiang, S.; Ni, L.; Wang, R.; Qiu, S.; Zhang, Z. The highly efficient photocatalysts of Co/TiO$_2$: Photogenerated charge-transfer properties and their applications in photocatalysis. *Chem. Phys. Lett.* **2014**, *615*, 111–116. [CrossRef]

238. Cao, C.; Hu, C.; Shen, W.; Wang, S.; Wang, J.; Tian, Y. Fabrication of a novel heterostructure of Co$_3$O$_4$-modified TiO$_2$ nanorod arrays and its enhanced photoelectrochemical property. *J. Alloys Compd.* **2013**, *550*, 137–143. [CrossRef]

239. Naseem, S.; Pinchuk, I.; Luo, Y.K.; Kawakami, R.; Khan, S.; Husain, S.; Khan, W. Epitaxial growth of cobalt doped TiO$_2$ thin films on LaAlO$_3$(100) substrate by Molecular Beam Epitaxy and their opto-magnetic based applications. *Appl. Surf. Sci.* **2019**, *493*, 691–702. [CrossRef]

240. Elmragui, A.; Logvina, Y.; Pinto da Silva, L.; Zegaoui, O.; Silva, J. Synthesis of Fe- and Co-Doped TiO$_2$ with Improved Photocatalytic Activity Under Visible Irradiation Toward Carbamazepine Degradation. *Materials* **2019**, *12*, 3874. [CrossRef]

241. Mi, C.; Han, E.; Sun, L.; Zhu, L. Effect of Ti^{4+} doping on LiNi$_{0.35}$Co$_{0.27}$Mn$_{0.35}$Fe$_{0.03}$O$_2$. *Solid State Ionics* **2019**, *340*, 114976. [CrossRef]

242. Ebrahimian, A.; Monazzam, P.; Fakhari Kisomi, B. Co/TiO$_2$ nanoparticles: Preparation, characterization and its application for photocatalytic degradation of methylene blue. *Desalin. Wtare Treat.* **2017**, *63*, 283–292. [CrossRef]

243. Iwasaki, M.; Hara, M.; Kawada, H.; Tada, H.; Ito, S. Cobalt Ion-Doped TiO$_2$ Photocatalyst Response to Visible Light. *J. Colloid Interface Sci.* **2000**, *224*, 202–204. [CrossRef]

244. Hamadanian, M.; Reisi-Vanani, A.; Majedi, A. Sol-gel preparation and characterization of Co/TiO$_2$ nanoparticles: Application to the degradation of methyl orange. *Chem. Soc* **2010**, *7*, 52–58. [CrossRef]

245. Shifu, C.; Wei, L.; Sujuan, Z.; Yinghao, C. Preparation and activity evaluation of relative p-n junction photocatalyst Co-TiO$_2$/TiO$_2$. *J. Sol-Gel Sci. Technol.* **2010**, *54*, 258–267. [CrossRef]

246. Amadelli, R.; Samiolo, L.; Andrea, M.; Molinari, A.; Mario, V.; Gazzoli, D. Preparation, Characterisation, and Photocatalytic Behaviour of Co-TiO$_2$ with Visible Light Response. *Int. J. Photoenergy* **2008**, *2008*, 853753. [CrossRef]

247. Nesfchi, M.; Ebrahimian, A.; Saraei, F.; Rojaee, F.; Mahdavi, F.; Rastegar, S. Fabrication of plasmonic nanoparticles/cobalt doped TiO$_2$ nanosheets for degradation of tetracycline and modeling the process by artificial intelligence techniques. *Mater. Sci. Semicond. Process.* **2021**, *122*, 105465. [CrossRef]

248. Elmragui, A.; Zegaoui, O.; Silva, J. Elucidation of the photocatalytic degradation mechanism of an azo dye under visible light in the presence of cobalt doped TiO$_2$ nanomaterials. *Chemosphere* **2020**, *266*, 128931. [CrossRef] [PubMed]

249. Pirbazari, A. Sensitization of TiO$_2$ Nanoparticles With Cobalt Phthalocyanine: An Active Photocatalyst for Degradation of 4-Chlorophenol under Visible Light. *Procedia Mater. Sci.* **2015**, *11*, 622–627. [CrossRef]

250. Alyani, S.; Ebrahimian, A.; Khalilsaraei, F.; Asasian, N.; Gilani, N. Growing Co-doped TiO$_2$ nanosheets on reduced graphene oxide for efficient photocatalytic removal of tetracycline antibiotic from aqueous solution and modeling the process by artificial neural network. *J. Alloys Compd.* **2019**, *799*, 169–182. [CrossRef]

251. Miao, Y.; Zhai, Z.; Jiang, L.; Shi, Y.; Yan, Z.; Duan, D.; Zhen, K.; Wang, J. Facile and new synthesis of cobalt doped mesoporous TiO$_2$ with high visible-light performance. *Powder Technol.* **2014**, *266*, 365–371. [CrossRef]

252. Hosaini, N.; Kamran-Pirzaman, A.; Aroon, M.; Ebrahimian, A. Photocatalytic degradation of 2,4-dichlorophenol by Co-doped TiO$_2$(Co/TiO$_2$) nanoparticles and Co/TiO$_2$ containing mixed matrix membranes. *J. Water Process Eng.* **2017**, *2017*, 124–134. [CrossRef]

253. Crisan, M.; Drăgan, N.; Crisan, D.; Ianculescu, A.; Nitoi, I.; Oancea, P.; Todan, L.; Stan, C.; Stanica, N. The effects of Fe, Co and Ni dopants on TiO$_2$ structure of sol-gel nanopowders used as photocatalysts for environmental protection: A comparative study. *Ceram. Int.* **2015**, *42*, 3088–3095. [CrossRef]

254. Preethi, T.; Abarna, B.; Vidhya, K.N.; Rajarajeswari, G.R. Sol-gel derived cobalt doped nano-titania photocatalytic system for solar light induced degradation of crystal violet. *Ceram. Int.* **2014**, *40*, 13159. [CrossRef]

255. Lee, B.-K. Rapid photo-degradation of 2-chlorophenol under visible light irradiation using cobalt oxide-loaded TiO$_2$/reduced graphene oxide nanocomposite from aqueous media. *J. Environ. Manag.* **2016**, *165*, 1–10. [CrossRef]

256. Drăgan, N.; Crisan, M.; Răileanu, M.; Crisan, D.; Ianculescu, A.; Oancea, P.; Somacescu, S.; Todan, L.; Stanica, N.; Vasile, B. The effect of Co dopant on TiO₂ structure of sol–gel nanopowders used as photocatalysts. *Ceram. Int.* **2014**, *40*, 12273–12284. [CrossRef]

257. Sevim, A. Synthesis and characterization of Zn and Co monocarboxy-phthalocyanines and investigation of their photocatalytic efficiency as TiO₂ composites. *J. Organomet. Chem.* **2017**, *832*, 18–26. [CrossRef]

258. Dong, F.; Guo, S.; Wang, H.; Li, X.; Wu, Z. Enhancement of the Visible Light Photocatalytic Activity of C-Doped TiO₂ Nanomaterials Prepared by a Green Synthetic Approach. *J. Phys. Chem. C* **2011**, *115*, 13285–13292. [CrossRef]

259. Ravishankar, T.N.; Vaz, M.d.O.; Ramakrishnappa, T.; Teixeira, S.R.; Dupont, J. Ionic liquid–assisted hydrothermal synthesis of Nb/TiO₂ nanocomposites for efficient photocatalytic hydrogen production and photodecolorization of Rhodamine B under UVvisible and visible light illuminations. *Mater. Today Chem.* **2019**, *12*, 373–385. [CrossRef]

260. Furubayashi, Y.; Hitosugi, T.; Yamamoto, Y.; Inaba, K.; Kinoda, G.; Hirose, Y.; Shimada, T.; Hasegawa, T. A transparent metal: Nb-doped anatase TiO₂. *Appl. Phys. Lett.* **2005**, *86*, 252101. [CrossRef]

261. De Trizio, L.; Buonsanti, R.; Schimpf, A.; Llordés, A.; Gamelin, D.; Simonutti, R.; Milliron, D. Nb-Doped Colloidal TiO₂ Nanocrystals with Tunable Infrared Absorption. *Chem. Mater.* **2013**, *25*, 3383–3390. [CrossRef]

262. Su, H.; Huang, Y.-T.; Chang, Y.-H.; Zhai, P.; Hau, N.; Cheung, P.; Yeh, W.-T.; Wei, T.; Feng, S.-P. The Synthesis of Nb-doped TiO₂ Nanoparticles for Improved-Performance Dye Sensitized Solar Cells. *Electrochim. Acta* **2015**, *182*, 230–237. [CrossRef]

263. Khan, S.; Cho, H.; Han, S.S.; Lee, K.; Cho, S.-H.; Song, T.; Choi, H. Defect engineering toward strong photocatalysis of Nb-doped anatase TiO₂: Computational predictions and experimental verifications. *Appl. Catal. B Environ.* **2017**, *206*, 520–530. [CrossRef]

264. Lim, J.; Murugan, P.; Lakshminarasimhan, N.; Kim, J.; Lee, J.S.; Lee, S.-H.; Choi, W. Synergic photocatalytic effects of nitrogen and niobium co-doping in TiO₂ for the redox conversion of aquatic pollutants under visible light. *J. Catal.* **2014**, *310*, 91–99. [CrossRef]

265. Lim, J.; Monllor-Satoca, D.; Jang, J.; Lee, S.; Choi, W. Visible light photocatalysis of fullerol-complexed TiO₂ enhanced by Nb doping. *Appl. Catal. B Environ.* **2014**, *152–153*, 233–240. [CrossRef]

266. Ferraz, N.; Marcos, F.; Nogueira, A.; Martins, A.; Lanza, M.; Assaf, E.; Asencios, Y. Hexagonal-Nb₂O₅/Anatase-TiO₂ mixtures and their applications in the removal of Methylene Blue Dye under various conditions. *Mater. Chem. Phys.* **2017**, *198*, 331–340. [CrossRef]

267. Kou, Y.; Yang, J.; Li, B.; Fu, S. Solar photocatalytic activities of porous Nb-doped TiO₂ microspheres by coupling with tungsten oxide. *Mater. Res. Bull.* **2015**, *63*, 105–111. [CrossRef]

268. Silva, A.; Muche, D.; Dey, S.; Hotza, D.; Castro, R. Photocatalytic Nb₂O₅-doped TiO₂ nanoparticles for glazed ceramic tiles. *Ceram. Int.* **2015**, *42*, 5113–5122. [CrossRef]

269. Lee, D.; Park, J.-H.; Kim, Y.-H.; Lee, M.-H.; Cho, N.-I. Effect of Nb doping on morphology, crystal structure, optical band gap energy of TiO₂ thin films. *Curr. Appl. Phys.* **2014**, *14*, 421–427. [CrossRef]

270. Ullah, I.; Haider, A.; Khalid, N.; Ali, S.; Ahmed, S.; Khan, Y.; Ahmed, N.; Zubair, M. Tuning the band gap of TiO₂ by tungsten doping for efficient UV and visible photodegradation of Congo red dye. *Spectrochim. Acta Part A Mol. Biomol. Spectrosc.* **2018**, *204*, 150–157. [CrossRef] [PubMed]

271. Yadav, M.; Yadav, A.; Fernandes, R.; Popat, Y.; Orlandi, M.; Dashora, A.; Kothari, D.C.; Miotello, A.; Ahuja, B.; Patel, N. Tungsten-doped TiO₂/reduced Graphene Oxide nano-composite photocatalyst for degradation of phenol: A system to reduce surface and bulk electron-hole recombination. *J. Environ. Manag.* **2017**, *203*, 364–374. [CrossRef] [PubMed]

272. Grabowska, E.; Nadolna, J.; Zaleska-Medynska, A. Mechanism of phenol photodegradation in the presence of pure and modified-TiO₂: A review. *Water Res.* **2012**, *46*, 5453–5471. [CrossRef]

273. Thomas, M.; Natarajan, T. TiO₂-High Surface Area Materials Based Composite Photocatalytic Nanomaterials for Degradation of Pollutants: A Review. In *Photocatalytic Nanomaterials for Environmental Applications*; MRF: Millersville, PA, USA, 2018; ISBN 978-1-945291-58-6.

274. Palmisano, L.; Sclafani, A.; Venezia, A.M.; Campostrini, R.; Carturan, G.; Martin, C.; Rives, V.; Solana, G. Influence of tungsten oxide on structural and surface properties of sol-gel prepared TiO₂ employed for 4-nitrophenol photodegradation. *J. Chem. Soc. Faraday Trans.* **1996**, *92*, 819–829. [CrossRef]

275. Keller, V.; Bernhardt, P.; Garin, F. Photocatalytic oxidation of butyl acetate in vapor phase on TiO₂, Pt/TiO₂ and WO₃/TiO₂ catalysts. *J. Catal.* **2003**, *15*, 129–138. [CrossRef]

276. Y, T.; Song, K.; Lee, W.; Choi, G.; Y, R. Photocatalytic Behavior of WO₃-Loaded TiO₂ in an Oxidation Reaction. *J. Catal.* **2000**, *191*, 192–199. [CrossRef]

277. Du, S.; Liao, Z.; Qin, Z.; Zuo, F.; Li, X. Polydopamine microparticles as redox mediators for catalytic reduction of methylene blue and rhodamine B. *Catal. Commun.* **2015**, *72*, 86–90. [CrossRef]

278. Li, J.; Luo, D.; Yang, C.; He, S.; Chen, S.; Lin, J.; Zhu, L.; Li, X. Copper(II) imidazolate frameworks as highly efficient photocatalysts for reduction of CO₂ into methanol under visible light irradiation. *J. Solid State Chem.* **2013**, *203*, 154–159. [CrossRef]

279. Cai, H.; Chen, X.; Li, Q.; He, B.; Tang, Q. Enhanced photocatalytic activity from Gd, La codoped TiO₂ nanotube array photocatalysts under visible-light irradiation. *Appl. Surf. Sci.* **2013**, *284*, 837–842. [CrossRef]

280. Ki, S.J.; Park, Y.-K.; Kim, J.-S.; Lee, W.-J.; Lee, H.; Jung, S.-C. Facile Preparation of Tungsten Oxide Doped TiO₂ Photocatalysts using Liquid Phase Plasma Process for Enhanced Degradation of Diethyl Phthalate. *Chem. Eng. J.* **2018**, *377*, 120087. [CrossRef]

281. Azadi, S.; Karimi-Jashni, A.; Javadpour, S. Modeling and Optimization of Photocatalytic Treatment of Landfill Leachate using Tungsten-doped TiO₂ Nano-photocatalysts: Application of Artificial Neural Network and Genetic Algorithm. *Process Saf. Environ. Prot.* **2018**, *117*, 267–277. [CrossRef]

282. Kondamareddy, K.; D, N.; Lu, D.; Peng, T.; Macias, M.; Wang, C.; Yu, Z.; Cheng, N.; Fu, D.; Zhao, X.-Z. Ultra-trace (parts per million-ppm) W^{6+} dopant ions induced anatase to rutile transition (ART) of phase pure anatase TiO_2 nanoparticles for highly efficient visible light-active photocatalytic degradation of organic pollutants. *Appl. Surf. Sci.* **2018**, *456*, 676–693. [CrossRef]

283. Mayoufi, A.; Nsib, M.; Houas, A. Doping level effect on visible-light irradiation W-doped TiO_2–anatase photocatalysts for Congo red photodegradation. *Comptes Rendus Chim.* **2014**, *17*, 818–823. [CrossRef]

284. Wang, X.; Sun, M.; Murugananthan, M.; Zhang, Y.; Zhang, L. Electrochemically Self-Doped WO_3/TiO_2 Nanotubes for Photocatalytic Degradation of Volatile Organic Compounds. *Appl. Catal. B Environ.* **2019**, *260*, 118205. [CrossRef]

285. Xu, H.; Liao, J.; Yuan, S.; Zhao, Y.; Zhang, M.; Wang, Z.; Shi, L. Tuning the morphology, stability and photocatalytic activity of TiO_2 nanocrystal colloids by tungsten doping. *Mater. Res. Bull.* **2014**, *51*, 326–331. [CrossRef]

286. Wang, Q.; Zhang, W.; Hu, X.; Xu, L.; Chen, G.; Li, X. Hollow spherical WO_3/TiO_2 heterojunction for enhancing photocatalytic performance in visible-light. *J. Water Process Eng.* **2021**, *40*, 101943. [CrossRef]

287. Fouad, K.; Gar Alalm, M.; Bassyouni, M.; Saleh, M. A novel photocatalytic reactor for the extended reuse of $W–TiO_2$ in the degradation of sulfamethazine. *Chemosphere* **2020**, *257*, 127270. [CrossRef] [PubMed]

288. Abraham, C.; Devi, L.G. One-pot facile sol-gel synthesis of W, N, C and S doped TiO_2 and its application in the photocatalytic degradation of thymol under the solar light irradiation: Reaction kinetics and degradation mechanism. *J. Phys. Chem. Solids* **2020**, *141*, 109350. [CrossRef]

289. Hunge, Y.; Mahadik, M.; Moholkar, A.; Bhosale, C. Photoelectrocatalytic degradation of oxalic acid using WO_3 and stratified WO_3/TiO_2 photocatalysts under sunlight illumination. *Ultrason. Sonochem.* **2016**, *35*, 233–242. [CrossRef]

290. Wattanawikkam, C.; Pecharapa, W. Structural studies and photocatalytic properties of Mn and Zn co-doping on TiO_2 prepared by single step sonochemical method. *Radiat. Phys. Chem.* **2020**, *171*, 108714. [CrossRef]

291. El-Mehasseb, I.; Kandil, S.; Elgindy, K. Advanced visible-light applications utilizing modified Zn-doped TiO_2 nanoparticles via non-metal in situ dual doping for wastewater detoxification. *Optik* **2020**, *213*, 164654. [CrossRef]

292. Sanchez-Dominguez, M.; Morales-Mendoza, G.; Rodriguez-Vargas, M.; Ibarra-Malo, C.; Rodríguez, A.; Vela-Gonzalez, A.; Perez, A.; Gomez, R. Synthesis of Zn-doped TiO_2 nanoparticles by the novel oil-in-water (O/W) microemulsion method and their use for the photocatalytic degradation of phenol. *J. Environ. Chem. Eng.* **2015**, *3*, 3037–3047. [CrossRef]

293. Michaelson, H.B. The work function of the elements and its periodicity. *J. Appl. Phys.* **2021**, *48*, 4729–4733. [CrossRef]

294. Linic, S.; Christopher, P.; Ingram, D. Plasmonic-metal nanostructures for efficient conversion of solar to chemical energy. *Nat. Mater.* **2011**, *10*, 911–921. [CrossRef]

295. Kochuveedu, S.; Jang, Y.H.; Kim, D.H. A Study on the Mechanism for the Interaction of Light with Noble Metal-Metal Oxide Semiconductor Nanostructures for Various Photophysical Applications. *Chem. Soc. Rev.* **2013**, *42*, 8467–8493. [CrossRef]

296. Ali, F.; Khan, S.; Kamal, T.; Alamry, K.; Asiri, A.M. Chitosan-titanium oxide fibers supported zero-valent nanoparticles: Highly efficient and easily retrievable catalyst for the removal of organic pollutants. *Sci. Rep.* **2018**, *8*, 6260. [CrossRef]

297. Naya, S.-I.; Niwa, T.; Kume, T.; Tada, H. Visible-Light-Induced Electron Transport from Small to Large Nanoparticles in Bimodal Gold Nanoparticle-Loaded Titanium (IV) Oxide. *Angew. Chem. Int. Ed. Engl.* **2014**, *53*, 7305–7309. [CrossRef] [PubMed]

298. Ahmad Rather, R.; Sharma, P.; Kumar, P.; Singh, S.; Pal, B. Plasmonic Stimulated Photocatalytic/Electrochemical Hydrogen Evolution from Water by (001) Faceted and bimetallic Loaded Titania Nanosheets under Sunlight Irradiation. *J. Clean. Prod.* **2017**, *175*, 394–401. [CrossRef]

299. Ghosh, S.; Mallik, A.; Basu, R. Enhanced photocatalytic activity and photoresponse of poly(3,4-ethylenedioxythiophene) nanofibers decorated with gold nanoparticle under visible light. *Sol. Energy* **2017**, *159*, 548–560. [CrossRef]

300. Wang, M.; Ye, M.; Iocozzia, J.; Lin, C.; Lin, Z. Plasmon-Mediated Solar Energy Conversion via Photocatalysis in Noble Metal/Semiconductor Composites. *Adv. Sci.* **2016**, *3*, 1600024. [CrossRef]

301. Li, G.; Li, J.; Li, G.; Jiang, G. N and Ti^{3+} co-doped 3D anatase TiO_2 superstructures composed of ultrathin nanosheets with enhanced visible light photocatalytic activity. *J. Mater. Chem. A* **2015**, *3*, 22073–22080. [CrossRef]

302. Cheng, L.; Zhang, D.; Liao, Y.; Li, F.; Zhang, H.; Xiang, Q. Constructing functionalized plasmonic Au/TiO_2 nanosheets with small Au nanoparticles for efficient photocatalytic hydrogen evolution. *J. Colloid Interface Sci.* **2019**, *555*, 94–103. [CrossRef]

303. Naya, S.; Tada, H. Dependence of the plasmonic activity of Au/TiO_2 for the decomposition of 2-naphthol on the crystal form of TiO_2 and Au particle size. *J. Catal.* **2018**, *364*, 328–333. [CrossRef]

304. Shoueir, K.; Kandil, S.; El-Hosainy, H. Tailoring the surface reactivity of plasmonic $Au@TiO_2$ photocatalyst bio-based chitosan fiber towards cleaner of harmful water pollutants under visible-light irradiation. *J. Clean. Prod.* **2019**, *230*, 383–393. [CrossRef]

305. Cojocaru, B.; Andrei, V.; Tudorache, M.; Lin, F.; Cadigan, C.; Richards, R.; Parvulescu, V. Enhanced photo-degradation of bisphenol pollutants onto gold-modified photocatalysts. *Catal. Today* **2016**, *284*, 153–159. [CrossRef]

306. Hazra Chowdhury, I.; Roy, M.; Kundu, S.; Naskar, M. TiO_2 hollow microspheres impregnated with biogenic gold nanoparticles for the efficient visible light-induced photodegradation of phenol. *J. Phys. Chem. Solids* **2019**, *129*, 329–339. [CrossRef]

307. Celebi, N.; Aydın, M.Y.; Soysal, F.; Ciftci, Y.; Salimi, K. Ligand-free fabrication of Au/TiO_2 nanostructures for plasmonic hot-electron-driven photocatalysis: Photoelectrochemical water splitting and organic-dye degredation. *J. Alloys Compd.* **2021**, *860*, 157908. [CrossRef]

308. Wang, Y.; Yang, C.; Chen, A.; Pu, W.; Gong, J. Influence of yolk-shell $Au@TiO_2$ structure induced photocatalytic activity towards gaseous pollutant degradation under visible light. *Appl. Catal. B Environ.* **2019**, *251*, 57–65. [CrossRef]

309. Nasirian, M.; Mehrvar, M. Modification of TiO$_2$ to Enhance Photocatalytic Degradation of Organics in Aqueous Solutions. *J. Environ. Chem. Eng.* **2016**, *4*, 4072–4082. [CrossRef]
310. Al-Hajji, L.; Ismail, A.; Bumajdad, A.; al Saidi, M.; Ahmed, S.A.; Almutawa, F.; Alhazza, A. Construction of Au/TiO$_2$ Heterojunction with high photocatalytic performances under UVA illumination. *Ceram. Int.* **2020**, *46*, 20155–20162. [CrossRef]
311. Tiwari, A.; Shukla, A.; Lalliansanga; Tiwari, D.; Lee, S. Au-nanoparticle/Nanopillars TiO$_2$ meso-porous thin films in the degradation of tetracycline using UV-A light. *J. Ind. Eng. Chem.* **2018**, *69*, 141–152. [CrossRef]
312. Singh, J.; Sahu, K.; Satpati, B.; Shah, J.; Kotnala, R.K.; Mohapatra, S. Facile synthesis, structural and optical properties of Au-TiO$_2$ plasmonic nanohybrids for photocatalytic applications. *J. Phys. Chem. Solids* **2019**, *135*, 109100. [CrossRef]
313. Nalenthiran, P.; Murugesan, S.; Sathishkumar, P.; Sambandam, A. Photocatalytic degradation of ceftiofur sodium in the presence of gold nanoparticles loaded TiO$_2$ under UV–visible light. *Chem. Eng. J.* **2014**, *241*, 401–409. [CrossRef]
314. Hernandez, R.; Olvera-Rodríguez, I.; Guzmán, C.; Medel, A.; Escobar-Alarcón, L.; Brillas, E.; Sirés, I.; Escalante, K. Microwave-assisted sol-gel synthesis of an Au-TiO$_2$ photoanode for the advanced oxidation of paracetamol as model pharmaceutical pollutant. *Electrochem. Commun.* **2018**, *96*, 42–46. [CrossRef]
315. Khaywah, M.; Jradi, S.; Louarn, G.; Lacroute, Y.; Toufaily, J.; Hamieh, T.; Adam, P.-M. Ultrastable, Uniform, Reproducible, and Highly Sensitive Bimetallic Nanoparticles as Reliable Large Scale SERS Substrates. *J. Phys. Chem.* **2015**, *119*, 26091–26100. [CrossRef]
316. Kallel, W.; Chaabene, S.; Bouattour, S. Novel (Ag,Y) doped TiO$_2$ plasmonic photocatalyst with enhanced photocatalytic activity under visible light. *Physicochem. Probl. Miner. Process.* **2019**, *55*, 745–759. [CrossRef]
317. Katchala, N.; Reddy, S.K.; Rao, T.; Anandan, S. Energy level matching for efficient charge transfer in Ag doped–Ag modified TiO$_2$ for enhanced visible light photocatalytic activity. *J. Alloys Compd.* **2019**, *794*. [CrossRef]
318. Ali, T.; Ahmed, A.; Alam, U.; Uddin, I.; Tripathi, P.; Muneer, M. Enhanced photocatalytic and antibacterial activities of Ag-doped TiO$_2$ nanoparticles under visible light. *Mater. Chem. Phys.* **2018**, *212*, 325–335. [CrossRef]
319. Peng, C.; Wang, W.; Zhang, W.; Liang, Y.; Zhuo, L. Surface plasmon-driven photoelectrochemical water splitting of TiO$_2$ nanowires decorated with Ag nanoparticles under visible light illumination. *Appl. Surf. Sci.* **2017**, *420*, 286–295. [CrossRef]
320. Bhavani, K.; Naresh, G.; Srinivas, B.; Venugopal, A. Plasmonic resonance nature of Ag-Cu/TiO$_2$ photocatalyst under solar and artificial light: Synthesis, characterization and evaluation of H$_2$O splitting activity. *Appl. Catal. B Environ.* **2016**, *199*, 282–291. [CrossRef]
321. Ryu, S.-Y.; Chung, J.W.; Kwak, S.-Y. Dependence of photocatalytic and antimicrobial activity of electrospun polymeric nanofiber composites on the positioning of Ag-TiO$_2$ nanoparticles. *Compos. Sci. Technol.* **2015**, *117*, 9–17. [CrossRef]
322. Du, M.; Xiong, S.; Wu, T.; Zhao, D.; Zhang, Q.; Fan, Z.; Zeng, Y.; Ji, F.; He, Q.; Xu, X. Preparation of a Microspherical Silver-Reduced Graphene Oxide-Bismuth Vanadate Composite and Evaluation of Its Photocatalytic Activity. *Materials* **2016**, *9*, 160. [CrossRef] [PubMed]
323. Rahul, T.K.; Sandhyarani, N. Plasmonic and Photonic Effects on Hydrogen Evolution over Chemically Modified Titania Inverse Opals. *ChemNanoMat* **2018**, *4*, 642–648. [CrossRef]
324. Low, J.; Qiu, S.; Xu, D.; Jiang, C.; Cheng, B. Direct evidence and enhancement of surface plasmon resonance effect on Ag-loaded TiO$_2$ nanotube arrays for photocatalytic CO$_2$ reduction. *Appl. Surf. Sci.* **2017**, *434*, 423–432. [CrossRef]
325. Perumal, S.; MonikandaPrabu, K.; Sambandam, C.G.; Mohamed, A.P. Synthesis and characterization studies of solvothermally synthesized undoped and Ag-doped TiO$_2$ nanoparticles using toluene as a solvent. *J. Eng. Res. Appl.* **2014**, *4*, 184–187.
326. Zhang, L.; Ni, C.; Jiu, H.; Xie, C.; Yan, J.; Qi, G. One-pot synthesis of Ag-TiO$_2$/reduced graphene oxide nanocomposite for high performance of adsorption and photocatalysis. *Ceram. Int.* **2017**, *43*, 5450–5456. [CrossRef]
327. Chen, P. A novel synthesis of Ti^{3+} self-doped Ag$_2$O/TiO$_2$ (p–n) nanoheterojunctions for enhanced visible photocatalytic activity. *Mater. Lett.* **2016**, *163*, 130–133. [CrossRef]
328. Wang, T.; Tang, T.; Gao, Y.; Chen, Q.; Zhang, Z.; Bian, H. Hydrothermal preparation of Ag-TiO$_2$-reduced graphene oxide ternary microspheres structure composite for enhancing photocatalytic activity. *Phys. E Low-Dimens. Syst. Nanostruct.* **2018**, *112*, 128–136. [CrossRef]
329. Devi, L.; Kavitha, R. A review on plasmonic metal-TiO$_2$ composite for generation, trapping, storing and dynamic vectorial transfer of photogenerated electrons across the Schottky junction in a Photocatalytic system. *Appl. Surf. Sci.* **2015**, *360*, 601–622. [CrossRef]
330. Khalid, N.R.; Ahmed, E.; Ahmad, M.; Niaz, N.A.; Ramzan, M.; Shakil, M.; Iqbal, T.; Majid, A. Microwave-assisted synthesis of Ag-TiO$_2$/graphene composite for hydrogen production under visible light irradiation. *Ceram. Int.* **2016**, *42*, 18257–18263. [CrossRef]
331. Rong, X.; Qiu, F.; Zhang, C.; Fu, L.; Wang, Y.; Yang, D. Preparation of Ag–AgBr/TiO$_2$–graphene and its visible light photocatalytic activity enhancement for the degradation of polyacrylamide. *J. Alloys Compd.* **2015**, *639*, 153–161. [CrossRef]
332. Quan, X.; Tan, H.; Zhao, Q.; Sang, X. Preparation of lanthanum-doped TiO$_2$ photocatalysts by coprecipitation. *J. Mater. Sci.* **2007**, *42*, 6287–6296. [CrossRef]
333. Ashraf, M.; Liu, Z.; Peng, W.-X.; Jermsittiparsert, K.; Hosseinzadeh, G.; Hosseinzadeh, R. Combination of sonochemical and freeze-drying methods for synthesis of graphene/Ag-doped TiO$_2$ nanocomposite: A strategy to boost the photocatalytic performance via well distribution of nanoparticles between graphene sheets. *Ceram. Int.* **2019**, *46*, 7446–7452. [CrossRef]
334. Demirci, S.; Dikici, T.; Yurddaskal, M.; Gültekin, S.; Toparli, M.; Çelik, E. Synthesis and characterization of Ag doped TiO$_2$ heterojunction films and their photocatalytic performances. *Appl. Surf. Sci.* **2016**, *390*, 591–601. [CrossRef]

335. Malfatti, L.; Carboni, D.; Pinna, A.; Lasio, B.; Marmiroli, B.; Innocenzi, P. In situ growth of Ag nanoparticles in graphene–TiO$_2$ mesoporous films induced by hard X-ray. *J. Sol-Gel Sci. Technol.* **2016**, *79*, 295–302. [CrossRef]

336. Zhou, G.; Meng, H.; Cao, Y.; Kou, X.; Duan, S.; Fan, L.; Xiao, M.; Zhou, F.; Li, Z.; Xing, Z. Surface Plasmon Resonance-Enhanced Solar-Driven Photocatalytic Performance from Ag Nanoparticles-Decorated Ti^{3+} Self-Doped Porous Black TiO$_2$ Pillars. *J. Ind. Eng. Chem.* **2018**, *64*, 188–193. [CrossRef]

337. Liu, R.; Wang, P.; Wang, X.; Yu, H.; Yu, J. UV- and Visible-Light Photocatalytic Activity of Simultaneously Deposited and Doped Ag/Ag(I)-TiO$_2$ Photocatalyst. *J. Phys. Chem. C* **2012**, *116*, 17721–17728. [CrossRef]

338. Hou, X.; Liu, A.-D.; Huang, M.-D.; Liao, B.; Wu, X.-L. First-Principles Band Calculations on Electronic Structures of Ag-Doped Rutile and Anatase TiO$_2$. *Chin. Phys. Lett.* **2009**, *26*, 077106. [CrossRef]

339. Xiong, Z.; Ma, J.; Ng, J.; Waite, T.; Zhao, X.S. Silver-Modified Mesoporous TiO$_2$ Photocatalyst for Water Purification. *Water Res.* **2011**, *45*, 2095–2103. [CrossRef]

340. Onkani, S.P.; Diagboya, P.; Mtunzi, F.; Klink, M.J.; Olu-Owolabi, B.; Pakade, V. Comparative study of the photocatalytic degradation of 2–chlorophenol under UV irradiation using pristine and Ag-doped species of TiO$_2$, ZnO and ZnS photocatalysts. *J. Environ. Manag.* **2020**, *260*, 110145. [CrossRef] [PubMed]

341. Komaraiah, D.; Radha, E.; Sivakumar, J.; Reddy, M.V.; Sayanna, R. Photoluminescence and photocatalytic activity of spin coated Ag$^+$ doped anatase TiO$_2$ thin films. *Opt. Mater.* **2020**, *108*, 110401. [CrossRef]

342. Kiran, T.; Ahmed, H.M.; Begum, N.; Manjunatha, K.G. Sun light driven photocatalytic performance of Ag decorated TiO$_2$ nanocomposite thin films by sol gel method. *Mater. Today Proc.* **2021**, *46*, 5948–5952. [CrossRef]

343. Abbad, S.; Guergouri, K.; Gazaout, S.; Djebabra, S.; Zertal, A.; Barille, R.; Zaabat, M. Effect of silver doping on the photocatalytic activity of TiO$_2$ nanopowders synthesized by the sol-gel route. *J. Environ. Chem. Eng.* **2020**, *8*, 103718. [CrossRef]

344. Ribao, P.; Corredor, J.; Rivero, M.; Ortiz, I. Role of reactive oxygen species on the activity of noble metal-doped TiO$_2$ photocatalysts. *J. Hazard. Mater.* **2018**, *372*, 45–51. [CrossRef] [PubMed]

345. Ling, L.; Yawei, F.; Li, H.; Chen, Y.; Wen, J.; Zhu, J.; Bian, Z. Microwave induced surface enhanced pollutant adsorption and photocatalytic degradation on Ag/TiO$_2$. *Appl. Surf. Sci.* **2019**, *483*, 772–778. [CrossRef]

346. Sui, M.; Dong, Y.; Wang, Z.; Wang, F.; You, H. A biocathode-driven photocatalytic fuel cell using an Ag-doped TiO$_2$/Ti mesh photoanode for electricity generation and pollutant degradation. *J. Photochem. Photobiol. A Chem.* **2017**, *348*, 238–245. [CrossRef]

347. Pazoki, M.; Parsa, M.; Farhadpour, R. Removal of the hormones dexamethasone (DXM) by Ag doped on TiO$_2$ photocatalysis. *J. Environ. Chem. Eng.* **2016**, *4*, 4426–4434. [CrossRef]

348. Scarisoreanu, M.; Ilie, G.; Goncearenco, E.; Banici, A.; Morjan, I.; Dutu, E.; Tanasă, E.; Fort, I.; Stan, M.; Mihailescu, C.; et al. Ag, Au and Pt decorated TiO$_2$ biocompatible nanospheres for UV & Vis photocatalytic water treatment. *Appl. Surf. Sci.* **2019**, *509*, 145217. [CrossRef]

349. Suwarnkar, M.; Dhabbe, R.; Kadam, A.; Garadkar, K. Enhanced photocatalytic activity of Ag doped TiO2 nanoparticles synthesized by a microwave assisted method. *Ceram. Int.* **2014**, *40*, 5489–5496. [CrossRef]

350. Zhang, P.; Li, X.; Wu, X.; Zhao, T.; Wen, L. Influence of In^{3+}-doping and Ag$_0$-depositing on the visible-light-induced photocatalytic activity of TiO$_2$. *J. Alloys Compd.* **2016**, *673*, 405–410. [CrossRef]

351. R, S.; Manoj, D.; Qin, J.; Highly Cited Researcher, M.; Gracia, F.; Lee, A.; Khan, M.M.; Pinilla, M.Á. Mechanothermal synthesis of Ag/TiO$_2$ for photocatalytic Methyl Orange degradation and hydrogen production. *Process Saf. Environ. Prot.* **2018**, *120*, 339–347. [CrossRef]

352. Vaiano, V.; Iervolino, G.; Sannino, D.; Murcia, J.; Hidalgo, M.; Ciambelli, P.; Navio, J.A. Photocatalytic removal of Patent Blue V dye on Au-TiO$_2$ and Pt-TiO$_2$ catalysts. *Appl. Catal. B Environ.* **2016**, *188*, 134–146. [CrossRef]

353. Masakazu, A.; Masato, T. The Design and Development of Highly Reactive Titanium Oxide Photocatalysts Operating under Visible Light Irradiation. *J. Catal.* **2003**, *216*, 505–516.

354. Alamelu, K.; Ali, J. TiO$_2$-Pt composite photocatalyst for photodegradation and chemical reduction of recalcitrant organic pollutants. *J. Environ. Chem. Eng.* **2018**, *6*, 5720–5731. [CrossRef]

355. Xu, T.; Zhao, H.; Zheng, H.; Zhang, P. Atomically Pt implanted nanoporous TiO$_2$ film for photocatalytic degradation of trace organic pollutants in water. *Chem. Eng. J.* **2019**, *385*, 123832. [CrossRef]

356. Kitsiou, V.; Zachariadis, G.; Lambropoulou, D.; Tsiplakides, D.; Poulios, I. Mineralization of the antineoplastic drug carboplatin by heterogeneous photocatalysis with simultaneous synthesis of platinum-modified TiO$_2$ catalysts. *J. Environ. Chem. Eng.* **2018**, *6*, 2409–2416. [CrossRef]

357. Alahmadi, N.; Amin, M.S.; Mohamed, R.M. Facile synthesis of mesoporous Pt-doped, titania-silica nanocomposites as highly photoactive under visible light. *J. Mater. Res. Technol.* **2020**, *9*, 14093–14102. [CrossRef]

358. Khan, H.; Rigamonti, M.; Boffito, D. Enhanced Photocatalytic Activity of Pt-TiO$_2$/WO$_3$ Hybrid Material with Energy Storage Ability. *Appl. Catal. B Environ.* **2019**, *252*, 77–85. [CrossRef]

359. Pol, R.; Guerrero, M.; García-Lecina, E.; Altube, A.; Rossinyol, E.; Garroni, S.; Baró, M.D.; Pons, J.; Sort, J.; Pellicer, E. Ni-, Pt- and (Ni/Pt)-doped TiO$_2$ nanophotocatalysts: A smart approach for sustainable degradation of Rhodamine B dye. *Appl. Catal. B Environ.* **2016**, *181*, 270–278. [CrossRef]

360. Nguyen-Phan, T.-D.; Luo, S.; Vovchok, D.; Llorca, J.; Sallis, S.; Kattel, S.; Xu, W.; Piper, L.; Polyansky, D.; Senanayake, S.; et al. Three-Dimensional Ruthenium-Doped TiO$_2$ Sea Urchins for Enhanced Visible-Light-Responsive H$_2$ Production. *Phys. Chem. Chem. Phys.* **2016**, *18*, 15972–15979. [CrossRef]

361. Ismael, M. High effective ruthenium-doped TiO_2 nanoparticles photocatalyst for visible-light-driven photocatalytic hydrogen production. *New J. Chem.* **2019**, *43*, 9596–9605. [CrossRef]

362. Wang, Z.; Liu, B.; Xie, Z.; Li, Y.-M.; Shen, Z.-Y. Preparation and Photocatalytic Properties of RuO_2/TiO_2 Composite Nanotube Arrays. *Ceram. Int.* **2016**, *42*, 13664–13669. [CrossRef]

363. González, A.; Solis-Cortazar, J.; Arellano, C.; Ramirez Morales, E.; Espinosa de los Monteros, A.; Silva Martínez, S. Synthesis of Ruthenium-Doped TiO_2 Nanotube Arrays for the Photocatalytic Degradation of Terasil Blue Dye. *J. Nanosci. Nanotechnol.* **2019**, *19*, 5211–5219. [CrossRef]

364. García-Ramírez, P.; Ramirez Morales, E.; Cortazar, J.; Sirés, I.; Silva Martínez, S. Influence of ruthenium doping on UV- and visible-light photoelectrocatalytic color removal from dye solutions using a TiO_2 nanotube array photoanode. *Chemosphere* **2020**, *267*, 128925. [CrossRef]

365. Fatimah, I.; Nurillahi, R.; Sahroni, I.; Muraza, O. TiO_2-pillared saponite and photosensitization using a ruthenium complex for photocatalytic enhancement of the photodegradation of bromophenol blue. *Appl. Clay Sci.* **2019**, *183*, 105302. [CrossRef]

366. Elsalamony, R.; Mahmoud, S. Preparation of nanostructured ruthenium doped titania for the photocatalytic degradation of 2-chlorophenol under visible light. *Arab. J. Chem.* **2017**, *10*, 194–205. [CrossRef]

367. Długokęcka, M.; Łuczak, J.; Polkowska, Ż.; Zaleska-Medynska, A. The effect of microemulsion composition on the morphology of Pd nanoparticles deposited at the surface of TiO_2 and photoactivity of Pd-TiO_2. *Appl. Surf. Sci.* **2017**, *405*, 220–230. [CrossRef]

368. Nguyen, C.H.; Fu, C.-C.; Juang, R.-S. Degradation of methylene blue and methyl orange by palladium-doped TiO_2 photocatalysis for water reuse: Efficiency and degradation pathways. *J. Clean. Prod.* **2018**, *202*, 413–427. [CrossRef]

369. Bai, X.; Lv, L.; Zhang, X.; Hua, Z. Synthesis and Photocatalytic Properties of Palladium-loaded Three Dimensional Flower-like Anatase TiO_2 with Dominant {001} Facets. *J. Colloid Interface Sci.* **2015**, *467*, 1–9. [CrossRef] [PubMed]

370. Dadsetan, S.; Baghshahi, S.; Farshidfar, F.; Hadavi, M. Photodeposition of Pd nanoparticles on TiO_2 Utilizing a Channel Type Quartz Reactor. *Ceram. Int.* **2017**, *43*, 9322–9326. [CrossRef]

371. Fodor, S.; Kovács, G.; Hernadi, K.; Danciu, V.; Baia, L.; Pap, Z. Shape tailored Pd nanoparticles' effect on the photocatalytic activity of commercial TiO_2. *Catal. Today* **2017**, *284*, 137–145. [CrossRef]

372. Niu, X.; Li, S.; Chu, H.; Zhou, J. Preparation, characterization of Y^{3+}-doped TiO_2 nanoparticles and their photocatalytic activities for methyl orange degradation. *J. Rare Earths* **2011**, *29*, 225–229. [CrossRef]

373. Ahmad, A.L.; Otitoju, T.A.; Ooi, B.S. Optimization of a high performance 3-aminopropyltriethoxysilane-silica impregnated polyethersulfone membrane using response surface methodology for ultrafiltration of synthetic oil-water emulsion. *J. Taiwan Inst. Chem. Eng.* **2018**, *93*, 461–476. [CrossRef]

374. Mazierski, P.; Lisowski, W.; Grzyb, T.; Winiarski, M.; Klimczuk, T.; Mikolajczyk, A.; Flisikowski, J.; Hirsch, A.; Kołakowska, A.; Puzyn, T.; et al. Enhanced photocatalytic properties of lanthanide-TiO_2 nanotubes: An experimental and theoretical study. *Appl. Catal. B Environ.* **2017**, *205*, 376–385. [CrossRef]

375. Nadolna, J.; Grzyb, T.; Wei, Z.; Klein, M.; Kowalska, E.; Ohtani, B.; Zaleska-Medynska, A. Photocatalytic activity and luminescence properties of RE^{3+}–TiO_2 nanocrystals prepared by sol–gel and hydrothermal methods. *Appl. Catal. B Environ.* **2016**, *181*, 825–837. [CrossRef]

376. Li, F.; Li, X.; Hou, M. Photocatalytic Degradation of 2-Mercaptobenzothiazole in Aqueous La^{3+}–TiO_2 Suspension for Odor Control. *Appl. Catal. B Environ.* **2004**, *48*, 185–194. [CrossRef]

377. Zhang, Y.; Zhang, H.; Xu, Y.; Wang, Y. Significant effect of lanthanide doping on the texture and properties of nanocrystalline mesoporous TiO_2. *J. Solid State Chem.* **2004**, *177*, 3490–3498. [CrossRef]

378. Ganesan, M.; Viswanathan, B.; Viswanath, R.P.; Varadarajan, T.K. Photocatalytic behavior of CeO_2-TiO_2 system for the degradation of methylene blue. *Indian J. Chem. Sect. A Inorg. Phys. Theor. Anal. Chem.* **2009**, *48*, 480–488.

379. Jo, W.; Kim, J.-T. Application of visible-light photocatalysis with nitrogen-doped or unmodified titanium dioxide for control of indoor-level volatile organic compounds. *J. Hazard Mater.* **2008**, *164*, 360–366. [CrossRef]

380. Li, F.; Li, X.; Hou, M.; Cheah, K.W.; Choy, W.C.H. Enhanced photocatalytic activity of Ce^{3+}–TiO_2 for 2-mercaptobenzothiazole degradation in aqueous suspension for odour control. *Appl. Catal. A Gen.* **2005**, *285*, 181–189. [CrossRef]

381. Cai, W.; Chen, F.; Shen, X.; Chen, L.; Zhang, J. Enhanced catalytic degradation of AO_7 in the CeO_2–H_2O_2 system with Fe^{3+} doping. *Appl. Catal. B Environ.* **2010**, *101*, 160–168. [CrossRef]

382. Vieira, G.; José, H.; Peterson, M.; Baldissarelli, V.; Alvarez, P.; Moreira, R. CeO_2/TiO_2 nanostructures enhance adsorption and photocatalytic degradation of organic compounds in aqueous suspension. *J. Photochem. Photobiol. A Chem.* **2017**, *353*, 325–336. [CrossRef]

383. Zhang, L.; Xie, J.; Li, G.; Zhang, H. Effect of Ce^{4+}-doping on structural and photocatalytic properties of sol-gel prepared titanium dioxide thin-films. *Bandaoti Guangdian/Semicond. Optoelectron.* **2013**, *34*, 98–102.

384. Tong, T.; Zhang, J.; Tian, B.; Chen, F.; He, D.; Anpo, M. Preparation of Ce-TiO_2 catalysts by controlled hydrolysis of titanium alkoxide based on esterification reaction and study on its photocatalytic activity. *J. Colloid Interface Sci.* **2007**, *315*, 382–388. [CrossRef] [PubMed]

385. Xiao, J.; Peng, T.; Li, R.; Peng, Z.; Yan, C. Preparation, Phase Transformation and Photocatalytic Activities of Cerium-Doped Mesoporous Titania Nanoparticles. *J. Solid State Chem.* **2006**, *179*, 1161–1170. [CrossRef]

386. Guangqin, L.; Liu, C.; Liu, Y. Different effects of cerium ions doping on properties of anatase and rutile TiO_2. *Appl. Surf. Sci.* **2006**, *253*, 2481–2486. [CrossRef]

387. Xie, J.; Jiang, D.; Chen, M.; Li, D.; Zhu, J.; Yan, C. Preparation and characterization of monodisperse Ce-doped TiO$_2$ microspheres with visible light photocatalytic activity. *Colloids Surfaces A Physicochem. Eng. Asp.* **2010**, *372*, 107–114. [CrossRef]

388. Aman, N.; Satapathy, P.; Mishra, T.; Mahato, M.; Das, N. Synthesis and photocatalytic activity of mesoporous cerium doped TiO$_2$ as visible light sensitive photocatalyst. *Mater. Res. Bull.* **2011**, *47*, 179–183. [CrossRef]

389. Singh, K.; Harish, S.; Kristy, P.; Vemulapalli, S.; Archana, J.; M, N.; Shimomura, M.; Hayakawa, Y. Erbium doped TiO$_2$ interconnected mesoporous spheres as an efficient visible light catalyst for photocatalytic applications. *Appl. Surf. Sci.* **2018**, *449*, 755–763. [CrossRef]

390. Manasa, M.; Chandewar, P.; Mahalingam, H. Photocatalytic degradation of ciprofloxacin & norfloxacin and disinfection studies under solar light using boron & cerium doped TiO$_2$ catalysts synthesized by green EDTA-citrate method. *Catal. Today* **2021**, *375*, 522–536. [CrossRef]

391. Shayegan, Z.; Haghighat, F.; Lee, C.-S. Surface Fluorinated Ce-doped TiO$_2$ Nanostructure Photocatalyst: A Trap and Remove Strategy to Enhance the VOC Removal from Indoor Air Environment. *Chem. Eng. J.* **2020**, *401*, 125932. [CrossRef]

392. Mureseanu, M.; Chivu, V.; Osiac, M.; Madalina, C.; Bucur, C.; Parvulescu, V.; Cioatera, N. New photoactive mesoporous Ce-modified TiO$_2$ for simultaneous wastewater treatment and electric power generation. *Catal. Today* **2021**, *366*, 164–176. [CrossRef]

393. Rapsomanikis, A.; Apostolopoulou, A.; Stathatos, E.; Lianos, P. Cerium-modified TiO$_2$ nanocrystalline films for Visible light photocatalytic activity. *J. Photochem. Photobiol. A Chem.* **2014**, *280*, 46–53. [CrossRef]

394. Chen, F.; Ho, P.-L.; Ran, R.; Chen, W.; Si, Z.; Wu, X.; Weng, D.; Huang, Z.; Lee, C. Synergistic effect of CeO$_2$ modified TiO$_2$ photocatalyst on the enhancement of visible light photocatalytic performance. *J. Alloys Compd.* **2017**, *714*, 560–566. [CrossRef]

395. Alvarez-Láinez, M.; Cano Franco, J.C. Effect of CeO2 content in morphology and optoelectronic properties of TiO$_2$-CeO$_2$ nanoparticles in visible light organic degradation. *Mater. Sci. Semicond. Process.* **2019**, *90*, 190–197. [CrossRef]

396. Liang, J.; Wang, J.; Yu, K.; Kexian, S.; Wang, X.; Liu, W.; Hou, J.; Liang, C. Enhanced Photocatalytic Performance of Nd^{3+}-Doped TiO$_2$ Nanosphere under Visible Light. *Chem. Phys.* **2019**, *528*, 110538. [CrossRef]

397. Nithya, N.; Bhoopathi, G.; Magesh, G.; Kumar, C. Neodymium doped TiO$_2$ nanoparticles by sol-gel method for antibacterial and photocatalytic activity. *Mater. Sci. Semicond. Process.* **2018**, *83*, 70–82. [CrossRef]

398. Nadolna, J.; Grzyb, T.; Sobczak, J.; Lisowski, W.; Gazda, M.; Ohtani, B.; Zaleska-Medynska, A. Visible light activity of rare earth metal doped (Er^{3+}, Yb^{3+} or Er^{3+}/Yb^{3+}) titania photocatalysts. *Appl. Catal. B Environ.* **2015**, *163*, 40–49. [CrossRef]

399. Zheng, Y.; Wang, W. Electrospun nanofibers of Er^{3+}-doped TiO$_2$ with photocatalytic activity beyond the absorption edge. *J. Solid State Chem.* **2014**, *210*, 206–212. [CrossRef]

400. Bhethanabotla, V.C.; Russell, D.R.; Kuhn, J.N. Assessment of mechanisms for enhanced performance of Yb/Er/titania photocatalysts for organic degradation: Role of rare earth elements in the titania phase. *Appl. Catal. B Environ.* **2017**, *202*, 156–164. [CrossRef]

401. Farbod, M.; Kajbafvala, M. Surface modification of TiO$_2$ nanoparticles by magnetic ions: Synthesis and application in enhancement of photocatalytic performance. *Appl. Catal. B Environ.* **2017**, *219*, 344–352. [CrossRef]

402. Parnicka, P.; Mazierski, P.; Lisowski, W.; Klimczuk, T.; Nadolna, J.; Zaleska-Medynska, A. A new simple approach to prepare rare-earth metals-modified TiO$_2$ nanotube arrays photoactive under visible light: Surface properties and mechanism investigation. *Results Phys.* **2019**, *12*, 412–423. [CrossRef]

403. Toloman, D.; Popa, A.; Stefan, M.; Pana, O.; Silipas, D.; Sergiu, M.; Barbu-Tudoran, L. Impact of Gd ions from the lattice of TiO$_2$ nanoparticles on the formation of reactive oxygen species during the degradation of RhB under visible light irradiation. *Mater. Sci. Semicond. Process.* **2017**, *71*, 61–68. [CrossRef]

404. Dal'Toé, A.; Lopes Colpani, G.; Padoin, N.; Fiori, M.; Soares, C. Lanthanum doped titania decorated with silver plasmonic nanoparticles with enhanced photocatalytic activity under UV-visible light. *Appl. Surf. Sci.* **2018**, *441*, 1057–1071. [CrossRef]

405. Zhang, J.; Wu, W.; Yan, S.; Chu, G.; Zhao, S.; Wang, X.; Li, C. Enhanced photocatalytic activity for the degradation of rhodamine B by TiO$_2$ modified with Gd$_2$O$_3$ calcined at high temperature. *Appl. Surf. Sci.* **2015**, *344*, 249–256. [CrossRef]

406. Nair, R.R.; Arulraj, J.; Devi, K.S. Ceria doped titania nano particles: Synthesis and photocatalytic activity. *Mater. Today Proc.* **2016**, *3*, 1643–1649. [CrossRef]

407. Jung, S.-C.; Bang, H.-J.; Lee, H.; Ha, H.-H.; Yu, Y.H.; Kim, S.-J.; Park, Y.-K. Assessing the photocatalytic activity of europium doped TiO$_2$ using liquid phase plasma process on acetylsalicylic acid. *Catal. Today* **2020**. In Press. [CrossRef]

408. Hu, Z.; Xu, T.; Liu, P.; Oeser, M. Microstructures and optical performances of nitrogen-vanadium co-doped TiO$_2$ with enhanced purification efficiency to vehicle exhaust. *Environ. Res.* **2021**, *193*, 110560. [CrossRef] [PubMed]

409. Teh, C.; Mohamed, A. Roles of titanium dioxide and ion-doped titanium dioxide on photocatalytic degradation of organic pollutants (phenolic compounds and dyes) in aqueous solutions: A review. *J. Alloy. Compd.* **2011**, *509*, 1648–1660. [CrossRef]

410. Skorb, E.; Antonouskaya, L.I.; Belyasova, N.; Shchukin, D.; Moehwald, H.; Sviridov, D. Antibacterial Activity of Thin-film Photocatalysts Based on Metal-modified TiO$_2$ and TiO$_2$:In$_2$O$_3$ Nanocomposite. *Appl. Catal. B Environ.* **2008**, *84*, 94–99. [CrossRef]

411. Li, C.; Ming, T.; Wang, J.; Wang, J.; Yu, J.; Yu, S. Ultrasonic aerosol spray-assisted preparation of TiO$_2$/In$_2$O$_3$ composite for visible-light-driven photocatalysis. *J. Catal.* **2014**, *310*, 84–90. [CrossRef]

412. Tahir, M.; Saidina Amin, N.A. Photocatalytic CO$_2$ reduction and kinetic study over In/TiO$_2$ nanoparticles supported microchannel monolith photoreactor. *Appl. Catal. A Gen.* **2013**, *467*, 483–496. [CrossRef]

413. Glez, V.; Moreno-Rodríguez, A.; May, M.; Tzompantzi, F.J.; Gomez, R. Slurry photodegradation of 2,4-dichlorophenoxyacetic acid: A comparative study of impregnated and sol–gel In$_2$O$_3$–TiO$_2$ mixed oxide catalysts. *J. Photochem. Photobiol. A Chem.* **2008**, *193*, 266–270. [CrossRef]

414. Yu, Y.; Wang, E.; Yuan, J.; Cao, Y. Enhanced photocatalytic activity of titania with unique surface indium and boron species. *Appl. Surf. Sci.* **2013**, *273*, 638–644. [CrossRef]

415. Zhou, J.; Zhang, Y.; Zhao, X.S.; Ray, A. Photodegradation of Benzoic Acid over Metal-Doped TiO$_2$. *Ind. Eng. Chem. Res.* **2006**, *45*, 3503–3511. [CrossRef]

416. Okajima, T.; Yamamoto, T.; Kunisu, M.; Yoshioka, S.; Tanaka, I.; Umesaki, N. Dilute Ga Dopant in TiO$_2$ by X-ray Absorption Near-Edge Structure. *Jpn. J. Appl. Phys.* **2006**, *45*, 7028. [CrossRef]

417. Umare, S.; Charanpahari, A.; Sasikala, R. Enhanced visible light photocatalytic activity of Ga, N and S codoped TiO$_2$ for degradation of azo dye. *Mater. Chem. Phys.* **2013**, *140*, 529–534. [CrossRef]

418. Mohamed, H.; Qarni, F.; Al-Omair, N. Design of porous Ga doped TiO$_2$ nanostructure for enhanced solar light photocatalytic applications. *Mater. Res. Bull.* **2021**, *133*, 111057. [CrossRef]

419. Liu, X.; Khan, M.; Liu, W.; Xiang, W.; Guan, M.; Jiang, P.; Cao, W. Synthesis of nanocrystalline Ga–TiO$_2$ powders by mild hydrothermal method and their visible light photoactivity. *Ceram. Int.* **2015**, *41*, 3075–3080. [CrossRef]

420. Deng, Q.; Han, X.; Gao, Y. Remarkable optical red shift and extremely high optical absorption coefficient of V-Ga co-doped TiO$_2$. *J. Appl. Phys.* **2012**, *112*. [CrossRef]

421. Lee, D.-K.; Yoo, H.-I. Electrical conductivity and oxygen nonstoichiometry of acceptor (Ga)-doped titania. *Phys. Chem. Chem. Phys.* **2008**, *10*, 6890–6898. [CrossRef]

422. Ahmad, A.; Senapati, S.; Khan, M.; Kumar, R.; Sastry, M. Extracellular Biosynthesis of Monodisperse Gold Nanoparticles by a Novel Extremophilic Actinomycete, *Thermomonospora* sp. *Langmuir* **2003**, *19*, 3550–3553. [CrossRef]

423. Hopper, M.; Sauvage, F.; Chandiran, A.K.; Graetzel, M.; Poeppelmeier, K.; Mason, T. Electrical Properties of Nb-, Ga-, and Y-Substituted Nanocrystalline Anatase TiO$_2$ Prepared by Hydrothermal Synthesis. *J. Am. Ceram. Soc.* **2012**, *95*, 3192–3196. [CrossRef]

424. Song, S.; Wang, C.; Hong, F.; He, Z.; Cai, Q.; Chen, J. Gallium and iodine-co-doped titanium dioxide for photocatalytic degradation of 2-chlorophenol in aqueous solution: Role of gallium. *Appl. Surf. Sci.* **2011**, *257*, 3427–3432. [CrossRef]

425. Chae, J.; Kim, D.; Kim, S.; Kang, M. Photovoltaic efficiency on dye-sensitized solar cells (DSSC) assembled using Ga-incorporated TiO$_2$ materials. *J. Ind. Eng. Chem.* **2010**, *16*, 906–911. [CrossRef]

426. Niyomkarn, S.; Puangpetch, T.; Chavadej, S. Mesoporous-assembled In$_2$O$_3$–TiO$_2$ mixed oxide photocatalysts for efficient degradation of azo dye contaminant in aqueous solution. *Mater. Sci. Semicond. Process.* **2014**, *25*, 112–122. [CrossRef]

427. An, G.; Mahadik, M.; Piao, G.; Chae, W.-S.; Park, H.; Cho, M.; Chung, H.-S.; Jang, J. Hierarchical TiO$_2$ @In$_2$O$_3$ heteroarchitecture photoanodes: Mechanistic study on interfacial charge carrier dynamics through water splitting and organic decomposition. *Appl. Surf. Sci.* **2019**, *480*, 1–12. [CrossRef]

428. Sangjan, S.; Wisasa, K.; Deddeaw, N. Enhanced photodegradation of reactive blue dye using Ga and Gd as catalyst in reduced graphene oxide-based TiO$_2$ composites. *Mater. Today Proc.* **2019**, *6*, 19–23. [CrossRef]

429. Ismail, A.; Abdelfattah, I.; Faisal, M.; Helal, A. Efficient Photodecomposition of Herbicide Imazapyr over Mesoporous Ga$_2$O$_3$-TiO$_2$ Nanocomposites. *J. Hazard Mater.* **2017**, *342*, In. [CrossRef] [PubMed]

430. Areerachakul, N.; Sakulkhaemaruethai, S.; Johir, M.A.H.; Kandasamy, J.; Vigneswaran, S. Photocatalytic degradation of organic pollutants from wastewater using aluminium doped titanium dioxide. *J. Water Process Eng.* **2019**, *27*, 177–184. [CrossRef]

431. Sengele, A.; Robert, D.; Keller, N.; Colbeau-Justin, C.; Keller, V. Sn-doped and porogen-modified TiO$_2$ photocatalyst for solar light elimination of sulfure diethyle as a model for chemical warfare agent. *Appl. Catal. B Environ.* **2018**, *245*, 279–289. [CrossRef]

432. Li, J.; Shi, J.; Li, Y.; Ding, Z.; Huang, J. A biotemplate synthesized hierarchical Sn-doped TiO$_2$ with superior photocatalytic capacity under simulated solar light. *Ceram. Int.* **2021**, *47*, 8218–8227. [CrossRef]

433. Zhu, X.; Han, S.; Feng, W.; Kong, Q.; Dong, Z.; Wang, C.; Lei, J.; Yi, Q. The effect of heat treatment on the anatase–rutile phase transformation and photocatalytic activity of Sn-doped TiO$_2$ nanomaterials. *RSC Adv.* **2018**, *8*, 14249–14257. [CrossRef]

434. Wang, J.; Ren, H.; Chen, W.-F.; Koshy, P.; Sorrell, C. Fabrication and Photocatalytic Performance of Sn-Doped Titania Hollow Spheres Using Polystyrene as Template. *Ceram. Int.* **2017**, *44*, 4981–4989. [CrossRef]

435. Mohammad, A.; Khan, M.; Cho, M.H.; Yoon, T. Fabrication of binary SnO$_2$/TiO$_2$ nanocomposites under a sonication-assisted approach: Tuning of band-gap and water depollution applications under visible light irradiation. *Ceram. Int.* **2021**, *47*, 15073–15081. [CrossRef]

436. Albornoz, L.; Wohlmuth da Silva, S.; Bortolozzi, J.; Banús, E.; Brussino, P.; Ulla, M.; Bernardes, A. Degradation and mineralization of erythromycin by heterogeneous photocatalysis using SnO$_2$-doped TiO$_2$ structured catalysts: Activity and stability. *Chemosphere* **2021**, *268*, 128858. [CrossRef] [PubMed]

437. Mugunthan, E.; Saidutta, M.B.; PonnanEttiyappan, J. Photocatalytic Degradation of Diclofenac using TiO$_2$-SnO$_2$ Mixed Oxide Catalysts. *Environ. Technol.* **2017**, *40*, 929–941. [CrossRef]

438. Rangel-Vázquez, I.; Del Angel, G.; Bertin, V.; González, F.; Vázquez-Zavala, A.; Arrieta, A.; Padilla, J.M.; Barrera, A.; Ramírez, E. Synthesis and characterization of Sn doped TiO$_2$ photocatalysts: Effect of Sn concentration on the textural properties and on the photocatalytic degradation of 2,4-dichlorophenoxyacetic acid. *J. Alloys Compd.* **2014**, *643*, S144–S149. [CrossRef]